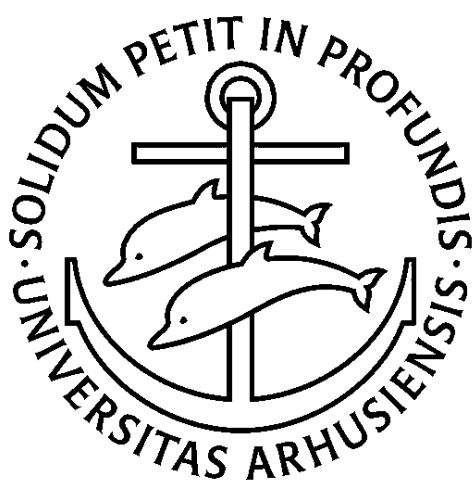PhD Thesis

# Linear Scaling Wave Function Optimization and Molecular Properties

Thomas Kjærgaard

The Lundbeck Foundation Center for Theoretical Chemistry

Department of Chemistry

University of Aarhus
July 2010

# Contents

# Chapter 1

# Preface

This thesis is submitted to the Faculty of Science at the University of Aarhus to fulfill the requirements for obtaining the PhD degree in chemistry. It contains the results of four years of PhD studies at the Center for Theoretical Chemistry, Department of Chemistry, University of Aarhus, under supervision of Poul Jørgensen from 2006 to 2010.

The focus of the thesis is on obtaining optimized density matrices for Hartree-Fock and Density Functional Theory, and optimized wave functions for Coupled-Cluster theory as well as linear scaling response properties within Hartree-Fock and Density Functional Theory. As will become evident, the focus has been mostly on methodological developments and less on applications.

## 1.1 Publications

The research I have participated in during my PhD studies has been documented in 9 articles:

**A. Thomas Kjærgaard**, Branislav Jansík, Poul Jørgensen, Sonia Coriani, and Josef Michl:
*Gauge-Origin-Independent Coupled Cluster Singles and Doubles Calculation of Magnetic Circular Dichroism of Azabenzenes and Phosphabenzene Using London Orbitals*
J. Phys. Chem. A 111, 11278 (2007)

**B. Thomas Kjærgaard**, Poul Jørgensen, Jeppe Olsen, Sonia Coriani, and Trygve Helgaker:
*Hartree-Fock and Kohn-Sham time-dependent response theory in a second-quantization atomic-orbital formalism suitable for linear scaling*
J. Chem. Phys. 129, 054106 (2008)

**C.** Simen Reine, Erik Tellgren, Andreas Krapp, **Thomas Kjærgaard**, Trygve Helgaker, Branislav Jansík, Stinne Høst, and Pawel Sałek:
*Variational and robust density fitting of four-center two-electron integrals in local metrics*
J. Chem. Phys. 129, 104101 (2008)

**D.** Kasper Kristensen, Joanna Kauczor, **Thomas Kjærgaard**, and Poul Jørgensen:

*Quasienergy formulation of damped response theory*

J. Chem. Phys. 131, 044112 (2009)

**E. Thomas Kjærgaard**, Poul Jørgensen, Andreas Johan Thorvaldsen, Pawel Sałek, and Sonia Coriani:

*Gauge-Origin Independent Formulation and Implementation of Magneto-Optical Activity within Atomic-Orbital-Density Based Hartree-Fock and Kohn-Sham Response Theories*

J. Chem. Theory Comput 5, 1997 (2009)

**F.** Sonia Coriani, **Thomas Kjærgaard**, Poul Jørgensen, Kenneth Ruud, Joonsuk Huh, and Robert Berger:

*An atomic-orbital based Lagrangian approach for calculating geometrical gradients of linear response properties*

J. Chem. Theory Comput, 6 1028 (2010)

**G.** Marcin Ziółkowski, Branislav Jansík, **Thomas Kjærgaard**, and Poul Jørgensen:

*Linear scaling coupled cluster method with correlation energy based error control*

J. Chem. Phys. 133, 014107 (2010)

**H.** Marcin Ziółkowski, Branislav Jansík, **Thomas Kjærgaard**, Kasper Kristensen, and Poul Jørgensen:

*The divide–expand–consolidate (DEC) coupled cluster method. A linear–scaling approach with correlation energy–based error control*

manuscript

**I. Thomas Kjærgaard**, Kasper Kristensen, Joanna Kauczor, Sonia Coriani, Andreas Johan Thorvaldsen, and Poul Jørgensen:

*Comparison of standard and damped response formulations of Magnetic Circular Dichroism*

manuscript

All papers are included at the end of this thesis.

## 1.2 Miscellaneous

Atomic units are used throughout this thesis unless otherwise stated.

All methods described have been implemented in a local development version of the quantum chemistry program DALTON [1] except for the DEC model of chapter 6 which constitute a separate PROGRAM [2].

## 1.3 Acknowledgments

I would first and foremost like to thank my supervisor Professor Poul Jørgensen, for his invaluable guidance through my years of study. Professor Jørgensen is extremely generous with his time,

his experiences, and his skills in debugging computer code. At times when my research seemed slow going and frustrating, Professor Jørgensen was a source of constant encouragement.

A number of people have helped me through my studies and have made the last four years a period of time I will look back on with joy. I am afraid that I do not always tell people how I feel and thank them for their support and friendship. I would in this respect like to thank Dr. Stinne Høst for many helpful discussions on all things related to wave function optimization. On a personal note, I appreciate that she took me under her wing and showed me the ropes, as only a older and wiser PhD student could.

I would like to thank Dr. Branislav Jansik for teaching me regarding a number of technical issues about compilers,shell scripts, unix systems, etc in addition to being my helpful office mate through the last four years. Dr. Sonia Coriani and I have had a very fruitful collaboration, and I would like to thank her for her help through an, at times, tough project.

During my stay in Oslo, I started a collaboration with Dr. Simen Reine and Professor Trygve Helgaker. I would like to thank both for invaluable collaboration and insight in the development of a new integral driver and especially Dr. Simen Reine for teaching me basically everything I know about integral evaluation, I would also like to thank Dr. Erik Tellgren, Dr. Andrew Teale, and the entire Oslo group for the good times I had in Oslo.

I would like to thank Dr. Pawel Sałek for his assistance with the exchange-correlation contributions, Professor Kenneth Ruud for his help with excited state optimizations, and Dr. Andreas Thorvaldsen for the collaboration on damped response theory.

Kasper Kristensen and Joanna Kauczor have during the last three–four years become good friends and good colleagues. I would especially like to thank Joanna for her moral support and the, at times, much needed hugs, and while I love to tease Kasper, I have great respect for his attention to details. I would also like to thank Peter Seidler and Dr. Mikkel Bo Hansen for their effort in getting me to run more, despite obvious reservations.

Late in my Ph.D. I have collaborated with Dr. Marcin Ziółkowski and would like to thank him for insightful discussions on Coupled Cluster theory. .

I would finally like to thank the entire quantum chemistry group in Aarhus for all the many good times, highly intellectual or drunken discussions, and many rich moments over the last four years.

A very special thanks goes to my friends for all their morale support, all the parties, the weekends, the golden spring, the challenging beer-bowling games, but also for listening to my problems, when needed.

I would also like to thank my family, for at least pretending to be interested, when I start rambling on about quantum chemistry.

Finally, I would like to thank Dr. Stinne Høst, Kasper Kristensen, Dr. Simen Reine and Dr. Mikkel Bo Hansen for proofreading this thesis.

# Chapter 2

# Introduction

Since the development of quantum mechanics in the 1920s, the area of quantum chemistry have transformed from an exotic area of chemistry, being merely of academic interest, into a powerful and fruitful branch of science, used extensively not only in chemistry and physics, but also in related branches of science such as molecular biology and drug design. For small molecular systems, state-of-the-art electronic structure calculations challenge the accuracy obtained from experiments [3, 4]. Unfortunately, as the size of the molecular systems increase, so does the required computational effort, and high accuracy calculations cannot be carried out for large molecular systems, but a qualitative calculation can be a useful tool in explaining e.g. reaction mechanisms. The toolbox of quantum chemistry therefore consist of everything from the computationally cheap qualitative–correct low-accuracy methods to the computationally expensive high-accuracy methods. Increasing the range of application of these methods will improve the usefulness of the toolbox provided by quantum chemistry, and increase the impact of quantum chemistry in the scientific community.

To obtain an accurate description of the electronic structure and properties of molecular systems, the Schrödinger equation must be set up and subsequently solved for a given molecular system. Since the exact solution to the Schrödinger equation is unattainable for all systems of chemical interest, approximations are required. A hierarchy of wave function based approximations provides a diverse set of tools, which range from the qualitative independent–particle Hartree–Fock (HF) approximation to the highly accurate hierarchy of coupled–cluster (CC) models.

An alternative approach is Density Functional Theory (DFT). DFT methods have become very popular, since DFT methods typically constitute a good compromise between cost and accuracy. The cost of DFT calculations is comparable to that of the simple wave function model, HF, but their accuracy significantly exceeds that of HF calculations.

A common characteristic of both DFT and wave function models is that in their standard formulation, their applicability is limited due to a poor scaling with system size. The simple HF as well as DFT formally have a quartic scaling, with respect to the size of the molecular system, denoted $\mathcal{O}(N^4)$, where $N$ is a quantity proportional to the size of the system. The

consequence is that doubling the size of a molecular system increases the computational time within the HF model by a factor of $2^4 = 16$, limiting the size of systems that can be treated using this model. The more accurate CC methods have an even steeper scaling behaviour. For instance the computational time of the accurate CCSD model scales as $\mathcal{O}(N^6)$ limiting its use to molecules containing approximately 40 atoms.

Much effort has been directed towards the development and implementation of algorithms of reduced scaling, ideally linear scaling $\mathcal{O}(N)$, such that doubling the system size implies only a doubling of the computational time. A linear scaling HF and DFT method have successfully been obtained, but both the HF and DFT methods can be accelerated through the use of density-fitting, which will be one subject of this thesis.

The present work focuses on two main topics. The first topic is how linear scaling may be obtained in CC theories. The impact of this method is expected to be profound as it will lead to an unprecedented accuracy and reliability for large molecular systems.

The second topic is how to obtain linear scaling molecular properties within HF and DFT theories. The calculation of molecular properties within HF or DFT have an inherent quartic scaling, identical to the standard formulation of the HF wave function optimization. However, many of the algorithms developed for the wave function optimization, can directly be exploited to obtain linear scaling molecular properties.

The many linear–scaling developments, which have been implemented in the DALTON program over the last decade, have made it necessary to implement a new integral program. This is a major task, which I have undertaken during my Ph.D., in collaboration with Dr. Simen Reine. The integral program exploit the current computer architecture and provides a flexible interface. This is required by, for instance, the linear scaling CC method presented in this thesis. The implementation of a new integral program have been, and will be, extremely important for further linear–scaling developments within the DALTON framework. The development of the new integral code has been a huge personal learning experience, but unfortunately, this work have not directly resulted in any articles.

This thesis is organized as follows:

**Electronic-Structure Theory:** We start with a short introduction to electronic structure theory, defining terms important in the following chapters on coupled cluster theory and molecular properties.

**Density Fitting:** We briefly summarize the key aspects of paper **C**, which have been implemented in the new integral code, and is the only paper which directly deals with integral evaluation.

**Coupled Cluster Theory:** Following a short introduction to coupled cluster theory, a brief summary are given concerning the status of reduced scaling coupled–cluster schemes.

**The Divide–Expand–Consolidate Coupled Cluster Model:** We present the first linear-scaling coupled-cluster method with correlation energy based error control. This chapter is

both a review of paper **G** and a more in depth description of the content of the unpublished paper **H**.

**Response Theory:** We start with an introduction to exact response theory, defining a notation used in the following chapters after which we introduce the damped response theory published in paper **D**

**Hartree–Fock and Kohn-Sham DFT response theory:** We review important aspects of paper **B** where we introduced a linear scaling second–quantization–atomic–orbital based response theory. Paper **B** deals with both a Hartree-Fock state and time–dependent density functional theory, but in this chapter we will limit the scope to Hartree-Fock theory. Later the Hartree-Fock response theory is extended to damped response theory.

**Geometric gradients of linear response properties:** We summarize the general linear scaling framework for obtaining molecular response properties that can be expressed as first derivative with respect to the nuclear displacements of a generic linear response function, its poles and its residues, introduced in paper **F**

**Magnetic Circular Dichroism:** We introduce the theory of Magnetic Circular Dichroism, using damped response theory described in the unpublished paper **I**, and briefly touch upon important features of papers **A** and **E**. Magnetic Optical Rotation have also been investigated in paper **E**, but this subject will not be discussed further in this thesis.

# Chapter 3

# Electronic-Structure Theory

The electronic energy E of a molecular system is obtained as the eigenvalue of the electronic time-independent (non-relativistic) Schrödinger equation[5], within the Born-Oppenheimer approximation

$$\hat{H}_e \Psi = E\Psi, \tag{3.1}$$

where the eigenfunction $\Psi$ is called the electronic wave function and contains all information needed to determine any property of the system. $\hat{H}_e$ is the electronic Hamiltonian which contains the kinetic energy operator for the electrons ($\hat{T}_e$), the external potential arising from the interaction between the electrons and the stationary nuclei ($\hat{V}_{ne}$), the interaction between the electrons ($\hat{V}_{ee}$), and the constant nuclear-nuclear repulsion term ($h_{nuc}$)

$$\hat{H}_e = \hat{T}_e + \hat{V}_{ne} + \hat{V}_{ee} + h_{nuc} = \sum_i^{N_e} \hat{h}_i + \sum_{i>j}^{N_e} \hat{g}_{ij} + h_{nuc}, \tag{3.2}$$

where $N_e$ is the number of electrons, and $\hat{h}_i$ and $\hat{g}_{ij}$ are one- and two-electron operators given by

$$\hat{h}_i = -\frac{1}{2}\nabla_i^2 - \sum_I^{N_n} \frac{Z_I}{|\boldsymbol{R}_I - \boldsymbol{r}_i|} \qquad \hat{g}_{ij} = \frac{1}{|\boldsymbol{r}_i - \boldsymbol{r}_j|}, \tag{3.3}$$

where $N_n$ is the number of nuclei, $Z_I$ the charge of the nuclei $I$, $|\boldsymbol{R}_I - \boldsymbol{r}_i|$ the distance between nuclei $I$ and electron $i$ and $|\boldsymbol{r}_i - \boldsymbol{r}_j|$ distance between electron $i$ and $j$.

In order to solve the Schrödinger equation, the many-electron wave function is traditionally expanded in terms of Slater determinants, which ensures that the Pauli principle is fulfilled. The Slater determinants are built from one-electron functions (spin orbitals). The exact solution to the Schrödinger equation is obtained in the limit of an infinite number of one-electron functions and all possible Slater determinants. Since this is not possible in practice, it is necessary to introduce two approximations. First, a finite number of one-electron functions (the basis set) is chosen. Second, only a limited number of all the possible Slater determinants are included in the wave function expansion.

If all possible Slater determinants are included the method is called the Full Configuration interaction (FCI) method, and the solution is exact within the chosen basis set. The method is

computationally expensive and intractable for all but the smallest of systems, and is therefore mainly used for benchmarking other less computationally expensive methods. In the following, the simplest non empirical of these approximations to the Schrödinger equation are introduced.

## 3.1 The Hartree-Fock Model

In the Hartree-Fock (HF) model, a single Slater determinant (or a minimal symmetry-adapted linear combination of Slater determinants, denoted a configuration state function) is included in the wavefunction expansion. For a closed-shell system (assumed throughout) of $N_e$ electrons, the HF wave function ansatz is given by

$$\Psi_{HF}(\boldsymbol{x}_1, \boldsymbol{x}_2, \cdots, \boldsymbol{x}_N) = |\psi_1(\boldsymbol{x}_1)\psi_2(\boldsymbol{x}_2)\cdots\psi_N(\boldsymbol{x}_N)|, \tag{3.4}$$

where $\psi$ are spin orbitals containing a spatial component $\phi$ ( denoted molecular orbitals (MOs)) and a spin component $\sigma$

$$\psi_i(\boldsymbol{x}_i) = \phi_i(\boldsymbol{r})\sigma(\boldsymbol{s}). \tag{3.5}$$

The energy is minimized with respect to variations in the MOs subject to the constraint that the MOs are orthonormal. This is equivalent to solving a set of effective one-electron equations

$$\hat{F}_i\phi_i = \sum_j \epsilon_{ij}\phi_j, \tag{3.6}$$

where $\epsilon_{ij}$ are Lagrangian multipliers and the Fock operator $\hat{F}$ is an effective one-electron operator

$$\hat{F}_i = \hat{h}_i + \sum_j (2\hat{J}_j - \hat{K}_j), \tag{3.7}$$

$\hat{J}$ and $\hat{K}$ are the Coulomb and exchange operators, which are most conveniently defined through their action on a MO

$$\hat{J}_j\phi_i(\boldsymbol{r}_1) = \phi_i(\boldsymbol{r}_1)\int \phi_j^*(\boldsymbol{r}_2)\frac{1}{|\boldsymbol{r}_1 - \boldsymbol{r}_2|}\phi_j(\boldsymbol{r}_2)d\boldsymbol{r}_2 \tag{3.8a}$$

$$\hat{K}_j\phi_i(\boldsymbol{r}_1) = \phi_j(\boldsymbol{r}_1)\int \phi_j^*(\boldsymbol{r}_2)\frac{1}{|\boldsymbol{r}_1 - \boldsymbol{r}_2|}\phi_i(\boldsymbol{r}_2)d\boldsymbol{r}_2, \tag{3.8b}$$

An infinite number of MOs fulfill Eq. (3.6) and Eq. (3.6) may be written in terms of canonical MOs (CMOs), which diagonalize $\epsilon$. The resulting equation are denoted the canonical HF equations

$$\hat{F}_i\phi_i = \epsilon_i\phi_i, \tag{3.9}$$

where $\epsilon_i$ are now interpreted as orbital energies. Since the Fock operator depends on the orbitals, the HF pseudo-eigenvalue equation of Eq. (3.9) must be solved using an iterative algorithm until a self consistent solution is found, after which the HF energy can be evaluated as

$$E_{\mathrm{HF}} = 2\sum_i^{N_{occ}} h_{ii} + 2\sum_{ij}^{N_{occ}} \int \phi_i^*(\boldsymbol{r}_1)\phi_i(\boldsymbol{r}_1)\frac{1}{|\boldsymbol{r}_1 - \boldsymbol{r}_2|}\phi_j^*(\boldsymbol{r}_2)\phi_j(\boldsymbol{r}_2)d\boldsymbol{r}_1 d\boldsymbol{r}_2 \tag{3.10}$$

$$- \sum_{ij}^{N_{occ}} \int \phi_i^*(\boldsymbol{r}_1)\phi_j(\boldsymbol{r}_1)\frac{1}{|\boldsymbol{r}_1 - \boldsymbol{r}_2|}\phi_j^*(\boldsymbol{r}_2)\phi_i(\boldsymbol{r}_2)d\boldsymbol{r}_1 d\boldsymbol{r}_2 + h_{nuc}, \tag{3.11}$$

where $h_{ii}$ are the expectation values of $\hat{h}_i$.

$$h_{ii} = \int \phi_i^*(\boldsymbol{r}_i) \left( -\frac{1}{2}\nabla_i^2 - \sum_I^{N_n} \frac{Z_I}{|\boldsymbol{R}_I - \boldsymbol{r}_i|} \right) \phi_i(\boldsymbol{r}_i) d\boldsymbol{r}_1. \tag{3.12}$$

The Coulomb contribution is a long-ranged contribution which has an inverse distance dependence on the two charge distributions described by $|\phi_i(\boldsymbol{r}_1)|^2$ and $|\phi_j(\boldsymbol{r}_2)|^2$. The exchange contribution is a consequence of the anti-symmetrization of the wave function and is for insulators a short-ranged contribution, which depend on the spatial separation of the two MOs $\phi_i$ and $\phi_j$.

The consequence of only using a single Slater determinant is that the instantaneous interaction between electrons are neglected, and thus the electrons interact only through the effective Fock operator, which contains a average potential generated from all other electrons. The HF model is sometimes denoted a mean-field model, as an individual electron only feels the mean potential generated by the other electrons.

For computational purposes, the MOs are typically expanded in a set of atomic orbitals (AOs) $\chi_\mu$

$$\phi_i = \sum_\mu C_{\mu i} \chi_\mu. \tag{3.13}$$

Note that throughout this thesis roman letters are used for the orthonormal MOs indices and greek letters for their atomic counterparts. Inserting this expansion into Eq. (3.9) yields the Roothaan-Hall equations

$$\mathbf{FC} = \mathbf{SC}\boldsymbol{\epsilon}, \tag{3.14}$$

where $\mathbf{S}$ is the overlap matrix in the AO basis

$$S_{\mu\nu} = \int \chi_\mu^*(\boldsymbol{r})\chi_\nu(\boldsymbol{r})d\boldsymbol{r} \tag{3.15}$$

The eigenvector matrix $\mathbf{C}$ in Eq. (3.14) contains the MO expansion coefficients of Eq. (3.13) and $\boldsymbol{\epsilon}$ is a diagonal matrix which contains the orbital energies. $\mathbf{F}$ is the Fock matrix in the AO basis

$$\mathbf{F} \;=\; \mathbf{h} + 2\mathbf{J}(\mathbf{D}) - \mathbf{K}(\mathbf{D}), \tag{3.16}$$

expressed in terms of the one-electron AO density matrix

$$\mathbf{D} = \mathbf{C}_o \mathbf{C}_o^\dagger, \tag{3.17}$$

where $\mathbf{C}_o$ denoted the subblock of occupied MO coefficients. The one-electron core hamiltonian $\mathbf{h}$, Coulomb $\mathbf{J}(\mathbf{D})$ and exchange $\mathbf{K}(\mathbf{D})$ matrices is defined as

$$h_{\mu\nu} = \int \chi_\mu^*(\boldsymbol{r}_1) \left( -\frac{1}{2}\nabla_1^2 - \sum_I^{N_n} \frac{Z_I}{|\boldsymbol{R}_I - \boldsymbol{r}_1|} \right) \chi_\nu(\boldsymbol{r}_1) d\boldsymbol{r}_1 \tag{3.18a}$$

$$J_{\mu\nu}(\mathbf{D}) = \sum_{\gamma\delta} \int \chi_\mu^*(\boldsymbol{r}_1)\chi_\gamma^*(\boldsymbol{r}_2) \frac{1}{|\boldsymbol{r}_1 - \boldsymbol{r}_2|} \chi_\nu(\boldsymbol{r}_1)\chi_\delta(\boldsymbol{r}_2) d\boldsymbol{r}_1 d\boldsymbol{r}_2 D_{\delta\gamma} \tag{3.18b}$$

$$K_{\mu\nu}(\mathbf{D}) = \sum_{\gamma\delta} \int \chi_\mu^*(\boldsymbol{r}_1)\chi_\gamma^*(\boldsymbol{r}_2) \frac{1}{|\boldsymbol{r}_1 - \boldsymbol{r}_2|} \chi_\delta(\boldsymbol{r}_1)\chi_\nu(\boldsymbol{r}_2) d\boldsymbol{r}_1 d\boldsymbol{r}_2 D_{\delta\gamma} \tag{3.18c}$$

The diagonalization of the Fock matrix according to Eq. (3.14) yields a set of MOs from which a new density can be constructed and the iterative procedure is thus established.

The evaluation of the molecular integrals of Eqs (3.18b),(3.18a),(3.18b) and (3.18c) is central to quantum chemistry, and is often one of the time-limiting steps. This is the subject of the next section, but before proceeding to this discussion, we note that a number of short hand notations have been used in the litterature, and we here introduce the Mulliken like notations, used in this thesis

$$(f|g) = = \int f^*(\boldsymbol{r}_1)\frac{1}{|\boldsymbol{r}_1-\boldsymbol{r}_2|}g(\boldsymbol{r}_2)d\boldsymbol{r}_1 d\boldsymbol{r}_2 \tag{3.19a}$$

$$(\mu\nu|\gamma\delta) = \int \chi_\mu^*(\boldsymbol{r}_1)\chi_\nu(\boldsymbol{r}_1)\frac{1}{|\boldsymbol{r}_1-\boldsymbol{r}_2|}\chi_\gamma^*(\boldsymbol{r}_2)\chi_\delta(\boldsymbol{r}_2)d\boldsymbol{r}_1 d\boldsymbol{r}_2 \tag{3.19b}$$

$$\langle f|w|g\rangle = \int f^*(\boldsymbol{r}_1)w(\boldsymbol{r}_1,\boldsymbol{r}_2)g(\boldsymbol{r}_2)d\boldsymbol{r}_1 d\boldsymbol{r}_2 \tag{3.19c}$$

$$g_{\mu\nu\gamma\delta} = \int \chi_\mu^*(\boldsymbol{r}_1)\chi_\gamma^*(\boldsymbol{r}_2)\frac{1}{|\boldsymbol{r}_1-\boldsymbol{r}_2|}\chi_\nu(\boldsymbol{r}_1)\chi_\delta(\boldsymbol{r}_2)d\boldsymbol{r}_1 d\boldsymbol{r}_2 = (\mu\nu|\gamma\delta) \tag{3.19d}$$

which means that

$$J_{\mu\nu}(\mathbf{D}) = \sum_{\gamma\delta}(\mu\nu|\gamma\delta)D_{\delta\gamma} = \sum_{\gamma\delta}g_{\mu\nu\gamma\delta}D_{\delta\gamma} \tag{3.20a}$$

$$K_{\mu\nu}(\mathbf{D}) = \sum_{\gamma\delta}(\mu\delta|\gamma\nu)D_{\delta\gamma} = \sum_{\gamma\delta}g_{\mu\delta\gamma\nu}D_{\delta\gamma} \tag{3.20b}$$

## 3.2 Linear-Scaling Hartree-Fock

Each iteration of a wavefunction optimization consists of two steps: the construction of the Fock matrix of Eq. (3.16), and a construction of the density from the solution to Eq. (3.14).

Linear-scaling methods for obtaining the solution to Eq. (3.14) have been developed and implemented, but this subject will not be included in this thesis. For extensive reviews see Refs. [6, 7].

The time dominating step in each iteration is the construction of the Fock matrix. During the last decades, much effort has been directed towards obtaining an efficient evaluation of each of the contributions entering the Fock matrix [8–10]. The construction of the AO integrals of Eqs. (3.18b) and (3.18c) is both of $\mathcal{O}(N^4)$ complexity. However, due to the exponential decay of the overlap distribution $\Omega_{\mu\nu}(\boldsymbol{r}) = \chi_\mu(\boldsymbol{r})\chi_\nu(\boldsymbol{r})$ with respect to the square of the distance between the centers of the two AOs, the number of significant overlap distributions scales as $\mathcal{O}(N)$. In order to preselect the significant integrals, a rigorous upper bound to the absolute value of two-electron repulsion integrals can be attained by the Cauchy-Schwarz (CS) screening of Häser and Ahlrichs [11],

$$|(\mu\gamma|\delta\nu)| \leq \sqrt{(\mu\gamma|\mu\gamma)}\sqrt{(\delta\nu|\delta\nu)} \tag{3.21}$$

The application of this inequality therefore reduces the scaling from $\mathcal{O}(N^4)$ to $\mathcal{O}(N^2)$. The CS screening does not, however account for the $1/r_{12}$ dependence. This dependence was later

incorporated into the multipole-based integral estimate (MBIE) of Lambrecht and Ochsenfeld [12].

For the Coulomb contribution, the scaling is reduced even further, by splitting the total interaction into a near-field (NF) short-range interaction and a far-field (FF) long-range interaction. The number of NF interactions grows linearly with the size of the system and is intrinsically linear scaling. the FF interactions grow quadratic with the system size, but using the Fast Multipole Method (FMM) [13], which was originally developed for point charges, but generalized to continuous charge distributions in the Continuous Fast Multipole Method (CFMM) [14], the Generalized-very-Fast-Multipole method (GvFMM) [15], and others [16, 17], linear scaling can be obtained.

The exchange matrix is intrinsically linear scaling provided that the density–matrix elements $D_{\gamma\delta}$ decay with distance. This can be seen by noting that the density–matrix elements couple basis functions belonging to different electrons, thus effectively damping the long ranged $1/r_{12}$ interaction. The decay behaviour of the density matrix elements may be illustrated introducing the first–order reduced density matrix

$$\rho(\boldsymbol{r}', \boldsymbol{r}) = \sum_{\gamma\delta} \chi_\gamma(\boldsymbol{r})\chi_\delta(\boldsymbol{r}')D_{\gamma\delta} \Rightarrow K_{\mu\nu}(\mathbf{D}) = \int \chi_\mu^*(\boldsymbol{r}_1)\frac{\rho(\boldsymbol{r}_1, \boldsymbol{r}_2)}{|\boldsymbol{r}_1 - \boldsymbol{r}_2|}\chi_\nu(\boldsymbol{r}_2)d\boldsymbol{r}_1 d\boldsymbol{r}_2. \qquad (3.22)$$

For insulators the first–order reduced density matrix decays exponentially with distance between $\boldsymbol{r}$ and $\boldsymbol{r}'$, for large distances, with the exponent proportional to the band gap of the system. For conductors, which do not have a band gap, the decay rate is only proportional to some power of $1/r_{12}$. For finite systems the situation is more complicated, but systems with small HOMO-LUMO gaps[1] behave similarly to conductors, whereas systems with large HOMO-LUMO gaps behave similarly to insulators.

Combining the CS screening and a reorganization of the integral loop structure, where the density-matrix elements are included in the integral estimates

$$|(\mu\gamma|\delta\nu)D_{\gamma\delta}| \leq \sqrt{(\mu\gamma|\mu\gamma)}\sqrt{(\delta\nu|\delta\nu)}\,|D_{\gamma\delta}|\,, \qquad (3.23)$$

leads to a linear scaling evaluation of the exchange matrix first implemented in the order N exchange (ONX) method [18, 19] and then later in the linear-scaling exchange (LinK) [20], implemented in DALTON [1].

Currently, the time dominating step in each iteration of the wave function optimization is the construction of the exchange matrix, despite the $\mathcal{O}(N)$ scaling, but both the calculation of the Coulomb and exchange matrix can be accelerated by using density-fitting techniques explained in chapter 4.

---

[1]A HOMO-LUMO gap is the energy difference between the highest occupied molecular orbital (HOMO) and lowest unoccupied molecular orbital (LUMO).

## 3.3 Density Functional Theory

In 1964, Hohenberg and Kohn [21] proved the Hohenberg-Kohn theorem, which established that
the exact ground-state electron density

$$\rho(\boldsymbol{r}) = N \int |\Psi(\boldsymbol{x}_1, \boldsymbol{x}_2, \cdots, \boldsymbol{x}_N)|^2 ds_1 d\boldsymbol{x}_2 \ldots d\boldsymbol{x}_N, \tag{3.24}$$

may be uniquely associated with one external potential $v_{\text{ext}}(\boldsymbol{r})$ (up to an additive constant).
It follows from the Hohenberg-Kohn theorem that the potential $v_{\text{ext}}(\boldsymbol{r})$ is a functional of the
electron density, $v_{\text{ext}}[\rho]$, and that the ground state energy $E_0$ is a functional of the electron
density, in the sense that the density uniquely determines the external potential, which in turn
determines the energy $E_0[v_{\text{ext}}]$, i.e.

$$E_0[v_{\text{ext}}] = E_0[v_{\text{ext}}(\rho)] = E_0[\rho]. \tag{3.25}$$

Hohenberg and Kohn further recast the variational principle in terms of the electron density,

$$E_0[v_{\text{ext}}] = \min_{\rho} \left( F[\rho] + \int \rho(\boldsymbol{r}) v_{\text{ext}}[\rho] d\boldsymbol{r} \right), \tag{3.26}$$

where the minimum is constrained to densities that are *v-representable*[1], and $F[\rho]$ is the universal
Hohenberg-Kohn functional, which is independent of the external potential, and defined by

$$F[\rho] = E_0[v_{\text{ext}}[\rho]] - \int \rho(\boldsymbol{r}) v_{\text{ext}}[\rho] d\boldsymbol{r}. \tag{3.27}$$

The ground state electron density therefore contains all the information needed to reconstruct
the external potential, and hence obtain both the wave function, and the ground state energy.
Unfortunately, the form of the universal functional $F[\rho]$ is not known. In 1965, Kohn and Sham
[22] derived the Kohn-Sham (KS) orbital equations, a set of equations for finding the density in
a self consistent fashion

$$\left( \hat{h}_i + \sum_j 2\hat{J}_j + \frac{\partial E_{\text{xc}}}{\partial \rho(\boldsymbol{r})} \right) \phi_i = \sum_j \epsilon_{ij} \phi_j, \tag{3.28}$$

where the density is given by $\rho(\boldsymbol{r}) = \sum_i |\phi_i(\boldsymbol{r})|^2$ and $E_{xc}$ is the unknown exchange-correlation
energy. However, various approximate exchange-correlation functionals have been developed.
The construction of exchange-correlation functionals is a key aspect of DFT, but this topic will
not be discussed in this thesis. Eq. (3.28) is similar to the HF orbital equation of Eq. (3.6) and
one may in a similar manner obtain a matrix equation formulation of the KS orbital equations

$$\mathbf{F}^{\text{KS}}\mathbf{C} = \mathbf{S}\mathbf{C}\boldsymbol{\epsilon}, \tag{3.29}$$

where $\mathbf{F}^{\text{KS}}$ is given by

$$\mathbf{F} = \mathbf{h} + 2\mathbf{J}(\mathbf{D}) + \mathbf{F}^{\text{xc}}(\mathbf{D}), \tag{3.30}$$

---

[1]An electron density is termed *v-representable* if it is associated with the ground state wave function of an
electronic Hamiltonian $\hat{H} = \hat{T} + \hat{V}_{ee} + \sum_i v_{\text{ext}}(\boldsymbol{r}_i)$.

where $\mathbf{F}^{\text{xc}}$ is the exchange-correlation matrix in the AO basis

$$F_{\mu\nu}^{\text{xc}}(\mathbf{D}) = \int \chi_\mu^*(\boldsymbol{r}_1)\chi_\nu(\boldsymbol{r}_2)v_{\text{xc}}(\boldsymbol{r})d\boldsymbol{r} = \int \chi_\mu^*(\boldsymbol{r}_1)\chi_\nu(\boldsymbol{r}_2)\frac{\partial E_{\text{xc}[\rho]}}{\partial \rho(\boldsymbol{r})}d\boldsymbol{r}. \qquad (3.31)$$

Here we have implicitly defined the exchange-correlation potential $v_{\text{xc}}(\boldsymbol{r})$ using

$$\rho(\boldsymbol{r}) = \sum_{\mu\nu} \chi_\mu^*(\boldsymbol{r})\chi_\nu(\boldsymbol{r})D_{\nu\mu}. \qquad (3.32)$$

Eq. (3.29) is very similar to Eq. (3.14) and the algorithm for solving Eq. (3.29) is identical, once the Kohn–Sham matrix of Eq. (3.30) have been built instead of the Fock matrix of Eq. (3.16), and theory developed for HF can therefore almost directly be applied to KS DFT theory as well, and HF and DFT are both denoted Self-Consistent-Field methods.

The most popular DFT functionals are of a local nature, and it should therefore be possible to obtain linear scaling. However, the exchange-correlation matrix is evaluated by numerical integration and the complexity depends both on the number of grid points and basis functions. By using partition functions to decompose the integrals, Pérez-Jordá and Yang [23] presented an $\mathcal{O}(N)$ scheme which is independent of the number of basis functions, and Stratmann *et al.*[24] developed an efficient atomic weight scheme for fast linearly scaling evaluation of the exchange-correlation contribution, and other methods have since been developed [25, 26], and this issue will not be discussed any further in this thesis.

Having established the basic theory and notation we may continue with the theory of density-fitting in the next chapter.

# Chapter 4

# Density Fitting

The evaluation of the molecular integrals of Eqs. (3.20a) and (3.20b) is often one of the time-limiting steps in quantum chemistry. Therefore approximations of these integrals have, in addition to improved integral evaluation schemes, been a concern from the early developments of quantum chemistry. The density-fitting methods (also called resolution–of–the–identity (RI) methods), have today been established as highly successful for approximating the Coulomb contribution (Eq. (3.18b)). The density-fitting approximation is today most often tributed to the 1973 contributions of Whitten [27] and of Baerends, Ellis and Ros [28], and to the developments by Dunlap, Connolly and Sabin [29, 30] in 1979, despite earlier contributions [31–35]. Density-fitting was originally introduced to accelerate the evaluation of the Coulomb matrix, but Weigend *et al.* [36] later extended the methodology to the exact exchange matrix.

In density-fitting the expensive evaluation of four-center integrals is replaced by the evaluation of two- and three-center integrals, and a set of linear equations for the fitting coefficients. Speed-ups in the range 3-30 are commonly observed [37], with errors well within the basis-set errors. Typical errors due to density fitting are about two orders of magnitude smaller than the basis-set errors.

In density fitting the electronic density of Eq. (3.32) is approximated by an expansion in single atom-centered auxiliary basis functions according to

$$\rho(\boldsymbol{r}) \approx \tilde{\rho}(\boldsymbol{r}) = \sum_{\alpha} \xi_{\alpha}(\boldsymbol{r}) c_{\alpha}, \tag{4.1}$$

where the tilde denotes an approximate quantity. The density and the fitted density, differ by an error $\Delta\rho$

$$\rho(\boldsymbol{r}) = \tilde{\rho}(\boldsymbol{r}) + \Delta\rho \tag{4.2}$$

Alternative to Eq. (4.1), individual overlap distributions $\Omega_{\mu\nu}(\boldsymbol{r}) = \chi_{\mu}(\boldsymbol{r})\chi_{\nu}(\boldsymbol{r})$ can be expanded in single auxiliary basis functions

$$\Omega_{\mu\nu} \approx \tilde{\Omega}_{\mu\nu} = \sum_{\alpha} \xi_{\alpha}(\boldsymbol{r}) c_{\alpha}^{\mu\nu}. \tag{4.3}$$

Examining Eq. (4.1) and Eq. (4.3) we obtain the relation

$$c_{\alpha} = \sum_{\mu\nu} D_{\mu\nu} c_{\alpha}^{\mu\nu}. \tag{4.4}$$

Different density fitting methods differ mainly in how the fitting coefficients $c_\alpha$ or $c_\alpha^{\mu\nu}$ are determined, and how the approximated overlap distributions are introduced into the expressions for integrals, the Coulomb matrix, or the Coulomb energy.

## 4.1  Robust and Variational Density Fitting

In this section we describe how a robust and variational fit can be obtained. According to [38] a robust fit is defined as a fitting method which correct the target function to first order in the error made by the fit. Using Eqs. (4.1) and (4.2) the Coulomb energy may be determined:

$$E_J = \frac{1}{2}(\rho|\rho) = \frac{1}{2}(\tilde{\rho}|\tilde{\rho}) + (\tilde{\rho}|\Delta\rho) + \frac{1}{2}(\Delta\rho|\Delta\rho). \tag{4.5}$$

If the fitting coefficients are determined in a manner, which ensures that the second term $(\tilde{\rho}|\Delta\rho)$ vanish, the fit constitutes a robust fit. Neglecting the second order term and finding the stationary points with respect to the fitting coefficients we obtain.

$$\frac{\partial}{\partial c_\alpha}\left(\frac{1}{2}(\tilde{\rho}|\tilde{\rho}) + (\tilde{\rho}|\Delta\rho)\right) = 0 \quad \Rightarrow \quad \sum_\beta (\alpha|\beta)c_\beta = (\alpha|\rho) \quad \Rightarrow \quad (\widetilde{\mu\nu}|\Delta\rho) = 0 \tag{4.6}$$

Which ensures $(\tilde{\rho}|\Delta\rho) = 0$, and thereby a robust fitting procedure if the fitting coefficients are obtained from Eq. (4.6).

It may be more convenient to fit the individual four-center integrals, and Dunlap [38] suggested the approximation

$$(\mu\nu|\gamma\delta) \approx (\widetilde{\mu\nu|\gamma\delta}) = (\mu\nu|\widetilde{\gamma\delta}) + (\widetilde{\mu\nu}|\gamma\delta) - (\widetilde{\mu\nu}|\widetilde{\gamma\delta}), \tag{4.7}$$

where the fitting coefficients $c_\alpha^{\mu\nu}$ are determined from Eq. (4.7) according to

$$\frac{\partial(\widetilde{\mu\nu|\gamma\delta})}{\partial c_\alpha^{\mu\nu}} = 0 \quad \Rightarrow \quad \sum_\beta (\alpha|\beta)c_\beta^{\gamma\delta} = (\alpha|\gamma\delta) \quad \Leftrightarrow \quad (\alpha|\Delta\gamma\delta) = 0 \tag{4.8}$$

which is equivalent to Eq. (4.6) using Eq. (4.4). Eqs. (4.7) and (4.8) constitutes a robust fitting procedure as the expression for the fitted Coulomb energy, is correct to second order in the fitting error

$$\tilde{E}_J \ = \ \frac{1}{2}(\rho|\tilde{\rho}) + \frac{1}{2}(\tilde{\rho}|\rho) - \frac{1}{2}(\tilde{\rho}|\tilde{\rho}) = \frac{1}{2}(\tilde{\rho}|\tilde{\rho}) + (\tilde{\rho}|\Delta\rho) = \frac{1}{2}(\tilde{\rho}|\tilde{\rho}), \tag{4.9}$$

It may also be shown that any function of $(\widetilde{\mu\nu|\gamma\delta})$ including the Coulomb and Exchange energy is variational with respect to the fitting coefficients $c_\alpha^{\mu\nu}$, if the fitting coefficients are determined from Eq. (4.8), i.e.

$$\frac{\partial f((\widetilde{\mu\nu|\gamma\delta}))}{\partial c_\alpha^{\mu\nu}} = \frac{\partial f((\widetilde{\mu\nu|\gamma\delta}))}{\partial(\widetilde{\mu\nu|\gamma\delta})}\frac{\partial(\widetilde{\mu\nu|\gamma\delta})}{\partial c_\alpha^{\mu\nu}} = 0. \tag{4.10}$$

We may therefore obtain a robust and variational fitting method if the approximation in Eq. (4.7) is used and the fitting coefficients are determined from Eq. (4.8). The variational feature ensures a continuous potential energy surface, important for the calculation of molecular properties.

The fitted Coulomb matrix may be obtained by differentiation of the approximate Coulomb energy with respect to the density matrix elements or simply by replacing the four-center integrals of Eq. (3.18b).

$$\tilde{J}_{\mu\nu} = \frac{\partial \tilde{E}_J}{\partial D_{\nu\mu}} = (\mu\nu|\tilde{\rho}) + (\widetilde{\mu\nu}|\rho) - (\widetilde{\mu\nu}|\tilde{\rho}) = (\mu\nu|\tilde{\rho}) + (\widetilde{\mu\nu}|\Delta\rho) = (\mu\nu|\tilde{\rho}) \tag{4.11}$$

The exchange matrix may be obtained in a similar manner

$$
\begin{aligned}
K_{\mu\nu}(\mathbf{D}) &= \sum_{\gamma\delta} (\mu\widetilde{\delta|\gamma}\nu)D_{\delta\gamma} = \sum_{i}^{N_{occ}} \sum_{\gamma\delta} (\mu\widetilde{\delta|\gamma}\nu)C_{\gamma i}C_{\delta i} \\
&= \sum_{i}^{N_{occ}} \sum_{\gamma\delta} \left( \sum_{\alpha}(\mu\delta|\alpha)c_\alpha^{\gamma\nu} + \sum_\alpha c_\alpha^{\mu\delta}(\alpha|\gamma\nu) - \sum_\alpha \sum_\beta c_\alpha^{\mu\delta}c_\beta^{\gamma\nu}(\alpha|\beta) \right)C_{\gamma i}C_{\delta i} \tag{4.12}
\end{aligned}
$$

Using Eq. (4.8) we may obtain the simplified equation

$$K_{\mu\nu}(\mathbf{D}) = \sum_{i}^{N_{occ}} \sum_{\gamma\delta} \left( \sum_{\alpha}(\mu\delta|\alpha)c_\alpha^{\gamma\nu} \right)C_{\gamma i}C_{\delta i}. \tag{4.13}$$

## 4.2   Linear Scaling Robust and Variational Density Fitting

For large molecular systems the fitting procedure in section 4.1 becomes problematic, due to the cubic scaling nature of the fitting equations (Eq. (4.8)).

When approximating the Coulomb matrix, this only becomes a problem for large systems of typically more than 10000 auxiliary basis functions, due to the low prefactor associated with these equations.

For the exchange matrix the different contraction and transformation steps becomes the computational bottleneck due to an $\mathcal{O}(N^4)$ scaling, and the large number of significant auxiliary functions which must be included in the expansion of the overlap distribution.

Within the field of density-fitting two different approaches have been implemented to achieve linear scaling. The first is based on the use of a local metric [28, 39, 40], and the second is based on a spatial partitioning of the electron density [28, 37, 41]. The method presented in paper **C** is based on a local metric and spatial partitioning will therefore not be discussed in this thesis.

Using a local metric, the fitting coefficients can be determined from a sparse set of linear equations, instead of the non-sparse set of linear equations (Eq. (4.8)). Exploiting the sparsity these sparse equations linear scaling can be obtained.

Using a local metric $w(\boldsymbol{r}_1, \boldsymbol{r}_2)$ we may determine the fitting coefficients according to

$$\sum_\beta \langle\alpha|w|\beta\rangle c_\beta^{\gamma\delta} = \langle\alpha|w|\gamma\delta\rangle \Leftrightarrow \langle\alpha|w|\Delta\gamma\delta\rangle = 0, \tag{4.14}$$

with $|\Delta\gamma\delta\rangle = |\gamma\delta\rangle - |\widetilde{\gamma\delta}\rangle$. However, using this equation to determine $c_\beta^{\mu\nu}$ means that the approximation of Eq. (4.7) no longer lead to a robust fit, nor a variational energy expression.

To make the integral in Eq. (4.7) variational in the fitting coefficients, we use Lagrange's method of undetermined multipliers, treating Eq. (4.14) as constraints on the integral. Multiplying these constraints by multipliers $\bar{c}_\alpha^{\mu\nu}$ and adding the resulting expressions to Eq. (4.7) we obtain

$$(\widetilde{\mu\nu|\gamma\delta}) = (\mu\nu|\widetilde{\gamma\delta}) + (\widetilde{\mu\nu}|\gamma\delta) - (\widetilde{\mu\nu}|\widetilde{\gamma\delta}) - \sum_\alpha \bar{c}_\alpha^{\mu\nu} \langle \alpha|w|\Delta\gamma\delta\rangle - \sum_\alpha \bar{c}_\alpha^{\gamma\delta} \langle \Delta\mu\nu|w|\alpha\rangle. \qquad (4.15)$$

Differentiating Eq. (4.15) with respect to the fitting coefficients and setting the result equal to zero, we obtain the following linear equations for the multipliers

$$\sum_\alpha \langle \beta|w|\alpha\rangle \bar{c}_\alpha^{\gamma\delta} = (\beta|\Delta\gamma\delta) \qquad \Rightarrow \qquad \sum_\alpha \langle \beta|w|\alpha\rangle \bar{c}_\alpha = (\beta|\Delta\rho); \qquad \bar{c}_\alpha = \sum_{\mu\nu} D_{\mu\nu} \bar{c}_\alpha^{\mu\nu}. \quad (4.16)$$

For the approximate Coulomb matrix the above approximation gives

$$\tilde{J} = (\mu\nu|\tilde{\rho}) + (\widetilde{\mu\nu}|\Delta\rho), \qquad (4.17)$$

which includes a first-order correction term, making the approximation correct to first order. Note that the second term vanishes in the Coulomb metric (Eq. (4.11)), due to Eq. (4.8).

Linear scaling robust and variational density-fitting can thus be achieved by replacing the cubic-scaling equations for obtaining the fitting coefficients using the Coulomb metric with an additional evaluation of the sparse two– and three–center integrals, and two sets of sparse linear equations, using a sparse metric $w(\boldsymbol{r}_1, \boldsymbol{r}_2)$. The algorithm is outlined in Fig. 4.1

Turning our attention to the exchange contribution, we see that by examining Eq. (4.12) and Eq. (4.14) we notice that similar to the LinK method, all integrals $(\mu\gamma|\delta\nu)$ where the density-matrix elements become sufficiently small can be neglected (see Eq. (3.23)). Therefore, the fitted integrals $(\widetilde{ac|bd})$ of $(ac|bd)$ is only required whenever

$$\sqrt{(ac|ac)}\sqrt{(bd|bd)}\,|D_{cd}| \geq \epsilon, \qquad (4.18)$$

for a given threshold $\epsilon$. The individual contributions in Eq. (4.12) may also be determined in a linear scaling manner, noting that the number of fitting coefficients $c_\alpha^{\mu\gamma}$ scales linearly with system size, as auxiliary basis functions $\xi_\alpha(\mathbf{r})$ sufficiently far away from the product overlaps $\Omega_{\mu\gamma}(\mathbf{r})$ do not contribute to the fitted product overlap $\tilde{\Omega}_{\mu\gamma}(\mathbf{r})$ [39].

The combined effects of locality in the density matrix and locality in the fit imply that the number of contributing three-center integrals $(\mu\gamma|\alpha)$ scales linearly with system size. The same argument holds for the two-center integrals appearing in the last term of Eq. (4.12). The algorithm is outlined in Fig. 4.2

## 4.3   Results

The linear-scaling robust and variational fitting procedure of Section 4.2 was applied to the benchmark set of Peach *et al.* [42]. Both a overlap and a Coulomb metric was examined, and for the Coulomb contribution, the overlap metric gave errors in the energy, which was only around

**Initialization:** *Non-Coulombic metric* $w$

Calculate $\langle\alpha|w|\beta\rangle$ and construct the inverse

**Each iteration:** *Fitted Coulomb matrix* $\tilde{J}_{\mu\nu}$

Calculate $\langle\alpha|w|\rho\rangle = \langle\alpha|w|\gamma\delta\rangle D_{\gamma\delta}$

Construct $c_\alpha = \langle\alpha|w|\beta\rangle^{-1}\langle\beta|w|\rho\rangle$

Calculate intermediate $\tilde{J}^I_{\mu\nu} = \sum_\alpha (\mu\nu|\alpha)c_\alpha = (\mu\nu|\tilde{\rho})$

Calculate $(\alpha|\rho) = \sum_{\gamma\delta}(\alpha|\gamma\delta)D_{\gamma\delta}$

Calculate $(\alpha|\tilde{\rho}) = \sum_\alpha (\alpha|\beta)c_\beta$

Construct $(\alpha|\Delta\rho) = (\alpha|\rho) - (\alpha|\tilde{\rho})$

Construct $\bar{c}_\alpha = \langle\alpha|w|\beta\rangle^{-1}(\beta|\Delta\rho)$

Calculate second intermediate $\tilde{J}^{II}_{\mu\nu} = (\widetilde{\mu\nu}|\Delta\rho) = c^{\mu\nu}_\alpha(\alpha|\Delta\rho) = \sum_\beta c^{\mu\nu}_\alpha\langle\alpha|w|\beta\rangle\bar{c}_\beta$

Finalize fitted Coulomb matrix $\tilde{J}_{\mu\nu} = \tilde{J}^I_{\mu\nu} + \tilde{J}^{II}_{\mu\nu}$

**Figure 4.1:** Outline of the algorithm employed for fitting the Coulomb matrix in a local metric. Note that the word calculate is used when integrals are evaluated. When both the Coulomb and Exchange matrix are calculated it is more convenient to follow a procedure more closely related to the outline for the construction of the exchange matrix in Fig. 4.2

**Initialization** *Non-Coulombic metric* $w$

Construct $G^w_{ab} = \sqrt{\langle ab|w|ab\rangle}$ and $G^w_\alpha = \sqrt{\langle\alpha|w|\alpha\rangle}$

Normalize $\{\xi_\alpha\}$ in metric $w$ (i.e. division with $G^w_\alpha$)

Construct $\langle\alpha|w|\beta\rangle$ and decompose to $\langle\alpha|w|\beta\rangle^{\pm\frac{1}{2}}$

Construct $\langle ab|w|\alpha\rangle \geq G^w_{ab}G^w_\alpha = G^w_{ab}$

Orthogonalize the auxiliary basis according to $c^{ab}_{\alpha'} = \langle ab|w|\alpha'\rangle = \sum_\alpha \langle ab|w|\alpha\rangle\langle\alpha|w|\alpha'\rangle^{-\frac{1}{2}}$

**Each iteration** *Fitted exchange matrix* $\tilde{K}_{ab}$

Construct Cholesky MO's by Cholesky decomposition of density matrix, $D_{ab} = \sum_i^{\text{occ}} L_{ai}L_{bi}$

MO half-transform according to $c^{ai}_{\alpha'} = \sum_b c^{ab}_{\alpha'}L_{bi}$, and $(ai|\alpha') = \sum_b L_{bi}(ab|\alpha')$

Build intermediate $\tilde{K}^I_{ab} = \sum_{i\alpha'}(ai|\alpha')c^{bi}_{\alpha'}$

Build intermediate $\tilde{K}^{II}_{ab} = \tilde{K}^I_{ab} + \sum_{i\alpha'}c^{ai}_{\alpha'}(bi|\alpha')$

Finalize fitted exchange matrix $\tilde{K}_{ab} = \tilde{K}^{II}_{ab} - \sum_{i\alpha'\beta'}c^{ai}_{\alpha'}(\alpha'|\beta')c^{bi}_{\beta'}$

**Figure 4.2:** Outline of the algorithm employed for fitting the exchange matries in a local metrics.

two times larger than when using the regular Coulomb metric; even when using auxiliary basis sets optimized for fitting in the Coulomb metric.

The errors introduced in the linear scaling robust and variational density-fitting method are therefore well within the regular basis-set error, and no significant loss of accuracy occurs when going from the robust and variational density-fitting method of Section 4.1 compared to the linear scaling version presented in Section 4.2.

Application of integral fitting to the calculation of Coulomb and exchange matrices provides a dramatic speedup of calculations. This is evident from Table 4.1 which presents example timings for B3LYP/cc-pVTZ(df-pVTZ) calculation on naphthalene, both with and without density-fitting. In both the Coulomb and exchange matrix cases, the evaluation is accelerated by approximately a factor 30 (when distributing the initialization evenly among the 14 Coulomb and exchange matrix construction) in agreement with what is commonly observed [37].

**Table 4.1:** Timings for a complete B3LYP/cc-pVTZ(df-pVTZ) calculation of the naphthalene molecule. The calculation converged in 14 SCF iterations. The timings were measured using a development version of Dalton [1].

| Method | Initialization [s] | Coulomb [s/iter] | exchange [s/iter] |
|---|---|---|---|
| J-engine + LinK | | 408 | 1394 |
| Coulomb and exchange fitting | 269 | 1.2 | 33.1 |

## 4.4 Conclusion

In this section, we studied the variational density-fitting technique of fitting the four-center two-electron integrals needed for calculation of Coulomb and exchange matrices.

We propose to use a local metric, which yields a sparse linear set of equations for fitting coefficients, allowing for their determination in time proportional to the system size. The method maintains the dramatic speedup commonly observed for density-fitting procedures. We show that a local metric can be chosen so that the accuracy of the calculation does not suffer. In the derivation of the formula, we enforce the variation principle, important for molecular properties.

# Chapter 5

# Coupled Cluster Theory

The HF method focuses on describing an average interaction of an electron with the field generated by all other electrons. The description of the electron-electron interaction is therefore severely limited and neglects the fact that the Coulomb interaction keeps the electrons instantaneously apart and thus that their motion is correlated. The effect of electron correlation must therefore be included to obtain chemical accuracy. The *correlation energy* $E_{\text{corr}}$ is usually defined as the difference between the exact energy $E_{\text{exact}}$ of the $N$-electron system and the HF energy $E_{\text{HF}}$

$$E_{\text{exact}} = E_{\text{HF}} + E_{\text{corr}}. \tag{5.1}$$

A common way to include the effect of electron correlation, is to include several Slater determinants in the wave function expansion. Many such methods have been proposed, among which the most successful is the coupled cluster (CC) method. In this context we introduce the CC correlation energy $E_{CC,corr}$ as

$$E_{\text{CC}} = E_{\text{HF}} + E_{\text{CC,corr}}. \tag{5.2}$$

The basic idea of CC theory is to include all the possible excited Slater determinants of a given reference wave function (e.g. the HF wave function). We define the cluster operator $\hat{T}$ as

$$\hat{T} = \sum_{\mu} t_{\mu} \hat{\tau}_{\mu} \tag{5.3}$$

where $\hat{\tau}_{\mu}$ is a general excitation operator with a corresponding amplitude (expansion coefficient) $t_{\mu}$. The cluster operator can be divided into terms containing a particular order of excitation, i.e. single (excitation of a single electron to an excited state), double (excitation of two electrons), triples and so on. This partitioning may be written as

$$\hat{T} = \hat{T}_1 + \hat{T}_2 + \hat{T}_3 + \hat{T}_4 + \cdots \tag{5.4}$$

19

where $\hat{T}_1$ is an operator performing single excitations etc.

$$\hat{T}_1 = \sum_{ai} t_i^a a_a^\dagger a_i \tag{5.5}$$

$$\hat{T}_2 = \sum_{\substack{a>b \\ i>j}} t_{ij}^{ab} a_a^\dagger a_i a_b^\dagger a_j \tag{5.6}$$

$$\vdots$$

$$\hat{T}_N = \sum_{\substack{a>b>c>\cdots \\ i>j>k>\cdots}} t_{ijk\cdots}^{abc\cdots} a_a^\dagger a_i a_b^\dagger a_j a_c^\dagger a_k \cdots \tag{5.7}$$

where $i, j, k$ refer to occupied indices, and $a, b, c$ refer to unoccupied indices. We have in Eqs. (5.5)-(5.7) used the language of second quantization [43], and we expect the reader to be familiar with this formulation. We refer to $t_i^a$ and $t_{ij}^{ab}$ as single and double cluster amplitudes, respectively.

In terms of the cluster operator, the CC exponential ansatz is given as

$$|\text{CC}\rangle = \exp(\hat{T})|\text{HF}\rangle \tag{5.8}$$

where the Dirac bra-ket notation was introduced and this notation will be used extensively in the next chapters. The exponential operator may be expanded in a Taylor series

$$\exp(\hat{T}) = 1 + \hat{T} + \frac{1}{2}\hat{T}^2 + \frac{1}{6}\hat{T}^3 + \cdots \tag{5.9}$$

Traditionally, the cluster operators of Eq. (5.9) are collected into sets which generate excited states with the same level of excitation, such as singles excitations **S**, doubles **D**, triples **T**, and so on

$$\exp(\hat{T}) = 1 + \underbrace{\hat{T}_1}_{\mathbf{S}} + \underbrace{\left(\hat{T}_2 + \frac{1}{2}\hat{T}_1^2\right)}_{\mathbf{D}} + \underbrace{\left(\hat{T}_3 + \hat{T}_2\hat{T}_1 + \frac{1}{6}\hat{T}_1^3\right)}_{\mathbf{T}} + \cdots \tag{5.10}$$

Inserting the CC wave function ansatz into the Schrödinger equation, we obtain

$$\hat{H}|\text{CC}\rangle = E_{CC}|\text{CC}\rangle \tag{5.11}$$

$$\hat{H}\exp(\hat{T})|\text{HF}\rangle = E_{CC}\exp(\hat{T})|\text{HF}\rangle \tag{5.12}$$

In contrast to the HF method, which is based on the variational principle, the CC method is usually based on projecting the reference wave function $\langle \text{HF}|$ against Eq. (5.11) to obtain the energy

$$E_{CC} = \langle \text{HF}|\hat{H}|\text{CC}\rangle \tag{5.13}$$

and projecting the excited states $\langle \mu|$ combined with an exponential cluster operator against Eq. (5.12) to obtain a set of amplitude equations

$$\langle \mu| \exp(-\hat{T})\hat{H}\exp(\hat{T})|\text{HF}\rangle = 0 \tag{5.14}$$

Since the presented CC equations include all levels of excitations, the obtained wave function therefore includes all possible Slater determinants and is equivalent to the FCI wave function.

The application of these equations is only possible for small molecules, but the cluster operator of Eq. (5.4) can be truncated. The truncations in the cluster operator are carried out by including excitations up to a particular level in Eq. (5.4). The exponential ansatz ensures that all excited state manifolds are included in the description independent on the level of truncation (see Eq. (5.10)). An important and related feature of CC theory is that the CC wave function obtained from a truncated cluster operator is size-extensive [43]. The truncations yields a hierarchy of CC methods denoted CCS[1],CCSD[2] [44],CCSDT[3] [45],.., which offers a systematic way of improving the description of the wave function, until eventually the FCI wave function is obtained. The energy expression for all CC methods (independently of truncation level) may be given explicitly in terms of single and double cluster amplitudes, but no higher order amplitudes.

$$E_{\text{corr}} = \sum_{ijab} \left( t_{ij}^{ab} + t_i^a t_j^b \right) \left( 2g_{iajb} - g_{ibja} \right) , \tag{5.15}$$

The hierarchy of CC methods can be expanded by including approximate methods, which rely on perturbative corrections for higher order of excitations (e.g. MP2[4] [46], CCSD(T)[5] [47], ..., which provide an excellent compromise between accuracy and cost. The full hierarchy of approximate methods of the CC theory are among the most trusted and reliable methods, due to the systematic error control, and the highly accurate results that can be obtained using these methods. CC methods can thus be used as a tool to predict and explain experimental data.

## 5.1   Reduced Scaling Coupled Cluster Method

The CC methods are computationally expensive and their scaling behavior prohibits the application of CC methods in their standard implementation for large molecular systems. During the last decade, much effort have been directed towards developing a formulation of CC theory with a reduced scaling behavior, but until now no formulation has been able to maintain the systematic error control that lead to the predictive power and success of CC theory. The Divide–Expand–Consolidate (DEC) CC method, which is the subject of the next chapter, does provide both linear-scaling and highly systematic error control. Before proceeding to this discussion of the DEC method we first look at some of the reduced-scaling methods

The optimal method should fulfill the requirements for a linear–scaling CC method, paraphrasing Prof. M. Head-Gordon [48]

- **Computational requirements:** The Computation time, required disk space and random access memory should scale at most linearly with increasing the size of the molecular system

---

[1]the coupled–cluster–singles

[2]the coupled–cluster–singles–doubles

[3]the coupled–cluster–singles–doubles-triples

[4]the second–order Møller-Plesset–perturbation–theory. Original a method of its own, it was later shown to be the second order wavefunction according to Coupled-cluster perturbation theory, it is therefore in this thesis considered as a CC method.

[5]the coupled–cluster–singles–doubles with perturbative triples

- **Basis set:** The algorithm should employ a non-redundant basis set. The basis set should not contain any linear dependencies or singularities.

- **Potential energy surface (PES):** A PES should be a smooth function of the nuclear coordinates.

- **Parameters** The theory should not include any ad-hoc parameters and should recover the CC energy. The algorithm should not include any adjustable parameters such as thresholds, cutoff lengths, or selection criteria that affect the result. The algorithm should keep al features of the standard formulation with respect to the input provided by the user, and thus maintain the black-box feature of the CC methods.

- **Size-extensivity** The theory should maintain the size-extensivity property of CC theory

- **Wave function** The algorithm should be general and provide the total energy of the molecular system, the wave function, and molecular properties such as molecular gradient.

Almlöf [49, 50] proposed how reduced scaling may be obtained in MP2 by applying a Laplace transformation to the energy denominator. This idea was implemented by other groups and linear scaling was obtained by Lambrecht *et al.* [51–53] by applying a rigorous multipole based integral estimates [12, 54] to obtain a state-of the-art Laplace-MP2 method, which do fulfill the requirements of a linear scaling method, although no molecular gradients have been presented. A Laplace transform may only be applied to the simplest correlated methods like MP2 [46] and CC2 [55] and another more general strategy must be employed to the hierarchy of CC methods.

During last decades, there has been an extensive amount of research in this area, and the intent in this section, is not to cover all developed methods, but to discuss some general aspects of these methods.

the standard CC calculations are expressed in the canonical HF basis. This is a highly delocalized basis where the individual HF orbitals extend over the whole molecular system. The description of local phenomena using a non–local basis is the reason for the high computational scaling of CC methods. To reduce the computational scaling, it has been attempted to express the CC wave function in a basis of local HF orbitals.

Local occupied orbitals may be obtained using the Least-Change algorithm [56] or by applying a standard localization procedure for the canonical occupied HF orbitals [57–65]. However, for the unoccupied HF orbital space, existing localization strategies have failed to give a set of local orbitals [56, 66]. So far, the only reliable way to obtain a local set of unoccupied MOs is by using the recently developed Least-Change method [56].

In the absence of local unoccupied HF orbitals various solutions have been proposed to bypass the problem of not having a set of local unoccupied HF orbitals, usually by projecting the occupied component out of the AO basis, thereby obtaining a non-redundant non–orthogonal basis.

After the pioneering work of Pulay in 1983 [67], Pulay and Saebø [68] introduced local correlation methods, based on local occupied molecular orbitals. This idea was adopted and

extended by a number of other groups [69–74], and linear scaling implementation was obtained using this methodology [71, 75–77].

A number of alternative reduced scaling coupled-cluster models have also been suggested over the last decades [78–84], e.g. the natural linear scaling approach [80], the cluster-in-molecule approach [81],the divide-and-conquer approach [82],the fragment MO approach [83], and the incremental approach [84].

The goal of all these reduced scaling CC methods have been to capture the major part of electronic correlation by exploiting the locality of electron correlation, meaning that the number of non-negligible amplitudes increases only linearly with the molecular system. The methods are therefore not a reformulation of the CC methods, and will not give the CC energy. Instead the reduced scaling CC methods are formulations where the reduce scaling is obtained through sever approximations and cutoff lengths, which recover around 99% of the CC correlation energy, at impressive computational speeds. If the thresholds and selection criteria were chosen sufficiently conservative the CC energy would be obtained, but this would significantly affect the efficiency and scaling of the models. In the reduced-scaling CC methods the error control in the correlation energy is in general lost. This may be due to a hardwired physical fragmentation of the molecular system. It may also be due to an a priori assignment of local orbital spaces which introduce local domain errors in the correlation energy for example when the completeness criteria of Pulay and Boughton [85] is used to assign fixed excitation spaces to the occupied HF orbitals. None of these methods therefore fulfill all the requirements of a linear-scaling CC model, in contrast to the Divide–Expand–Consolidate CC method presented in chapter 6

# Chapter 6

# The Divide–Expand–Consolidate Coupled Cluster Model

In a standard CC calculation, cluster amplitudes are determined by solving the cluster amplitude equations of Eq (5.14). The error in the calculated CC correlation energy is proportional to the threshold that is used for the residual norm in the cluster amplitude equations. The threshold for the residual norm thus controls the error in the correlation energy, and tightening this threshold gives a more precise correlation energy. The error control in the correlation energy is important as energy derivatives then become well–defined, and one can obtain e.g. nuclear forces that are continuous on a potential energy surface. In the reduced scaling CC Methods of Section 5.1 the error control have been sacrificed for speed and linear scaling.

In this section, a linear-scaling CC method with full error control is presented. The algorithm is denoted the Divide–Expand–Consolidate (DEC) model.

In the DEC model, the CC wave function is expanded in a set of local occupied and unoccupied HF orbitals [56]. In this local basis, a CC calculation on a large molecular system can be expressed in terms of CC calculations on small fragments of the full MO space. The determination of the fragments is black-box in the sense that no user-provided fragmentation of the molecule is necessary; rather, the orbital spaces are carefully selected and expanded to give fragment energies to a preset energy threshold. Adding these fragment energies yields the correlation energy of the full molecular system. Error control in the correlation energy is obtained because the precision of the total correlation energy is determined by the preset energy threshold for the fragment energies.

The algorithm is denoted the Divide–Expand–Consolidate method because the MO space is initially divided among the atomic sites. These orbital spaces are then used to generate atomic fragment orbital spaces, which are in turn expanded and optimized to give consolidated fragment energies, which are converged to a preset energy threshold. The fragment energies add up to the full CC correlation energy with an error in the correlation energy that is proportional to the energy threshold of the fragment energies.

In the following sections it is shown how a CC calculation on a large molecular system can
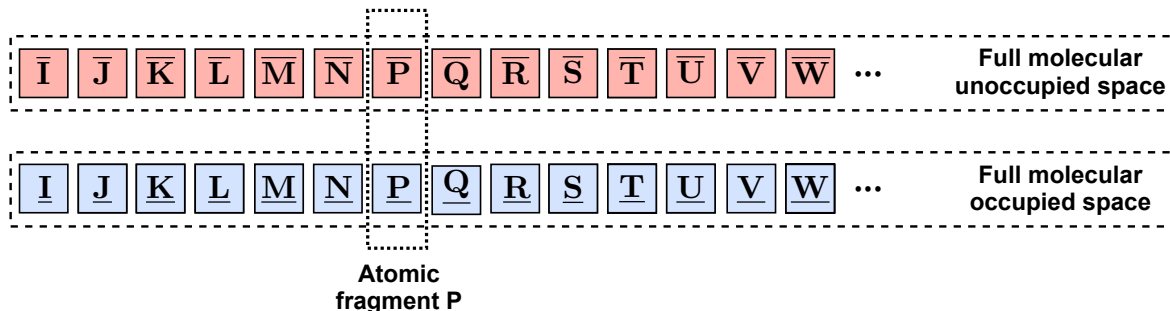
**Figure 6.1:** Molecular system divided into atomic sites I,J, …,P, … where each site has been assigned a set of occupied (light blue) and a set of unoccupied (light red) HF orbitals. Each column of squares represents an atom, the lower and upper square represents the occupied and unoccupied orbitals assigned to that atom

be expressed in terms of CC calculations on small fragments of the full MO space.

In Section 6.1, we examine the correlation energy expression in Eq. (5.15), and then in section 6.2, we discuss the amplitude equations in Eq. (5.14). In Section 6.3 the optimization of excitation spaces is discussed. In section 6.4 linear scaling is discussed, and in Section 6.5 various details about the DEC model are described. Finally an overview of the spaces employed in a DEC calculation is given in Section 6.6, and results are presented in 6.7.

## 6.1 The Coupled Cluster Energy for Local Hartree–Fock Orbitals

In a conventional CC calculation the CC wave function is expanded in the non–local canonical HF orbital basis [56], and therefore all integrals and cluster amplitudes in $E_{\text{corr}}$ (Eq. (5.15)) are non–vanishing. The evaluation of $E_{\text{corr}}$ therefore has a fourth power scaling in system size.

The scaling can be reduced by using a local HF orbital basis. For each local HF orbital $i$, we determine the gross Mulliken charge [61] on all atoms $A$

$$Q_A^i = \sum_{\mu \in A} \sum_{\nu} C_{\mu i} C_{\nu i} S_{\mu \nu},$$

(6.1)

and assign the orbital to the atomic site with the largest Mulliken charge. In this way, each atomic site is assigned a set of local occupied and a set of local unoccupied HF orbitals. The set of occupied HF orbitals assigned to atomic site $P$ is denoted $\underline{P}$ and the set of unoccupied HF orbitals assigned to atomic site $P$ is denoted $\overline{P}$.

A cartoon illustrating how a one–dimensional molecular system is divided into atomic sites and assigned a set of occupied and unoccupied HF orbitals is given in Fig. 6.1.

Having assigned the local HF occupied and unoccupied orbitals to atomic sites, the correlation energy in Eq. (5.15) can be expressed in terms of atomic fragment energies $E_{\text{P}}$ and atomic pair fragment energies $E_{\text{PQ}}$

$$E_{\text{P}} = \sum_{\substack{ij \in \underline{P} \\ ab}} \left( t_{ij}^{ab} + t_i^a t_j^b \right) \left( 2 g_{iajb} - g_{ibja} \right),$$

(6.2)

$$E_{\text{PQ}} = \sum_{\substack{ij \in \underline{P} \cup \underline{Q} \\ ab}} \left( t_{ij}^{ab} + t_i^a t_j^b \right) \left( 2g_{iajb} - g_{ibja} \right) , \tag{6.3}$$

giving

$$E_{\text{corr}} = \sum_{\text{P}} E_{\text{P}} + \sum_{P>Q} \Delta E_{\text{PQ}} , \tag{6.4}$$

where the sums run over atomic sites and where the pair fragment interaction energy $\Delta E_{\text{PQ}}$ is defined as

$$\Delta E_{\text{PQ}} = E_{\text{PQ}} - E_{\text{P}} - E_{\text{Q}} . \tag{6.5}$$

The sum over the two occupied orbital indices in Eq. (5.15) is in Eq. (6.4) replaced by sums over the occupied orbitals of the atomic fragments and atomic pair fragments. Eq. (5.15) is therefore equivalent to Eq. (6.4). Eq. (6.4) may be reminiscent of the Bethe-Goldstone expansion introduced into quantum chemistry by Nesbet [86, 87], and used in the incremental scheme, but neither the theory nor the basic idea is the same a that of the incremental scheme.

The first term in Eq. (6.4) describes the electron-electron interaction while the second term for larger PQ distances describes dispersion effects. In the local HF orbital basis, the integral $g_{iajb}$ is non-vanishing only if the orbital pair indices $ia$ refer to the same atomic site or atomic sites in the neighborhood of each other and similarly for $jb$. Therefore the integral $g_{iajb}$ is non-vanishing only if $i \in \underline{P}$ and $a \in [\overline{P}]$, where $[\overline{P}]$ refers to the unoccupied HF orbital space in the neighborhood of $\overline{P}$ (including $\overline{P}$) and similarly for $jb$. The requirements for a non-vanishing integral may thus be summarized as.

$$g_{iajb} : i \in \underline{P} , \, a \in [\overline{P}] , \, j \in \underline{Q} , \, b \in [\overline{Q}] \qquad \forall P, Q \tag{6.6}$$

When the atomic fragment energy $E_{\text{P}}$ in Eq. (6.2) is calculated, both occupied indices belong to the atomic site $P$. Since the integral $(2g_{iajb} - g_{ibja})$ in $E_{\text{P}}$ is non-vanishing only if $a, b \in [\overline{P}]$, we may restrict the virtual index summation in Eq. (6.2) and evaluate $E_{\text{P}}$ as

$$E_{\text{P}} = \sum_{\substack{ij \in \underline{P} \\ ab \in [\overline{P}]}} \left( t_{ij}^{ab} + t_i^a t_j^b \right) \left( 2g_{iajb} - g_{ibja} \right) , \tag{6.7}$$

where the summation over the unoccupied indices has been restricted to atomic sites which are local to $P$. Similarly, the locality of the integral $(2g_{iajb} - g_{ibja})$ in Eq. (6.3) implies that the atomic pair fragment energy $E_{\text{PQ}}$ may be evaluated as

$$E_{\text{PQ}} = \sum_{\substack{ij \in \underline{P} \cup \underline{Q} \\ ab \in [\overline{P}] \cup [\overline{Q}]}} \left( t_{ij}^{ab} + t_i^a t_j^b \right) \left( 2g_{iajb} - g_{ibja} \right) , \tag{6.8}$$

where the unoccupied index summation has been restricted to the union of unoccupied spaces which are local to $\overline{P}$ and $\overline{Q}$. Note that the orbital space for evaluating $E_{\text{PQ}}$ is the union of orbital spaces for evaluating $E_{\text{P}}$ and $E_{\text{Q}}$.

The atomic fragment energy $E_{\text{P}}$ depends on the singles and doubles amplitudes

$$t_i^a : i \in \underline{P}, \, a \in [\overline{P}] , \tag{6.9a}$$

$$t_{ij}^{ab} : i, j \in \underline{P}, \, a, b \in [\overline{P}] , \tag{6.9b}$$
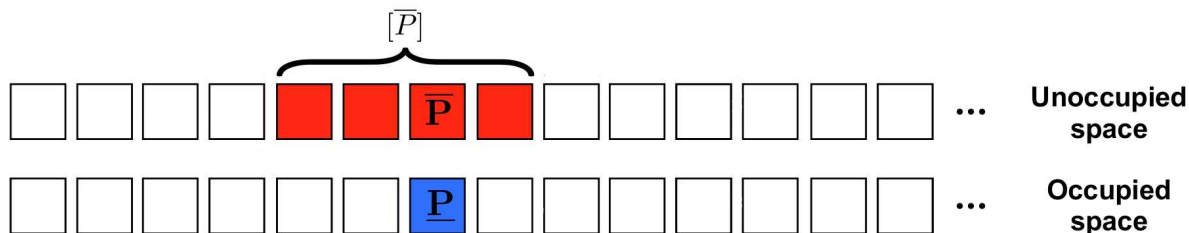
**Figure 6.2:** Molecular fragment $P$. The atomic fragment energy $E_\mathrm{P}$ is evaluated using the effective occupied (dark blue) and unoccupied (dark red) space, denoted energy orbital space (EOS).

The orbital space defined by Eq. (6.9) will be denoted the *atomic fragment energy orbital space* (atomic fragment EOS)

The atomic pair fragment energy $E_\mathrm{PQ}$ depends on the singles and doubles amplitudes

$$t_i^a \, : \, i \in \underline{P} \cup \underline{Q} \, , \, a \in [\overline{P}] \cup [\overline{Q}] \, . \tag{6.10a}$$

$$t_{ij}^{ab} \, : \, i,j \in \underline{P} \cup \underline{Q} \, , \, a,b \in [\overline{P}] \cup [\overline{Q}] \, . \tag{6.10b}$$

and the orbital space defined by Eq. (6.10a) will be denoted the *atomic pair fragment* EOS. $E_P$ and $E_{PQ}$ can be determined by carrying out calculations referencing small fragments of the full MO space. An illustration of the orbital spaces that are in use when the atomic fragment energy $E_\mathrm{P}$ is evaluated is displayed in Fig. 6.2

## 6.2 The Coupled Cluster Amplitude Equations for Local Hartree–Fock Orbitals

Eq. (6.7) and Eq. (6.8) both depend on CC amplitudes and in order to ensure that the amplitudes that determine $E_P$ and $E_{PQ}$ are accurately determined we find that the CC calculation which determines the amplitudes must include buffer regions for the occupied and unoccupied space.

Paper **H** presents a thorough locality analysis of the amplitude equations for MP2 and CCSD models. The purpose of the locality analysis is to show that buffer regions must be included in the amplitude equations to justify that the amplitude equations can be carried out in terms of calculations referencing only small fragments of the full MO space.

In this context we simply summarize the results and refer the reader to paper **H** for more details.

The MP2 amplitude equations must be solved in an iterative fashion due to the non-orthogonality of the local HF orbitals[1]. Using such an iterative algorithm, the MP2 amplitude equations may be solved in the *amplitude orbital space* (AOS)

$$\mathcal{F}_\mathrm{P} = [\underline{P}] + [[\overline{P}]] \qquad \mathcal{F}_\mathrm{PQ} = \mathcal{F}_\mathrm{P} \cup \mathcal{F}_\mathrm{Q} \tag{6.11}$$

---

[1]The non-orthogonality is discussed in section 6.5.1

**Figure 6.3:** Molecular fragment $P$. The correlated wave function calculation is carried out using the amplitude orbital space $\mathcal{F}_P$ (blue and red markings), while the atomic fragment energy $E_P$ is evaluated using the effective occupied (dark blue) and unoccupied (dark red) space.

where $[[\overline{P}]]$ refers to unoccupied orbitals assigned to atoms that are local to $[\overline{P}]$ (including $[\overline{P}]$ itself). The AOS is larger than the EOS in order to include all significant couplings among the amplitudes.

While Eq. (6.11) give a visual picture (see Fig. 6.3 ), the optimal sizes of the fragment orbital spaces are of course not known *a priori*. Instead they are optimized during the calculation to ensure that the atomic fragment and pair fragment energies have converged to a predefined energy threshold. In this way it is ensured that the fragment sizes are sufficiently large to ensure that only truly small terms are neglected.

In Sec. 6.3 we discuss in more detail how the optimization of fragment spaces is carried out in a DEC calculation. Before proceeding to this discussion we first look at the locality analysis for CCSD.

The CCSD locality analysis is more cumbersome than the corresponding analysis for MP2, but from a locality point of view, the CCSD amplitude equations contain three different types of terms discussed in Secs. IVB of Paper **H**. Type 1 and type 3 terms may relatively easy be dealt with, whereas type 2 terms are more troublesome because fragment calculations neglect some small long–range effects present in these terms. However, as discussed in Sec. IVB2 these terms are very small, and the omission of these terms has a negligible effect on the total CCSD energy.

Thus, the analysis substantiates from a theoretical point of view that the fragment calculations may be carried out in orbital spaces of finite size, and that the AOS is the EOS augmented by buffer regions. For future discussions we introduce the notation $\mathcal{B}_{\underline{P}}$ and $\mathcal{B}_{\overline{P}}$ for the occupied and unoccupied buffer region, respectively (see Fig. 6.4)

The CCSD analysis therefore have the same conclusion as the MP2 analysis, that it is indeed possible to carry out a full CCSD calculation in terms of small independent fragment calculations.
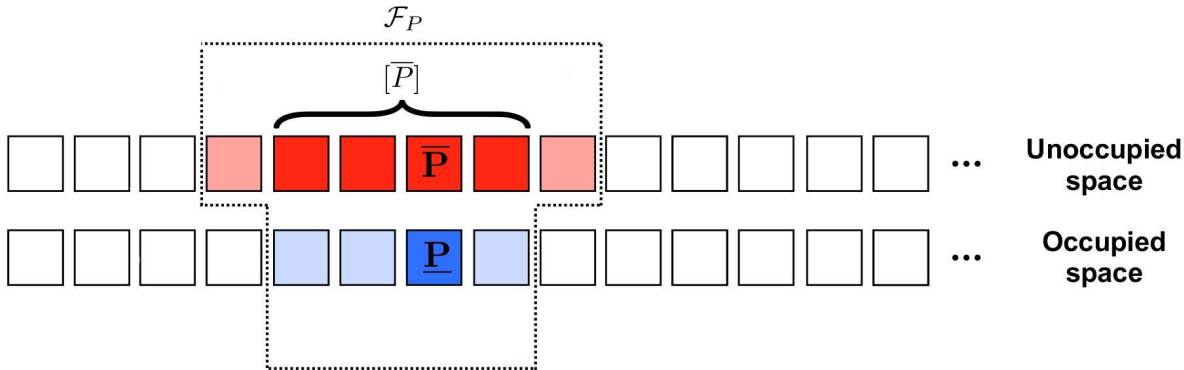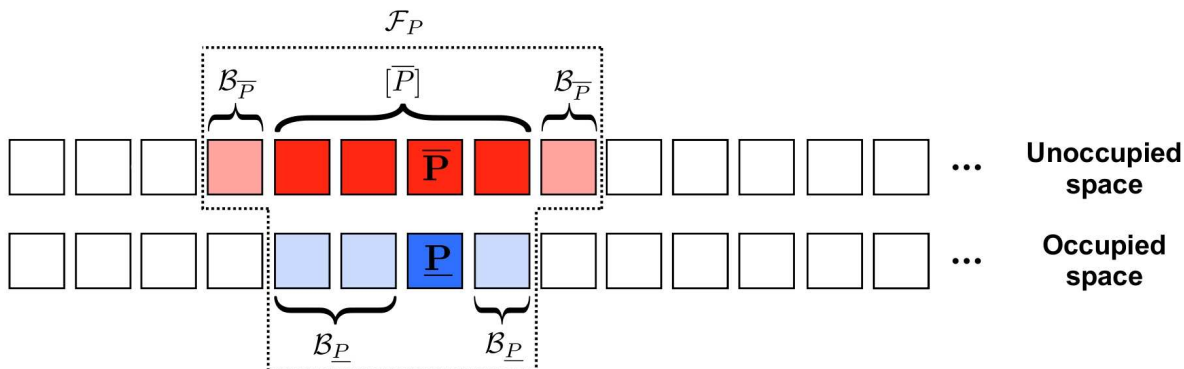
**Figure 6.4:** Molecular fragment $P$. The correlated wave function calculation is carried out using the amplitude orbital space $\mathcal{F}_P$ (blue and red markings), while the atomic fragment energy $E_P$ is evaluated using the effective occupied (dark blue) and unoccupied (dark red) space.

## 6.3   Optimization of Fragment Orbital Spaces

As described above an atomic fragment calculation for fragment $P$ is carried out using the atomic fragment (AOS) $\mathcal{F}_P$ in Fig. 6.3, and the atomic fragment energy is calculated from the amplitudes referencing the EOS (see fig. 6.2 and Eq. (6.9)).

We may now write up the algorithm to determine the optimal orbital space $\mathcal{F}_P$ visualized in Figure 6.5. In Fig. 6.5 A-D we have illustrated how the effective unoccupied space $[\overline{P}]$ (dark red) and the buffer region $\mathcal{B}_{\underline{P}}$ (light blue) and $\mathcal{B}_{\overline{P}}$ (light red) may gradually be increased to ensure that $E_P$ is determined to a given energy tolerance.

**A.** Initially a starting guess is made for the size of the molecular fragment.

- All atoms within an initial radius $\mathbf{R}_{[\overline{P}]}$ from the atomic site $\mathbf{P}$ is included in the effective unoccupied space $[\overline{P}]$.

- All atoms outside $\mathbf{R}_{[\overline{P}]}$ but inside the initial radius $\mathbf{R}_{\mathcal{B}_{\overline{P}}}$ is included in the unoccupied buffer region $\mathcal{B}_{\overline{P}}$.

- All atoms within an initial radius $\mathbf{R}_{\mathcal{B}_{\underline{P}}}$ is included in the occupied buffer region $\mathcal{B}_{\underline{P}}$, except the atom $P$.

The amplitudes are determined using the atomic fragment AOS $\mathcal{F}_P$, and $E_P$ is evaluated using the atomic fragment EOS

**B.** The effective unoccupied space $[\overline{P}]$ is then expanded using a constant step size, to increase $\mathbf{R}_{[\overline{P}]}$, and include atoms, which are spatially close to the current $\overline{P}$. The energy $E_P$ is evaluated using the expanded EOS, until $E_P$ remain unchanged

**C.** The occupied buffer $\mathcal{B}_{\underline{P}}$ is expanded by increasing $\mathbf{R}_{\mathcal{B}_{\underline{P}}}$, the amplitude equations solved, and the energy $E_P$ is evaluated until convergence

**D.** The unoccupied buffer $\mathcal{B}_{\overline{P}}$ is expanded by increasing $\mathbf{R}_{\mathcal{B}_{\overline{P}}}$, the amplitude equations solved, and the energy $E_P$ is evaluated until convergence

The steps in **B**,**C** and **D** are repeated until the size of all spaces remain unchanged.

In Fig. 6.5 E we illustrate how the atomic–pair–fragment EOS and AOS for evaluating $E_{PQ}$ is formed as the union of the atomic–fragment EOS and AOS for evaluating $E_P$ and $E_Q$. The locality analysis in paper **H** substantiate that it is not necessary to carry out additional fragment size optimizations for the combined $PQ$ space as the locality has been defined by the atomic fragment calculations on $P$ and $Q$. The numerical results presented in Sec. 6.7 also support this.

The fragment optimization discussed above applies both to MP2 and CCSD fragment calculations. In a CCSD calculation we may take advantage of the fact that the locality of the CCSD amplitude equations is similar to the one for MP2 equations, except for a more extensive coupling among the amplitudes. Therefore the MP2 fragment spaces serve as good starting guesses for the optimal CCSD fragment spaces. We then systematically increase the size of the CCSD fragments spaces until the CCSD atomic fragment energies are converged to within a given threshold.

The optimization of fragment orbital spaces, is a time-limiting step, and this method can be improved. Work in this direction is ongoing.

## 6.4  Computational Scaling in DEC Coupled Cluster Calculations

In Sec. 6.3 we demonstrate how the sizes of the orbital fragments that are used to evaluate both the atomic fragment energies in Eq. (6.7) and the atomic–pair–fragment energies in Eq. (6.8), may systematically be increased to ensure that the fragment energies are determined to a preset threshold. Since the major task of a CC calculation is to describe short–ranged phenomena in the wave function and dispersion effects, the fragment sizes are to a large extent system independent. The number of atomic fragments scales as the number of atoms in the molecular system and the calculation of atomic fragment energies therefore is linearly scaling.

The number of atomic–pair–fragment energies in Eq. (6.5) has a quadratic scaling with system size but this scaling is reduced to linear for large systems because the pair fragment calculations only need to be carried out for pair–atomic distances where the dispersion forces are non–negligible. A conservative distance cutoff have thus been implemented.

The above scheme is straightforward paralllizable. The evaluation of the atomic fragment energies may first be done independently of each other; second the atomic pair fragment energies that are needed may also be calculated independently of each other. Provided a sufficient number of processors are available the "wall time" for a parallelized correlated wave function calculation therefore is the sum of a single atomic fragment calculation and a single atomic pair fragment energy calculation, not considering the time for the initial Hartree-Fock calculation whose efficient evaluation has been discussed previously and may be done using a linear-scaling
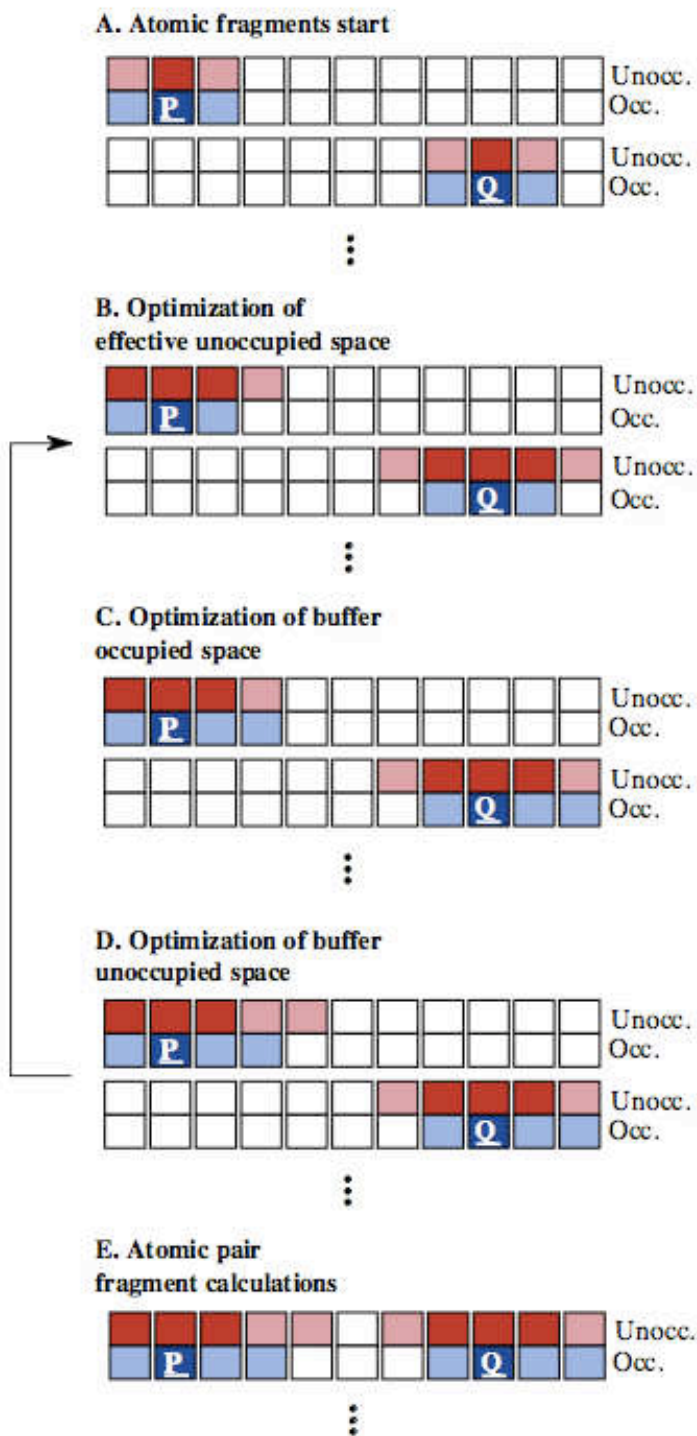
**Figure 6.5:** Main steps in the linear-scaling DEC algorithm. Initially a starting guess is made for the size of the molecular fragment for evaluating $E_P$ and $E_Q$ (A). The effective unoccupied space is then determined (B) followed by an iterative optimization of the occupied and unoccupied buffer spaces (C and D). The steps in B, C and D are thus repeated until the sizes of all spaces remain unchanged. In (E) it is illustrated that the union of $P$ and $Q$ fragments are used for calculating $E_{PQ}$.

algorithm[88].

## 6.5   Details about the DEC Model

In this section we describe various details about the DEC model. In Sec. 6.5.1 we discuss how to improve the locality of the MOs used in a DEC fragment calculation. The fragment calculations are carried out as standard MP2 and CCSD calculations as we detail in Sec. 6.5.2. In Sec. 6.5.3 we discuss how the pair interaction energy $\Delta E_{\mathrm{PQ}}$ may be calculated without introducing counterpoise-like errors.

### 6.5.1   Defining locality of molecular orbitals and atomic fragment extents

For a local occupied HF orbital $\phi_i^P = \sum_\mu \chi_\mu c_{\mu i}^P$ associated with atomic site $P$, we may introduce an approximation $\tilde{\phi}_i^P = \sum_{\tilde{\mu}} \chi_{\tilde{\mu}} \tilde{c}_{\tilde{\mu}i}^P$ by restricting $\tilde{\mu}$ to be a subset of the full set of atomic basis functions, and thereby remove the tail region of the occupied MOs. The expansion coefficients of $\tilde{\phi}_i^P$ may be determined from a least-squares fit

$$f(\tilde{\mathbf{c}}^P) = \langle \tilde{\phi}_i^P - \phi_i^P | \tilde{\phi}_i^P - \phi_i^P \rangle \tag{6.12}$$

giving

$$\tilde{c}_{\tilde{\mu}i}^P = \sum_{\tilde{\nu}\eta} (\mathbf{S}^{-1})_{\tilde{\mu}\tilde{\nu}} S_{\tilde{\nu}\eta} c_{\eta i}^P. \tag{6.13}$$

To identify the extent of $\phi_i^P$, the nonvanishing Mulliken charges are determined for $\phi_i^P$ and arranged in order of decreasing size to prioritize the importance of the atomic sites. We may then restrict $\tilde{\mu}$ to be the AOs centered on the atomic sites which have a Mulliken charge larger than a given threshold, and for this threshold determine the expansion coefficients $\tilde{c}_{\tilde{\mu}i}^P$ from Eq. (6.13). Using $1 - \langle \tilde{\phi}_i^P | \tilde{\phi}_i^P \rangle$ as a measure of the quality of the least-squares fit, we now determine the largest Mulliken charge for which

$$1 - \langle \tilde{\phi}_r^P | \tilde{\phi}_r^P \rangle \leq \delta \tag{6.14}$$

where $\delta$ is a prefixed small positive number. The atomic sites defined by the Mulliken charge threshold determine the extent of orbital $\phi_i^P$ denoted $\{\phi_i^P\}$. The union of extents for the HF orbitals assigned to atomic site $P$ determine the atomic extent $\{P\}$. This case is depicted in Fig. 6.6 for a one–dimensional system.

We note that a screening of atomic centers in accordance with Eq. (6.14), was used by Boughton and Pulay [85] for the occupied HF orbitals as a completeness criteria for the assignment of excitation spaces for the occupied HF orbitals.

When solving the amplitude equations for the atomic fragment calculation we use the MOs of the AOS $\mathcal{F}_{\mathrm{P}}$. The MOs may have expansion coefficients on atomic sites outside the $\mathcal{F}_{\mathrm{P}}$ space. The atomic sites, where atomic integrals have to be evaluated to ensure that the MO integrals in $\mathcal{F}_{\mathrm{P}}$ are properly evaluated, consist of the union of atomic extents for all atoms in $\mathcal{F}_{\mathrm{P}}$. We
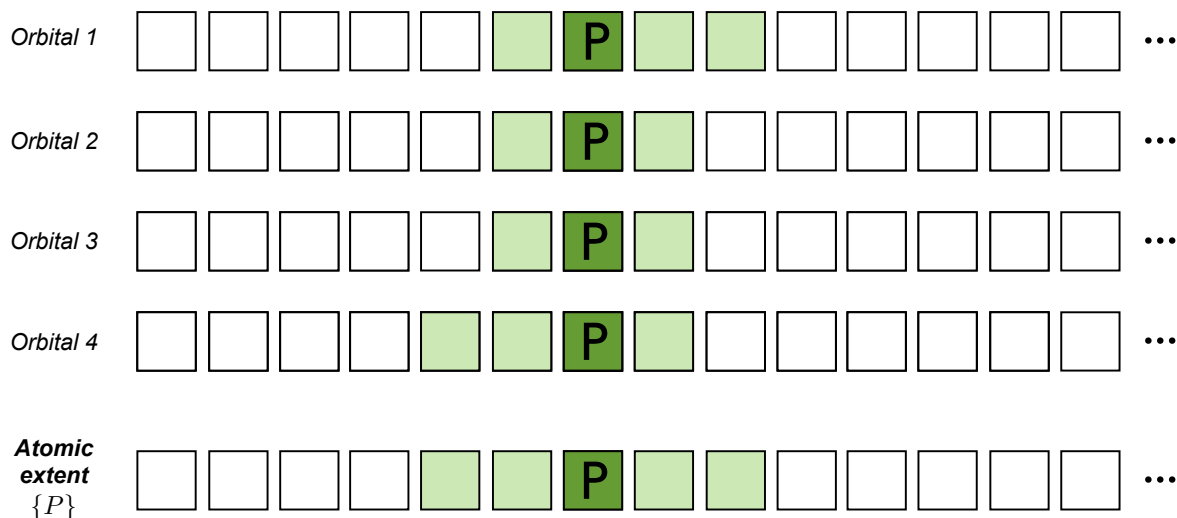
**Figure 6.6:** One-dimensional illustration of the atomic extent for atomic site $P$. Light green squares denote atomic sites where the molecular expansion coefficients are non–vanishing, the orbital extent $\{\phi_i^P\}$. The total atomic extent $\{P\}$ is the union of atomic sites for the individual occupied orbitals. In this example four orbitals have been assigned to $P$ illustrated by the dark green color.

denote this space *the atomic–fragment–extent* $\{\mathcal{F}_P\}$. If for example we consider the case where $\mathcal{F}_P$ contains the atomic sites $L$, $M$, $N$, $P$, $Q$, and $R$, then

$$\{\mathcal{F}_P\} = \{L\} \cup \{M\} \cup \{N\} \cup \{P\} \cup \{Q\} \cup \{R\} \tag{6.15}$$

This case is depicted in Fig. 6.7 for a one–dimensional system.

We have now defined the AOS $\mathcal{F}_P$, where the amplitude calculation is carried out, and the atomic centers in terms of which the MOs are expanded, $\{\mathcal{F}_P\}$. The MOs that are used in an atomic–fragment calculation are then obtained from an expansion of the form,

$$\tilde{\phi}_r^X = \sum_{\tilde{\mu} \in \{\mathcal{F}_P\}} \chi_{\tilde{\mu}} \tilde{c}_{\tilde{\mu}r}^X; \qquad (X \in \mathcal{F}_P) \tag{6.16}$$

The expansion coefficients in Eq. (6.16) may be determined from Eq. (6.13) and gives the best uniform description of the MOs in $\mathcal{F}_P$ confined to the space $\{\mathcal{F}_P\}$.

We further require that the orbitals are normalized

$$\langle \tilde{\phi}_r^X | \tilde{\phi}_r^X \rangle = \sum_{\tilde{\mu}\tilde{\nu}} \tilde{c}_{\tilde{\mu}r}^X S_{\tilde{\mu}\tilde{\nu}} \tilde{c}_{\tilde{\nu}r}^X = 1 \tag{6.17}$$

Using Eq. (6.17) the orbitals are nolonger orthonormal, and the MP2 amplitude equations must be solved in an iterative fashion.

The quality of the least–squares fit, which determine the MOs, depends on the parameter $\delta$ in Eq. (6.14), as $\delta$ was used to determine $\{\mathcal{F}_P\}$. Tightening the threshold $\delta$ will lead to an extension of $\{\mathcal{F}_P\}$ and thus a better least-squares fit.

We have now established the locality of an atomic–fragment calculation in terms of the spaces $\mathcal{F}_P$ and $\{\mathcal{F}_P\}$ and identified the MOs that should be used in the amplitude calculations.
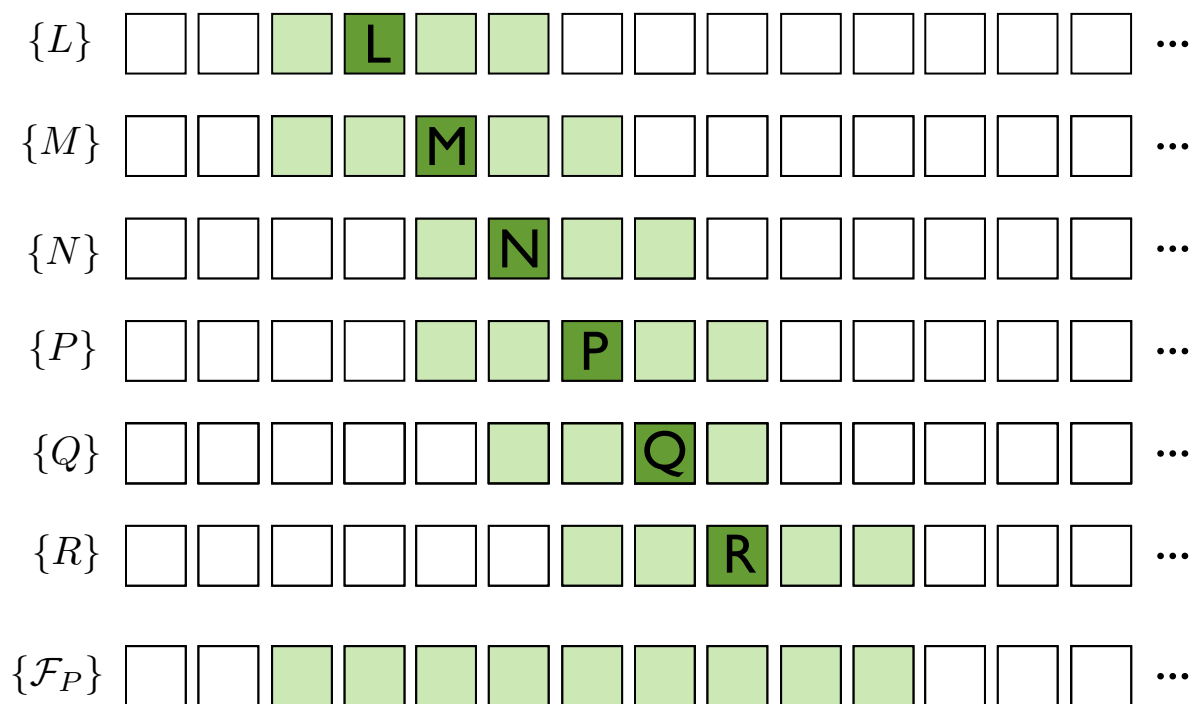
**Figure 6.7:** One-dimensional illustration of the atomic fragment extent $\{\mathcal{F}_P\}$ where the molecular orbitals in the atomic orbital space $\mathcal{F}_P$ are expanded. $\{\mathcal{F}_P\}$ is the union of atomic extents for the atomic sites in $\mathcal{F}_P$. In this example $\mathcal{F}_P$ contains six atoms $L$, $M$, $N$, $P$, $Q$, and $R$. For simplicity we do not consider occupied and virtual spaces separately. Light green squares denote atomic sites where the molecular expansion coefficients are non–vanishing, the orbital extent $\{\phi_i^P\}$, and dark green denote the atomic site where the molecular orbitals are assigned.

For clarity let us now summarize the main steps for fragment $P$:

- Choose a $\delta$ value which is a measure of how much the approximated orbitals $\tilde{\phi}_i$ deviate from the original orbitals $\phi_i$.

- For each atom $L$ in the atomic orbital space $\mathcal{F}_P$ construct the *atomic extent* $\{L\}$ by

  - For each approximated orbital assigned to atom $L$ add atoms based on decreasing Mulliken charge until Eq. (6.14) is satisfied. This newly generated list of atoms constitute the *orbital extent* $\{\phi\}$ for each orbital.

  - construct the *atomic extent* $\{L\}$ as the union of orbital extents for all orbitals assigned to atom $L$. (Fig. 6.6).

- Construct the atomic fragment extent $\{\mathcal{F}_P\}$ as the union of atomic extents for all atoms in the fragment (Fig. 6.7).

- Determine the local MOs using Eq. (6.16), where the MO coefficients are determined from Eq. (6.13). Subsequently the MOs may be normalized according to Eq. (6.17)

### 6.5.2 Coupled Cluster Calculations on Atomic Fragments and Atomic Pair Fragments

The MP2 and CCSD atomic–fragment and atomic–pair–fragment calculations are carried out as standard MP2 and CCSD calculations using the local HF orbitals and the atomic–fragment or atomic–pair–fragment orbital spaces. The MP2 amplitude equations constitute a set of linear equations involving a symmetric matrix and are solved using the conjugate residual with optimal trial vectors (CROP) algorithm where only the last three trial vectors need to be stored to maintain the information of all previous trial vectors (see Ref. [89]). For CCSD a non–linear set of amplitude equations are solved. For CCSD we also use the conjugate residual method in the CROP implementation. For the small non–linearity in the CCSD equations, storing the last three trial vectors is also sufficient to maintain the information content of all the previous trial vectors. In our actual CCSD calculations we store 3–5 trial vectors.

### 6.5.3 Avoiding Counterpoise-like Errors in Pair Energy Calculations

The calculation of pair energies requires special attention because the equations presented in Sec. 6.1 may be subject to counterpoise-like errors. We now demonstrate how this problem may easily be circumvented.

The expression for the atomic pair–fragment interaction energy in Eq. (6.5), $\Delta E_{PQ} = E_{PQ} - E_P - E_Q$, is correct as it stands. However, the amplitudes used for calculating $E_P$, $E_Q$, and $E_{PQ}$ are obtained from fragment calculations in different AOSs, i.e. $\mathcal{F}_P$, $\mathcal{F}_Q$, and $\mathcal{F}_{PQ} = \mathcal{F}_P \cup \mathcal{F}_Q$. The orbital space employed for the $PQ$ atomic–pair–fragment calculations is thus larger than the orbital spaces used for the $P$ and $Q$ atomic–fragment calculations. This means that the
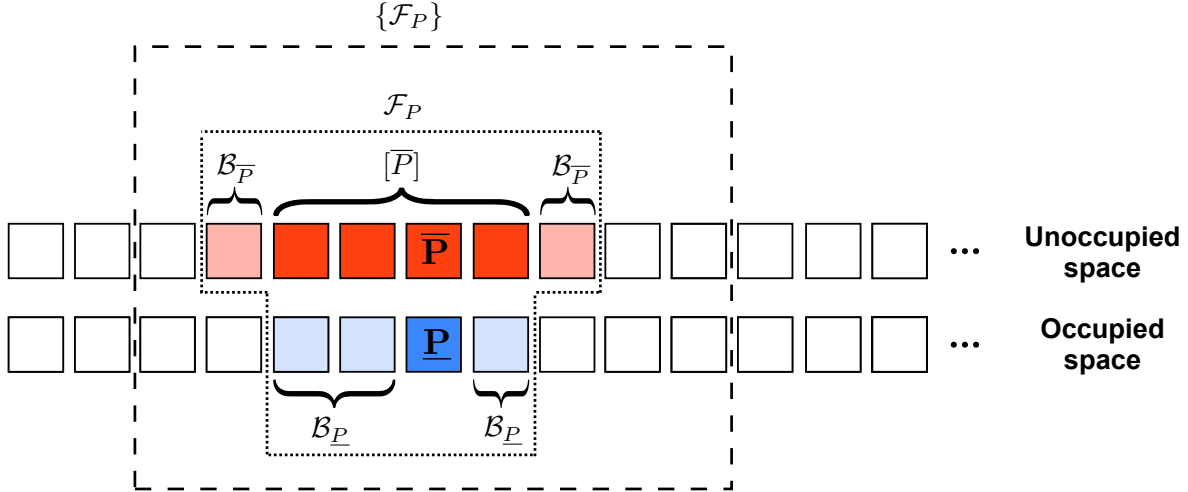
**Figure 6.8:** Molecular fragment $P$. The correlated wave function calculation is carried out using the amplitude orbital space $\mathcal{F}_{\mathrm{P}}$ (blue and red markings), while the atomic fragment energy $E_{\mathrm{P}}$ is evaluated using the effective occupied (dark blue) and unoccupied (dark red) space. The orbitals in the molecular fragment $P$ are confined to the atoms in the atomic fragment extent $\{\mathcal{F}_{\mathrm{P}}\}$. Thus, two-electron integrals in the AO basis need to be calculated for atoms in the $\{\mathcal{F}_{\mathrm{P}}\}$ space.

amplitudes used to determine $E_{\mathrm{PQ}}$ are determined slightly more accurately than the amplitudes used to determine $E_{\mathrm{P}}$ and $E_{\mathrm{Q}}$, and therefore counterpoise-like errors will be introduced when calculating the interaction energy $\Delta E_{\mathrm{PQ}} = E_{\mathrm{PQ}} - E_{\mathrm{P}} - E_{\mathrm{Q}}$.

To avoid such counterpoise problems we may use Eqs. (6.7) and (6.8) to express $\Delta E_{\mathrm{PQ}}$ as,

$$
\begin{aligned}
\Delta E_{\mathrm{PQ}} \;=\; & E_{\mathrm{PQ}} - E_{\mathrm{P}} - E_{\mathrm{Q}} \\
=\; & \sum_{\substack{ij \in \underline{P} \cup \underline{Q} \\ ab \in [\overline{P}] \cup [\overline{Q}]}} \left( t_{ij}^{ab} + t_i^a t_j^b \right) \left( 2g_{iajb} - g_{ibja} \right) \\
& - \sum_{\substack{ij \in \underline{P} \\ ab \in [\overline{P}]}} \left( t_{ij}^{ab} + t_i^a t_j^b \right) \left( 2g_{iajb} - g_{ibja} \right) \\
& - \sum_{\substack{ij \in \underline{Q} \\ ab \in [\overline{Q}]}} \left( t_{ij}^{ab} + t_i^a t_j^b \right) \left( 2g_{iajb} - g_{ibja} \right)
\end{aligned}
\tag{6.18}
$$

and evaluate $\Delta E_{\mathrm{PQ}}$ in Eq. (6.18) using only amplitudes from the pair–fragment calculation. We thereby determine $\Delta E_{\mathrm{PQ}}$ in line with a counterpoise–corrected interaction energy.

## 6.6 Overview of the Spaces Employed in a DEC Calculation

It is now in place to summarize the various spaces employed in the atomic–fragment and atomic–pair–fragment calculations.

In Fig. 6.8 we summarize the various spaces used in an atomic fragment calculation. The amplitude equation is solved for MO indices assigned to atoms in the AOS $\mathcal{F}_{\mathrm{P}}$, and the fragment–energy $E_{\mathrm{P}}$ is calculated using only the EOS, see Eq. (6.7). The spaces in $\mathcal{F}_{\mathrm{P}}$ are optimized during

the calculation as we discussed in Sec. 6.3. The MOs in atomic fragment $P$ have non–vanishing expansion coefficients only for the atomic sites in the $\{\mathcal{F}_P\}$ space. Thus, when solving the amplitude equations in the $\mathcal{F}_P$ space, we need two-electron integrals in the AO basis for atomic sites in the $\{\mathcal{F}_P\}$ space to properly describe the MO integrals which are used in the amplitude equation.

For the atomic pair fragment calculations we employ the union of spaces from the atomic fragment calculations. As an example consider the $PQ$ pair. The amplitude equations are solved using the $\mathcal{F}_P \cup \mathcal{F}_Q$ space, and the atomic pair fragment interaction energy $\Delta E_{PQ}$ is determined as described in Sec. 6.5.3. The MOs are described in terms of atoms in the $\{\mathcal{F}_P\} \cup \{\mathcal{F}_Q\}$ space and two-electron integrals are therefore calculated for the $\{\mathcal{F}_P\} \cup \{\mathcal{F}_Q\}$ space.

## 6.7 Illustrative Results

In this section we present calculations demonstrating that MP2 and CCSD correlation energies for a full molecular system may be determined from DEC fragment calculations with full control of the errors introduced.

The initial results indicate that the maximum atomic fragment size is independent of the size of the molecule. This is closely related to the fact that the maximum orbital spread obtained using the least-change molecular basis (see Ref. [56] for a discussion of orbital spreads) is roughly independent of the size of the molecule. We are therefore able to carry out MP2 calculations on all atomic fragments and atomic pair fragments encountered — irrespectively of the size of the molecule. This implies that the size of the largest molecule that we can treat in a DEC-MP2 calculation is limited only by the initial Hartree—Fock calculation.)

Using the linear $C_{14}H_2$ molecule as a test system we now compare DEC–MP2/cc-pVDZ calculations to full molecular MP2/cc-pVDZ calculations. In subsection 6.7.1 we discuss the errors in the total energies as a function of the *fragment optimization threshold* (FOT). We then analyze the errors of the individual atomic fragment and atomic pair interaction energies in Sec. 6.7.2.

### 6.7.1 Total Energy Errors

Let us consider the single and pair contributions to the total energy errors. In Table 6.7.1 we have listed the sums of the single atomic fragment and atomic pair interaction energy errors compared to a full space calculation for $\delta = 0.01$. We henceforth denote $\sum_P E_P$ as the *total single energy* and $\sum_{P>Q} \Delta E_{PQ}$ as the *total pair interaction energy*. In Table 6.1 it is seen that the total single energy and total pair interaction energy errors systematically decrease when tightening the fragment optimization threshold (FOT). Furthermore, total single and total pair interaction energy errors are of similar magnitude, substantiating that pair fragments may be determined as unions of atomic fragments without carrying out additional fragment optimizations as discussed in Sec. 6.3.

| Threshold | $\Delta(\sum_{\mathrm{P}} E_{\mathrm{P}})$ | $\Delta(\sum_{\mathrm{P>Q}} \Delta E_{\mathrm{PQ}})$ | $\Delta E_{\mathrm{corr}}$ | % of $E_{\mathrm{corr}}$ |
|---|---|---|---|---|
| $10^{-3}$ | 0.006793 | 0.008313 | 0.015106 | 99.1313 |
| $10^{-4}$ | 0.000422 | 0.000250 | 0.000672 | 99.9614 |
| $10^{-5}$ | 0.000136 | 0.000148 | 0.000284 | 99.9837 |
| $10^{-6}$ | 0.000012 | 0.000011 | 0.000022 | 99.9987 |
| $10^{-7}$ | 0.000002 | 0.000001 | 0.000004 | 99.9998 |

**Table 6.1:** Energy errors [a.u.] for single, pair, and total correlation energies using various fragment optimization thresholds compared to a full molecular calculation. The calculations have been carried out on the $C_{14}H_2$ molecule at the MP2 level of theory using a cc-pVDZ basis and $\delta = 0.01$.
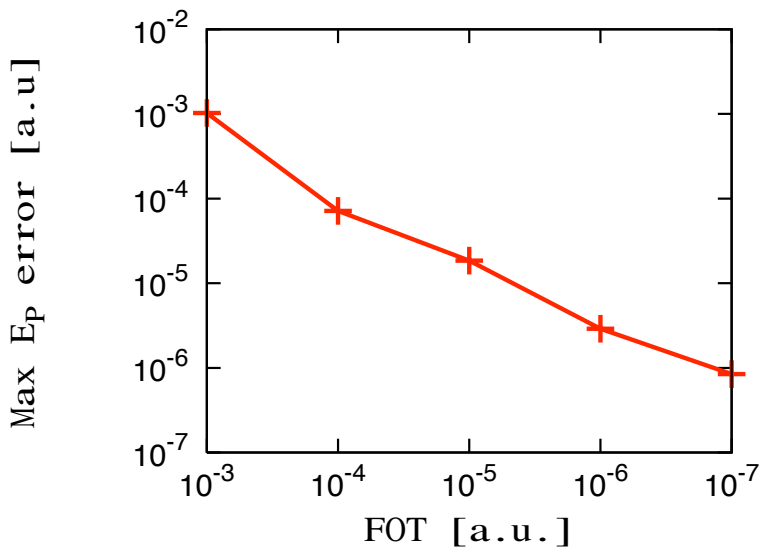


**Figure 6.9:** Maximum errors of atomic fragment energies $\Delta E_P$ as a function of the fragment threshold (FOT). The calculations have been carried out on the $C_{14}H_2$ molecule at the MP2 level of theory using a cc-pVDZ basis and $\delta = 0.01$.

### 6.7.2 Individual Fragment Energy Errors

Having analyzed the total errors we now consider the errors in the individual atomic fragment and atomic pair interaction energies.

In Fig. 6.9 we have plotted the maximum errors in the individual atomic fragment energies $E_{\mathrm{P}}$. It is seen that the maximum atomic fragment energy error decreases uniformly when tightening the threshold. We do note that for the lowest FOTs ($10^{-6}$ and $10^{-7}$) the maximum atomic fragment energy errors are slightly larger than the FOTs. This is an artifact of the simple fragment optimization procedure in Fig. 6.5 where we only allow one single orbital space to expand in each step. We are currently working on solving this problem.

In Fig. 6.10 we have plotted the absolute pair interaction energies obtained in a full DEC calculation (red-solid curve) as a function of the pair distance along with the maximum absolute
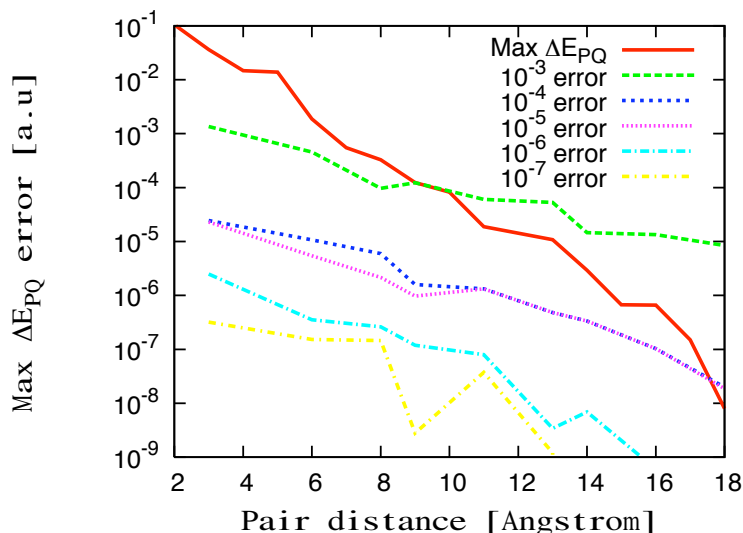
**Figure 6.10:** Maximum atomic pair interaction energies $\text{Max}\Delta E_{\text{PQ}}$ and maximum errors of atomic pair interaction energies $\Delta E_{\text{PQ}}$ as a function of the distance between pairs $R_{\text{PQ}}$ for various atomic fragment optimization thresholds. **Red solid curve**: Maximum atomic pair interaction energies from full space DEC calculation. **Other curves**: Maximum *errors* in atomic pair interaction energies for the fragment optimization thresholds indicated in the figure. The calculations have been carried out on the $C_{14}H_2$ molecule at the MP2 level of theory using a cc-pVDZ basis and $\delta = 0.01$.

pair interaction energy errors for various fragment calculations. From the red-solid curve we see that the pair interaction energies decrease rapidly as a function of distance. This supports the discussion in Sec. 6.4, where it was stated that the pair fragment calculations do not need to be carried out for large pair distances where dispersion forces are negligible. In Fig. 6.10 we also see that in general the maximum pair interaction energy error systematically decreases by tightening the threshold. We note that for the molecule under consideration the errors for $\text{FOT} = 10^{-4}$ is coincidentally lower than expected. Finally, the maximum pair interaction energy errors in Fig. 6.10 are comparable in magnitude to the maximum atomic fragment energy errors in Fig. 6.9. This is in line with the conclusion that pair fragments may be formed simply as unions of atomic fragments.

## 6.8 Conclusion and Comparison with Reduced Scaling Coupled Cluster Methods

We have presented an algorithm for a linear scaling CC calculations, which fulfills all requirements of a linear scaling CC model presented in section 5.1

Calculations in the presented algorithm are made on a linear scaling number of atomic fragments and pairs of atomic fragments. The main effort is shifted towards optimization of atomic fragments for selection of optimal excitation and correlation spaces. The optimization

is necessary to recover the full correlation energy, and ensure a continuous potential energy surface. The scaling for the atomic and atomic pair fragments is similar to the standard CC model, but the calculations for each fragment may be done independently and the model is therefore straightforward parallizable.

The presented algorithm is general and may be applied to the full hierarchy of CC methods, including the perturbative methods like MP2 and CCSD(T). The algorithm provides both the CC correlation energy, the wave function in terms of the CC amplitudes, and molecular properties may be evaluated using this method. An implementation of the MP2 and CCSD molecular gradient is in progress.

The DEC algorithm requires no ad-hoc parameters and maintains the black-box property of the CC hierarchy.

The DEC algorithm, relies on a local occupied and unoccupied HF orbital basis. This basis is a non-redundant basis set, but at the moment the Least-Change algorithm [56] have a high scaling ($\mathcal{O}(N^5)$), which is a bottleneck of the current implementation.

None of the local CC methods of section 5.1, fulfill all requirements of a linear scaling CC algorithm, in contrast to DEC. However, the most distinguishing feature of DEC is probably the optimization of atomic fragments for selection of optimal excitation and correlation space, which is lacking in the local CC methods of section 5.1. The fixed excitation space prohibit the local CC methods from recover the full CC correlation energy, and the important error control is lost in favour of speed and linear scaling.

# Chapter 7

# Response Theory

## 7.1  Introduction

In the previous chapters, the focus has been on obtaining efficient linear–scaling methods for solving the time-independent Schrödinger equation. The resulting wave function can be used to calculate simple expectation values such as the permanent dipole moment. However, once a molecular system is subjected to an external perturbation like for instance a time–dependent electric field, the solution to the time-independent Schrödinger equation is no longer valid and we must solve the time–dependent Schrödinger equation. Assuming that the external perturbation is small, we can expect the unperturbed and perturbed wave functions to be very similar, and we may use the original unperturbed time-independent solution as a starting point, for obtaining the time-dependent solutions. This approach is called *response theory* but is actually just time-dependent perturbation theory in the frequency domain, applied to molecular systems within an approximate quantum chemistry wave function model. The goal of standard response theory is to obtain the perturbed property (e.g. the induced dipole moment), and not the wave function itself nor the actual time–development of the system. Response theory therefore describes how an observable responds when a molecular system is subjected to an external field.

## 7.2  Exact Response Theory

Imagine a system described by a wave function $|0\rangle$, which fulfills the time–independent Schrödinger equation $H_0|0\rangle = E_0|0\rangle$. Now imagine that the system is perturbed by a first-order time-dependent perturbation $\hat{V}(t)$

$$\hat{V}(t) = \int_{-\infty}^{\infty} V(\omega)e^{-i\omega t+\epsilon t}d\omega = \int_{-\infty}^{\infty} \hat{V}^{\omega}e^{-i\omega t+\epsilon t}d\omega \qquad (7.1)$$

where $\epsilon$ is a positive infinitely small number such that the perturbation vanishes at $t = -\infty$. For $t > -\infty$, the fields are gradually applied, until $t = 0$. This gradual change in the external conditions characterizes an adiabatic process and ensures that the system remains in the initially populated state at all times. In response to the perturbation, the wave function changes ($|0\rangle \rightarrow |\tilde{0}\rangle$) and so do the molecular properties.

43

As mentioned, response theory describes how the expectation value $\langle 0|\hat{A}|0\rangle$ of an operator $\hat{A}$ is affected by the time-dependent perturbation. An exponential parametrization is used to describe the perturbed time-dependent wave function $|\tilde{0}\rangle$ [90],

$$|\tilde{0}\rangle = e^{i\hat{X}(t)}|0\rangle \tag{7.2}$$

where $\hat{X}(t)$ is a Hermitian operator describing how the molecular system changes due to the perturbation (see Ref. [90] ).

$$\hat{X}(t) = \sum_{p<0} x_p(t)\hat{R}_p + \sum_{p>0} x_p(t)\hat{R}_p \tag{7.3}$$

Since $\hat{X}(t)$ is a Hermitian operator, the time-dependent response parameters for positive and negative indices are related as

$$\hat{R}_p = \begin{cases} |p\rangle\langle 0|, & p > 0 \\ |0\rangle\langle p|, & p < 0 \end{cases} \qquad x_p(t) = \begin{cases} x_p(t), & p > 0 \\ x^*_{-p}(t), & p < 0 \end{cases} \tag{7.4}$$

where $|p\rangle$ denotes an excited state $p$ which fulfills the time–independent Schrödinger equation

$$H_0|p\rangle = E_p|p\rangle \tag{7.5}$$

and which is orthogonal to all other excited states

$$\langle p|n\rangle = \delta_{pn} \tag{7.6}$$

### 7.2.1 The Time Evolution of an Expectation Value

The Hermitian operator $\hat{X}(t)$ may be expanded in orders of the external perturbation

$$\hat{X}(t) = \hat{X}^{(1)}(t) + \hat{X}^{(2)}(t) + \cdots \tag{7.7}$$

To second order in the external perturbation, we obtain the expansion

$$\begin{aligned} \langle \tilde{0}|\hat{A}|\tilde{0}\rangle &= \langle 0|\hat{A}|0\rangle - \mathrm{i}\langle 0|[\hat{X}^{(1)}(t), \hat{A}]|0\rangle \\ &- \tfrac{1}{2}\langle 0|[\hat{X}^{(1)}(t), [\hat{X}^{(1)}(t), \hat{A}]]|0\rangle - \mathrm{i}\langle 0|[\hat{X}^{(2)}(t), \hat{A}]|0\rangle. \end{aligned} \tag{7.8}$$

The first term is the expectation value in absence of a perturbation. The second term determines the first order correction due to the applied field, while the remaining terms represent second order corrections.

Since the external perturbation is usually a homogenous periodic electric or magnetic field defined by a single frequency component, it is convenient to operate in the frequency domain rather than the time domain. The wave-function corrections are therefore introduced in the frequency domain. By analogy to Eq. (7.1)

$$\hat{X}^{(1)}(t) = \int_{-\infty}^{\infty} \hat{X}^{(1)}(\omega)e^{-i\omega t + \epsilon t}\mathrm{d}\omega \tag{7.9a}$$

$$\hat{X}^{(2)}(t) = \iint_{-\infty}^{\infty} \hat{X}^{(2)}(\omega_1, \omega_2)e^{-i(\omega_1+\omega_2)t+2\epsilon t}\mathrm{d}\omega_1\mathrm{d}\omega_2 \tag{7.9b}$$

where we require the second-order corrections to be symmetric in the frequencies: $\hat{X}^{(2)}(\omega_1, \omega_2) = \hat{X}^{(2)}(\omega_2, \omega_1)$. Inserting the frequency expansions of the wave-function corrections of Eq. (7.9) into Eq. (7.8), we obtain

$$
\begin{aligned}
\langle\tilde{0}|\hat{A}|\tilde{0}\rangle = \langle 0|\hat{A}|0\rangle &- \mathrm{i}\int_{-\infty}^{\infty}\langle 0|[\hat{X}^{(1)}(\omega), \hat{A}]|0\rangle e^{-i\omega t + \epsilon t}\mathrm{d}\omega \\
&- \frac{1}{2}\iint_{-\infty}^{\infty}\langle 0|[\hat{X}^{(1)}(\omega_1), [\hat{X}^{(1)}(\omega_2), \hat{A}]]|0\rangle e^{-i(\omega_1+\omega_2)t+2\epsilon t}\mathrm{d}\omega_1\mathrm{d}\omega_2 \\
&- \frac{1}{2}\iint_{-\infty}^{\infty}\langle 0|[\hat{X}^{(1)}(\omega_2), [\hat{X}^{(1)}(\omega_1), \hat{A}]]|0\rangle e^{-i(\omega_1+\omega_2)t+2\epsilon t}\mathrm{d}\omega_1\mathrm{d}\omega_2 \\
&- \mathrm{i}\iint_{-\infty}^{\infty}\langle 0|[\hat{X}^{(2)}(\omega_1, \omega_2), \hat{A}]|0\rangle e^{-i(\omega_1+\omega_2)t+2\epsilon t}\mathrm{d}\omega_1\mathrm{d}\omega_2
\end{aligned}
\tag{7.10}
$$

We now Introduce the linear and quadratic response functions.

$$
\langle\langle A; V^{\omega}\rangle\rangle_{\omega} = -\mathrm{i}\langle 0|[\hat{X}^{(1)}(\omega), \hat{A}]|0\rangle \tag{7.11a}
$$

$$
\begin{aligned}
\langle\langle A; V^{\omega_1}, V^{\omega_2}\rangle\rangle_{\omega_1,\omega_2} = &-\frac{1}{2}\langle 0|[\hat{X}^{(1)}(\omega_1), [\hat{X}^{(1)}(\omega_2), \hat{A}]]|0\rangle \\
&- \frac{1}{2}\langle 0|[\hat{X}^{(1)}(\omega_2), [\hat{X}^{(1)}(\omega_1), \hat{A}]]|0\rangle - 2\mathrm{i}\langle 0|[\hat{X}^{(2)}(\omega_1, \omega_2), \hat{A}]|0\rangle
\end{aligned}
\tag{7.11b}
$$

Eq. (7.10) may then be written as

$$
\begin{aligned}
\langle\tilde{0}|\hat{A}|\tilde{0}\rangle = \langle 0|\hat{A}|0\rangle &+ \int_{-\infty}^{\infty}\langle\langle A; V^{\omega}\rangle\rangle_{\omega} e^{-i\omega t + \epsilon t}\mathrm{d}\omega \\
&+ \frac{1}{2}\iint_{-\infty}^{\infty}\langle\langle A; V^{\omega_1}, V^{\omega_2}\rangle\rangle_{\omega_1,\omega_2} e^{-i(\omega_1+\omega_2)t+2\epsilon t}\mathrm{d}\omega_1\mathrm{d}\omega_2
\end{aligned}
\tag{7.12}
$$

With the definitions of Eq. (7.11a) and Eq. (7.11b), the linear response function represents the first-order correction to the expectation value due to the applied field, while the quadratic response function represents the second-order correction.

### 7.2.2 Time Evolution according to Ehrenfest's Theorem

Once the response parameters $x_p(t)$ of Eq. (7.4) are determined, it is possible to determine the response functions. The main task of response theory is therefore to determine the response parameters $x_p(t)$. The time evolution of $|\tilde{0}\rangle$ in the presence of the time-dependent perturbation may be determined using Ehrenfest's theorem [91] Using the operator of Eq. (7.4).

$$
\mathrm{i}\frac{\mathrm{d}}{\mathrm{d}t}\langle\tilde{0}|\hat{R}_p|\tilde{0}\rangle = \mathrm{i}\langle\tilde{0}|(\frac{\partial\hat{R}_p}{\partial t}|\tilde{0}\rangle + \langle\tilde{0}|[\hat{R}_p, \hat{H}_0 + \hat{V}(t)]|\tilde{0}\rangle
\tag{7.13}
$$

Since $\hat{R}_p$ is time-independent, Eq. (7.13) reduces to

$$
\mathrm{i}\frac{\mathrm{d}}{\mathrm{d}t}\langle\tilde{0}|\hat{R}_p|\tilde{0}\rangle = \langle\tilde{0}|[\hat{R}_p, \hat{H}_0 + \hat{V}(t)]|\tilde{0}\rangle
\tag{7.14}
$$

Using the Ehrenfest theorem results in a set of nonlinear equations which define the time-dependence of $\hat{X}(t)$. These equations are solved order by order to determine the parameters $\hat{X}^{(i)}(\omega)$. Inserting Eqs. (7.2) and (7.7) into Eq. (7.14), expanding in orders of the external

perturbation, and collecting the terms linear in the perturbation, the first-order time-dependent equations are obtained

$$\langle 0|[X^{(1)}, [\hat{R}_p, \hat{H}_0]]|0\rangle + i\langle 0|[\hat{R}_p, \hat{V}(t)]|0\rangle - i\langle 0|[\dot{X}^{(1)}, \hat{R}_p]|0\rangle = 0 \tag{7.15}$$

To solve this time-dependent equation, the frequency expansions of the wave function corrections of Eq. (7.9) and of the external perturbations Eq. (7.1) are used.

$$\int_{-\infty}^{\infty} \left( \langle 0|[X^{(1)}(\omega), [\hat{R}_p, \hat{H}_0]]|0\rangle + i\langle 0|[\hat{R}_p, \hat{V}^\omega]|0\rangle - \omega\langle 0|[X^{(1)}(\omega), \hat{R}_p]|0\rangle \right) e^{-i\omega t + \epsilon t}\mathrm{d}\omega = 0 \tag{7.16}$$

Extracting the integrand, which must also be zero and rearranging using (7.3) we obtain

$$\sum_{q\neq 0} \left( \langle 0|[[\hat{R}_p, \hat{H}_0], \hat{R}_q]|0\rangle - \omega\langle 0|[\hat{R}_p, \hat{R}_q]|0\rangle \right) x_q = -i\langle 0|[\hat{V}^\omega, \hat{R}_p]|0\rangle. \tag{7.17}$$

The perturbation $\hat{V}^\omega$ is usually called $B$ in order to clearly distinguish between the different perturbing components of the external potential. Defining the generalized Hessian and metric matrices $\boldsymbol{E}^{[2]}$ and $\boldsymbol{S}^{[2]}$, and the gradient vector $\boldsymbol{g}^b$ by

$$E_{pq}^{[2]} = \langle 0|[[\hat{R}_p, \hat{H}_0], \hat{R}_q]|0\rangle \tag{7.18}$$

$$S_{pq}^{[2]} = \langle 0|[\hat{R}_p, \hat{R}_q]|0\rangle \tag{7.19}$$

$$g_p^b = \langle 0|[\hat{R}_p, \hat{B}]|0\rangle \tag{7.20}$$

the first-order response equation may be written as

$$(\boldsymbol{E}^{[2]} - \omega_b \boldsymbol{S}^{[2]})\boldsymbol{x}^b = i\boldsymbol{g}^b \tag{7.21}$$

Inserting the explicit expression for $R_p$ in Eq. (7.4) into Eqs. (7.18) and (7.19), and using Eqs. (7.5) and (7.6), $\boldsymbol{E}^{[2]}$ and $\boldsymbol{S}^{[2]}$ may be written in the diagonal forms,

$$\boldsymbol{E}^{[2]} = \begin{pmatrix} \boldsymbol{\omega}_k & \mathbf{0} \\ \mathbf{0} & \boldsymbol{\omega}_k^* \end{pmatrix} \qquad \boldsymbol{S}^{[2]} = \begin{pmatrix} \mathbf{1} & \mathbf{0} \\ \mathbf{0} & -\mathbf{1} \end{pmatrix} \tag{7.22}$$

where $\boldsymbol{\omega}_k$ is a diagonal matrix containing the excitation energies. For reasons which will become evident in section 7.3, we have retained the complex conjugation in the lower right block of $\boldsymbol{E}^{[2]}$, but in standard response theory, the excitation energies are real ($\boldsymbol{\omega}_k^* = \boldsymbol{\omega}_k$). Using the diagonal structure of the matrices in Eq. (7.22), we may write the first-order standard response equation in Eq. (7.21) as

$$\begin{pmatrix} ^1\boldsymbol{x}^b \\ ^2\boldsymbol{x}^b \end{pmatrix} = i \begin{pmatrix} (\boldsymbol{\omega}_k - \boldsymbol{\omega}_b)^{-1} & \mathbf{0} \\ \mathbf{0} & (\boldsymbol{\omega}_k^* + \boldsymbol{\omega}_b)^{-1} \end{pmatrix} \begin{pmatrix} ^1\boldsymbol{g}^b \\ ^2\boldsymbol{g}^b \end{pmatrix} \tag{7.23}$$

where $\boldsymbol{\omega}_b$ is a diagonal matrix with the frequency $\omega_b$ in all diagonal elements. We have divided $\boldsymbol{x}^b$ and $\boldsymbol{g}^b$ into two sub-vectors to emphasize that the upper and the lower part of $\boldsymbol{x}^b$ are decoupled due to the diagonal structure of $\boldsymbol{E}^{[2]}$ and $\boldsymbol{S}^{[2]}$. Note that $^1\boldsymbol{x}^b$ and $^2\boldsymbol{x}^b$ refer to positive and

negative indices, respectively, contrary to the right-hand side vector where $^1\boldsymbol{g}^b$ and $^2\boldsymbol{g}^b$ refer to negative and positive indices, respectively,

$$
\begin{pmatrix} ^1x^b_k \\ ^2x^b_{-k} \end{pmatrix} = i \begin{pmatrix} (\omega_k - \omega_b)^{-1} & 0 \\ 0 & (\omega_k^* + \omega_b)^{-1} \end{pmatrix} \begin{pmatrix} B^{k0} \\ -B^{0k} \end{pmatrix}
\tag{7.24}
$$

where we have used Eq. (7.20) and introduced the short-hand notation,

$$
B^{k0} = \langle k|\hat{B}|0\rangle; \qquad B^{0k} = \langle 0|\hat{B}|k\rangle
\tag{7.25}
$$

Inserting Eq. (7.24) into Eq. (7.11a), we obtain a sum-over-states (SOS) expression for the linear response function

$$
\langle\langle A; B\rangle\rangle_\omega = \sum_{p\neq 0}\left( -\frac{A^{0p}B^{p0}}{\omega_p - \omega_b} - \frac{V^{0p}A^{p0}}{\omega_p^* + \omega_b} \right) = \sum_{p\neq 0}\left( \frac{A^{0p}B^{p0}}{\omega_b - \omega_p} + \frac{V^{0p}A^{p0}}{\omega_b + \omega_p^*} \right)
\tag{7.26}
$$

The linear response function determine the first order correction to the expectation value, and the residue of the linear response function give information about the dipole transition matrix element between the reference state $|0\rangle$ and excited state $|n\rangle$

$$
\lim_{\omega_b\to\omega_n} (\omega_b - \omega_n)\langle\langle A; B\rangle\rangle_\omega = A^{0n}B^{n0},
\tag{7.27}
$$

from which the oscillator strength may be determined.

Likewise, the quadratic response equation determining the second order wave function-corrections may be determined from (7.14) by collecting terms which are second-order in the external perturbation, and the same may be done for higher order response equations.

For future discussions, we note that the quadratic response function may be shown to be

$$
\begin{aligned}
\langle\langle A; B, C\rangle\rangle_{\omega_b, \omega_c} = &\sum_{p\neq 0}\sum_{q\neq 0} \frac{B^{0p}\tilde{A}^{pq}C^{q0}}{(\omega_p + \omega_b)(\omega_q - \omega_c)} + \frac{C^{0q}\tilde{A}^{qp}B^{p0}}{(\omega_p - \omega_b)(\omega_q + \omega_c)} \\
&+ \sum_{p\neq 0}\sum_{q\neq 0} \frac{A^{0p}\tilde{B}^{pq}C^{q0}}{(\omega_p + \omega_a)(\omega_q - \omega_c)} + \frac{C^{0q}\tilde{B}^{qp}A^{p0}}{(\omega_p - \omega_a)(\omega_q + \omega_c)} \\
&+ \sum_{p\neq 0}\sum_{q\neq 0} \frac{A^{0p}\tilde{C}^{pq}B^{q0}}{(\omega_p + \omega_a)(\omega_q - \omega_b)} + \frac{B^{0q}\tilde{C}^{qp}A^{p0}}{(\omega_p - \omega_a)(\omega_q + \omega_b)},
\end{aligned}
\tag{7.28}
$$

and that in paper **D** it is shown that all response equations have the same form

$$
(\boldsymbol{E}^{[2]} - \omega_{b\dots f}\boldsymbol{S}^{[2]})\boldsymbol{x}^{b\dots f} = i\boldsymbol{g}^{b\dots f}
\tag{7.29}
$$

here shown for the $f$'th order response equation, where the right-hand side vector $\mathbf{g}^{b\dots f}$ only contains response parameters of orders $f-1$ and below.

## 7.3   Damped Response Theory

The response functions derived in Section 7.2 have singularities when one or more of the optical frequencies coincides with an excitation energy $(\omega_b = \omega_p)$(see (7.26)). This leads to an unphysical behavior for molecular properties in the resonance region, such as divergence of dispersion

curves and absorption spectra with infinitely narrow absorption peaks, i.e. stick spectra. This unphysical behavior is due to the fact that the excited states have infinite lifetimes when the standard response functions are derived in Section 7.2.

### 7.3.1   Phenomenological Damping of Excited States

Consider a molecular system described by the Hamiltonian $H_0$, characterized by Eqs. (7.5) and (7.6). The time-dependent excited state $|n(t)\rangle$, which is obtained by multiplying $|n\rangle$ by an exponential phase factor,

$$|n(t)\rangle = e^{-iE_n t}|n\rangle \tag{7.30}$$

trivially satisfies the time-dependent Schrödinger equation,

$$i\frac{\partial |n(t)\rangle}{\partial t} = H_0|n(t)\rangle = E_n|n(t)\rangle \tag{7.31}$$

The norm of $|n(t)\rangle$ is constant in time, $\langle n(t)|n(t)\rangle = \langle n|n\rangle = 1$, so no decay occurs from the excited state to the ground state (or other excited states). In other words, the lifetime of the excited state $|n(t)\rangle$ is infinite.

In reality, an excited state has a finite lifetime which is not readily described by the Hamiltonian $H_0$. However, we may introduce a phenomenological description of the lifetime by multiplying Eq. (7.30) by an exponential damping factor $e^{-\frac{1}{2}\Gamma_n t}$ to obtain the damped excited state $|\bar{n}(t)\rangle$ [92, 93]

$$|\bar{n}(t)\rangle = e^{-\frac{1}{2}\Gamma_n t}|n(t)\rangle = e^{-i(E_n - \frac{i}{2}\Gamma_n)t}|n\rangle \tag{7.32}$$

The norm of the damped excited state $|\bar{n}(t)\rangle$ decays exponentially in time

$$\langle \bar{n}(t)|\bar{n}(t)\rangle = e^{-\Gamma_n t} \tag{7.33}$$

and $\Gamma_n^{-1}$ may therefore be interpreted as the lifetime of the excited state $|\bar{n}(t)\rangle$, i.e. the time it takes before the population of the excited state has decreased by a factor of $e^{-1}$.

The non-damped state $|n(t)\rangle$ in Eq. (7.31) has a real energy $E_n$. By contrast, the damped excited state $|\bar{n}(t)\rangle$ does not possess a well-defined real energy due to its finite lifetime,

$$i\frac{\partial |\bar{n}(t)\rangle}{\partial t} = (E_n - \tfrac{i}{2}\Gamma_n)|\bar{n}(t)\rangle \tag{7.34}$$

By comparing Eqs. (7.30) and (7.32) we see that the damping of the excited states is effectively obtained by introducing complex excitation energies $\bar{E}_n$

$$E_n \to \bar{E}_n = E_n - i\gamma_n; \qquad \gamma_n = \tfrac{1}{2}\Gamma_n \tag{7.35}$$

for all excited states $|n(t)\rangle$.

In standard response theory of Section 7.2, transitions between the ground and excited states are described in terms of oscillator strengths which are obtained from residues of response functions. This gives rise to a delta-peaked residue spectrum (absorption spectrum). In an experimental absorption spectrum, the peaks are broadened and the oscillator strength is obtained

by integration over the absorption band representing the electronic transition. The broadening of the electronic absorption bands may be associated with contributions arising from different physical phenomena:

- The isolated, non-moving molecule possesses a finite lifetime due to spontaneous emission which gives rise to an energy uncertainty manifested in a broadening of the absorption bands.

- The vibrational substructure of electronic absorption spectra leads to a broadening of the absorption bands.

- In an experiment, the molecules are moving relative to the detector which leads to Doppler broadening.

- Collisions among molecules perturb the electron densities and hence the excited state energies, leading to a broadening of the absorption bands.

For a rigorous treatment of molecular properties which reproduces the correct physical behavior at resonance frequencies, the finite lifetime of an excited molecular system has to be taken into account, and the Hamiltonian $H_0$ must be modified accordingly.

This is not readily done using a standard quantum chemical description, and finite lifetimes have therefore been introduced using a phenomenological description. An effective lifetime is introduced to account for the above physical phenomena [92–96] by multiplying the excited states by a damping factor [92, 93].

In practice it is virtually impossible, to assign individual lifetimes to each excited state encompassing all the above phenomena, and therefore the same common empirical *effective lifetime parameter* $\Gamma^{-1} = (2\gamma)^{-1}$ has previously been used for all excited states [94, 96]. In that case Eq. (7.35) simplifies to

$$E_n \rightarrow \bar{E}_n = E_n - i\gamma. \tag{7.36}$$

In response theory, the excited state energy $E_n$ always enters in combination with the ground state energy $E_0$ as the excitation energy $\omega_n = E_n - E_0$, and Eq. (7.36) then corresponds to making the replacement,

$$\omega_n \rightarrow \bar{\omega}_n = \omega_n - i\gamma. \tag{7.37}$$

since the lifetime of the ground state is infinite and consequently $\Gamma_0 = 0$. The introduction of finite lifetimes is therefore equivalent to introducing complex excitation energies.

When complex excitation energies are introduced and the domain of the response functions thereby is extended to the complex plane, the singularities of the response functions at resonance frequencies are removed. For real perturbation operators, dispersion processes are then described by the real part of the response functions, whereas absorption spectra (residues of standard response functions) are obtained from the imaginary part of the response functions. When real excitation energies have been replaced by complex excitation energies, the result is called *damped response theory*.

Molecular absorption properties in damped response theory will have an imposed Lorentzian lineshape function. The lineshape function associated with pure Doppler broadening is Gaussian, whereas the lineshape function describing pure collision broadening is Lorentzian (see e.g. Ref. [97]). The true experimental lineshape function is more complicated, as it encompasses all the phenomena discussed above, but the structure of an absorption spectrum obtained using damped response theory will be qualitatively correct.

Excitation energies and transition strengths are in standard response theory determined by solving a generalized eigenvalue problem (See Eqs. (7.21) and (7.29)). Using this approach, the lowest excitations may easily be addressed, and for small molecules this is in most cases sufficient to obtain the desired absorption spectrum. However, for large molecules where the density of low lying excited states may be very high, it may in practice be difficult to determine an absorption spectrum using standard response theory.

Damped response theory may be used to determine absorption spectra for *any* frequency range. Damped response theory therefore becomes a very useful tool for calculating molecular absorption spectra at arbitrary frequencies, also for large molecules.

The absorption spectra determined using damped response theory are identical to those obtained using standard response theory, when Lorentzian lineshape functions are superimposed onto the stick spectra of standard response theory. For this reason, we consider damped response theory to be an empirical tool for determining absorption spectra in arbitrary frequency regions, where standard response theory is not applicable in practice. This relates not only to simple one-photon absorption spectra, but also to e.g. Magnetic Circular Dichroism spectra, discussed in chapter 9 and other absorption properties, which may be determined from residues of standard response functions.

Throughout this chapter, a bar denotes a quantity in damped response theory, whereas the bar is omitted for the corresponding quantity in standard (non-damped) response theory.

We now show that to any order in the perturbation, the replacement in Eq. (7.37) may effectively be carried out by solving a set of damped response equations for complex frequencies.

### 7.3.2   Application of Damped Response Theory

We now consider the application of damped response function theory. We start out by identifying excitation energies in the standard response function expressions. Let us first consider the response parameters, which are obtained by solving response equations of the form in Eq. (7.21). All response parameters contain excitation energies due to the form of $\mathbf{E}^{[2]}$ in Eq. (7.22). In damped response theory, we thus have to carry out the replacement in Eq. (7.37) in $\mathbf{E}^{[2]}$ to obtain the damped generalized Hessian $\bar{\mathbf{E}}^{[2]}$,

$$\mathbf{E}^{[2]} \to \bar{\mathbf{E}}^{[2]} = \begin{pmatrix} \bar{\omega}_k & \mathbf{0} \\ \mathbf{0} & \bar{\omega}_k^{\star} \end{pmatrix} = \begin{pmatrix} \omega_k - i\gamma & \mathbf{0} \\ \mathbf{0} & \omega_k + i\gamma \end{pmatrix} = \mathbf{E}^{[2]} - i\gamma\mathbf{S}^{[2]} \qquad (7.38)$$

where we have used Eq. (7.22), and where $\gamma$ is a diagonal matrix containing the damping parameters.

Since all response equations have the same form (see Eq. (7.29)), all singularities may be removed by replacing $(\mathbf{E}^{[2]} - \omega_{b...f}\mathbf{S}^{[2]})$ in the $f$'th order response equation in Eq. (7.29) according to Eq. (7.38),

$$\mathbf{E}^{[2]} - \omega_{b...f}\mathbf{S}^{[2]} \rightarrow \mathbf{E}^{[2]} - (\omega_{b...f} + i\gamma)\mathbf{S}^{[2]} \tag{7.39}$$

In the following, we consider the structure of the damped response equations in detail.

### 7.3.3 Analysis of Damped Response Equations

Let us first consider the first-order damped response equation, which is obtained by carrying out the replacement in Eq. (7.39) in the standard first order equation in Eq. (7.21),

$$\left[\mathbf{E}^{[2]} - (\omega_b + i\gamma)\mathbf{S}^{[2]}\right]\bar{\mathbf{x}}^b = i\mathbf{g}^b \tag{7.40}$$

or written out explicitly,

$$\begin{pmatrix} {}^{1}\bar{\mathbf{x}}^b \\ {}^{2}\bar{\mathbf{x}}^b \end{pmatrix} = i \begin{pmatrix} (\boldsymbol{\omega}_k - \boldsymbol{\omega}_b - i\boldsymbol{\gamma})^{-1} & \mathbf{0} \\ \mathbf{0} & (\boldsymbol{\omega}_k + \boldsymbol{\omega}_b + i\boldsymbol{\gamma})^{-1} \end{pmatrix} \begin{pmatrix} {}^{1}\mathbf{g}^b \\ {}^{2}\mathbf{g}^b \end{pmatrix} \tag{7.41}$$

where $\bar{\mathbf{x}}^b$ is a complex damped response vector,

$$\bar{\mathbf{x}}^b = \bar{\mathbf{x}}^b_R + i\bar{\mathbf{x}}^b_I \tag{7.42}$$

The first–order right–hand–side vector $\mathbf{g}^b$ is not barred because it is identical to the right–hand–side vector in the standard theory of Eq. (7.20) since it does not depend on the excitation energies. The damped response vector $\bar{\mathbf{x}}^b$ is complex in contrast to standard theory, where (for real wave functions) the response vector $\mathbf{x}^b$ is either purely real (e.g. when the perturbing operator $B$ is an electric dipole operator) or purely imaginary (e.g. when $B$ is a magnetic dipole operator).

The elements of the $[\mathbf{E}^{[2]} - (\omega_b + i\gamma)\mathbf{S}^{[2]}]^{-1}$ matrix may be written in terms of their real and imaginary parts

$$[\mathbf{E}^{[2]} - (\omega_b + i\gamma)\mathbf{S}^{[2]}]^{-1} = \begin{pmatrix} \frac{\omega_k - \omega_b}{(\omega_k - \omega_b)^2 + \gamma^2} & 0 \\ 0 & \frac{\omega_k + \omega_b}{(\omega_k + \omega_b)^2 + \gamma^2} \end{pmatrix} + i \begin{pmatrix} \frac{\gamma}{(\omega_k - \omega_b)^2 + \gamma^2} & 0 \\ 0 & -\frac{\gamma}{(\omega_k + \omega_b)^2 + \gamma^2} \end{pmatrix} \tag{7.43}$$

and similarly for the right-hand side vector $\mathbf{g}^b = \mathbf{g}^b_R + i\mathbf{g}^b_I$. We now introduce the dispersion $\mathcal{D}$ and the absorption $\mathcal{A}$ lineshape functions as,

$$\mathcal{D}_k(\omega) = \frac{\omega_k - \omega}{(\omega_k - \omega)^2 + \gamma^2}; \qquad \mathcal{D}_k(-\omega) = \frac{\omega_k + \omega}{(\omega_k + \omega)^2 + \gamma^2} \tag{7.44a}$$

$$\mathcal{A}_k(\omega) = \frac{\gamma}{(\omega_k - \omega)^2 + \gamma^2}; \qquad \mathcal{A}_k(-\omega) = \frac{\gamma}{(\omega_k + \omega)^2 + \gamma^2} \tag{7.44b}$$

We use the index convention that $\omega_k = \omega_{-k}$ and thus $\mathcal{D}_k = \mathcal{D}_{-k}$ and $\mathcal{A}_k = \mathcal{A}_{-k}$. $\mathcal{D}_k(\omega)$ and $\mathcal{D}_k(-\omega)$ are antisymmetric and are zero at $\omega = \omega_k$ and $\omega = -\omega_k$, respectively, whereas the
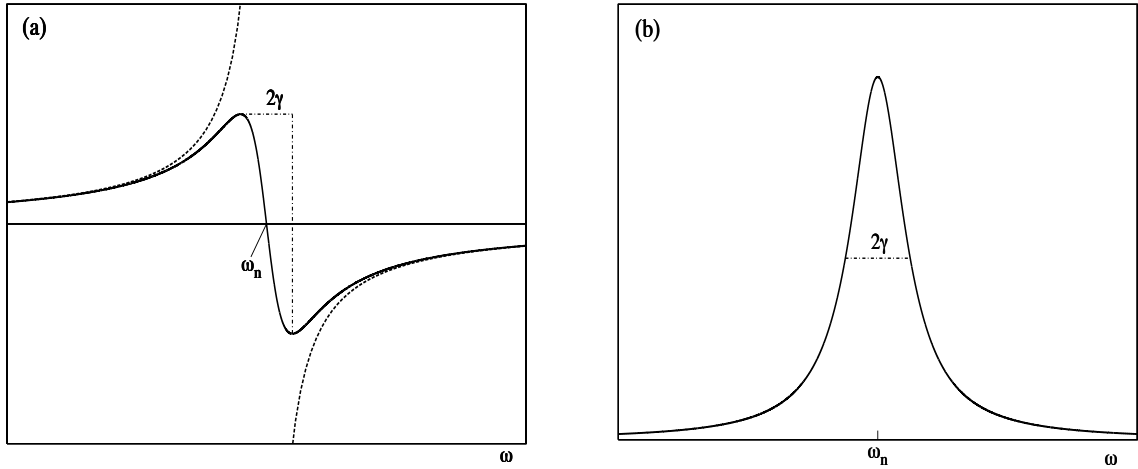
(a) $\mathcal{D}_n(\omega) = \frac{\omega_n - \omega}{(\omega_n - \omega)^2 + \gamma^2}$        (b) $\mathcal{A}_n(\omega) = \frac{\gamma}{(\omega_n - \omega)^2 + \gamma^2}$

**Figure 7.1:** Lineshape functions in damped response theory: **Left**: The solid line depicts the dispersion lineshape function $\mathcal{D}_n(\omega)$ for $\gamma \neq 0$, while the dashed line depicts $\mathcal{D}_n(\omega)$ for $\gamma = 0$, where a pole is obtained at $\omega = \omega_n$. Note that the two functions approach each other when $\omega$ is far-off-resonance **Right**: The absorption lineshape function $\mathcal{A}_n(\omega)$, where the full width at half maximum equals the inverse lifetime $\Gamma = 2\gamma$.

Lorentzian functions $\mathcal{A}_k(\omega)$ and $\mathcal{A}_k(-\omega)$ are symmetric and reach their maximum values at $\omega = \omega_k$ and $\omega = -\omega_k$, respectively. $\mathcal{D}_n(\omega)$ and $\mathcal{A}_n(\omega)$ are plotted in Fig. 7.1.

For real wave functions, $\mathbf{g}^b$ will be either purely real or purely imaginary as discussed above. Assuming that the right–hand–side vector is real $\mathbf{g}^b = \mathbf{g}_R^b$, the structure of damped response vector can be investigated at different frequencies. The analysis in paper **D** may be summarized as follows. Assuming that the excited states are all non-degenerate and that the spacing between adjacent excitation energies is considerably larger than the inverted effective lifetime, i.e. $\gamma <<$ $|\omega_{n+1} - \omega_n|$, we consider two cases:

- The resonant case, where the optical frequency is close to an excitation energy, $\omega_b \approx \omega_n$ (assuming $\gamma << \omega_b$.). The real part of the damped response function is associated with a dispersion lineshape function and the imaginary part is associated with an absorption lineshape function

$$\langle\langle \overline{A; B} \rangle\rangle_{\omega_b}^R \quad \approx \quad \mathcal{D}_n(\omega_b) A^{0n} B^{n0} \qquad (\omega_b \approx \omega_n) \tag{7.45}$$

$$\langle\langle \overline{A; B} \rangle\rangle_{\omega_b}^I \quad \approx \quad -\mathcal{A}_n(\omega_b) A^{0n} B^{n0} \qquad (\omega_b \approx \omega_n) \tag{7.46}$$

- The far-off-resonance case, where $\omega_b$ is not close to any excitation energy. In this case, the imaginary part vanishes, and the real part becomes approximately identical to the standard response function.

$$\langle\langle \overline{A; B} \rangle\rangle_{\omega_b}^R \approx \langle\langle A; B \rangle\rangle_{\omega_b} \qquad \langle\langle \overline{A; B} \rangle\rangle_{\omega_b}^I \approx 0 \tag{7.47}$$

If A and B are components of the electric dipole operator $\mu_\alpha$, then $\langle\langle\mu_\alpha;\mu_\beta\rangle\rangle_{\omega_b}$ describes a component of the polarizability

$$\alpha_{\alpha\beta} \;\;=\;\; -\langle\langle\mu_\alpha;\mu_\beta\rangle\rangle_\omega \qquad\qquad (7.48)$$

and $\mu_\alpha^{0n}\mu_\beta^{n0}$ describes a component of the dipole transition strength matrix for the $|0\rangle \rightarrow |n\rangle$ transition. $\langle\langle\overline{A;B}\rangle\rangle_{\omega_b}^I$ thus represents a residue spectrum with a peak broadening of $\Gamma = 2\gamma$ at full width half maximum. In the limit $\gamma \rightarrow 0$, $\langle\langle\overline{A;B}\rangle\rangle_{\omega_b}^I$ represents a delta-peaked residue spectrum. Thus, we explicitly see that the phenomenologically introduced damping factor $\gamma$ does indeed represent a broadening of absorption spectra, and it is therefore appropriate to interpret $\Gamma^{-1}$ as a common effective lifetime for the excited states.

The replacement in Eq. (7.39) may be applied to higher–order response equations (see Eq. (7.29)), and since damped response equations to all orders have the same form, our formulation is well–suited for the determination of damped response functions to arbitrary orders in exact as well as approximate theories.

In standard response theory, the computational effort for determining molecular properties from response functions and their residues may be minimized by applying rules for eliminating higher-order response parameters from the response function expressions, e.g. Wigner's $2n + 1$ rule [98] or alternative elimination rules described in Ref. [99]. In paper **D** we use the quasienergy formulation of response theory [100, 101] and the response parameter elimination rules of Ref. [99] to obtain simple expressions for standard response functions in terms of standard response parameters. The standard response parameters are then replaced by the corresponding damped response parameters giving damped response functions which comply with the optimal elimination rule. Due to the fact that the generalized Hellmann-Feynman theorem does not apply in phenomenologically damped response theory, the explicit structure of a damped response function depends on the chosen elimination rule. However, this does not pose any practical problems as long as the molecular property of interest is identified using the same rule as the exact and approximate levels of theory.

## 7.4   Hartree–Fock and Kohn-Sham DFT Response Theory

Time-dependent perturbation theory for Hartree–Fock states has a long history. The theory of first-order molecular properties was first given by Ball and McLacland, using the *time-dependent Hartree–Fock approximation* [102, 103]. Second- and higher-order molecular properties in Hartree–Fock theory were subsequently evaluated [104, 105]. Response-function theory as it is used today—where response functions are subjected to pole and residue analysis to determine molecular properties for both ground and excited states and for the transitions between these states—was developed in the eighties [90] and has since been used to calculate a large variety of molecular properties.

The quasi-energy approach developed in the nineties [100, 101] has tied response function theory closely to energy-derivative techniques. Through the quasi-energy approach, response

functions may straightforwardly be derived for both variational and non-variational wave functions and used to calculate molecular properties for both ground and excited states, as well as transition properties between these states [90, 101].

This section is a brief summary of Paper **B**. It is demonstrated that the AO based formulation can be parametrized in a manner similar to the parametrization used in MO based response theory. Using this approach, all previous MO based second quantization formulations may be rewritten in the AO based formulation with only minor modifications. Paper **B** therefore provides the tools for transforming an MO based formulation to an AO based formulation, suitable for linear-scaling.

### 7.4.1 Second Quantization-Based AO Theory

In this section, we look at the aspects of second quantization that are relevant for deriving response functions within a second quantization AO-based formalism.

We will roughly follow the outline of Section 7.2, but the wave function $|0\rangle$ will in this case be a HF wave function, and the parametrization will be done in an AO basis in order to obtain a linear–scaling formulation. The focus of this section is to demonstrate how the language of second quantization can be used to parametrize the perturbed wave function similarly to Eq. (7.2) for exact theory.

The atomic orbital based second quantization used here has not previously been used to derive response functions, and it is relevant to review some of the details presented in Paper **B**.

In HF theory, the wave function is a single determinant given by

$$|0\rangle = a_i^\dagger a_j^\dagger \ldots a_l^\dagger |\text{vac}\rangle \tag{7.49}$$

where $\{a_i^\dagger a_j^\dagger \ldots a_l^\dagger\}$ refers to the set of occupied molecular spin orbitals that are occupied in $|0\rangle$.

Now consider a set of non-orthogonal atomic spin orbitals $\chi_\mu$ with the Hermitian metric **S**. The creation and annihilation operators of the AOs fulfill the anticommutation relations [43]

$$[a_\mu^\dagger, a_\nu^\dagger]_+ = 0 \quad [a_\mu, a_\nu]_+ = 0 \qquad [a_\mu^\dagger, a_\nu]_+ = S_{\nu\mu} \tag{7.50}$$

For a single-determinant state $|0\rangle$, we may define the MO density matrix

$$D_{pq}^{\text{MO}} = \langle 0|a_p^\dagger a_q|0\rangle \qquad \boldsymbol{D}^{\text{MO}} = \begin{pmatrix} \mathbf{1} & \mathbf{0} \\ \mathbf{0} & \mathbf{0} \end{pmatrix}. \tag{7.51}$$

In a similar manner we may define a matrix $\Delta$ as the expectation value of the AO creation and annihilation operators.

$$\Delta_{\mu\nu} = \langle 0|a_\mu^\dagger a_\nu|0\rangle \tag{7.52}$$

The orthonormal spin orbitals may be expanded in the AO basis (see Eq. (3.13)) and so may the creation and annihilation operators

$$a_i^\dagger = \sum_\alpha C_{\alpha i} a_\alpha^\dagger \tag{7.53}$$

The AO density matrix $\mathbf{D} = \mathbf{C}\mathbf{D}^{\mathrm{MO}}\mathbf{C}^{\dagger}$ is related to $\boldsymbol{\Delta}$ by the transformation

$$\boldsymbol{\Delta} = \mathbf{S}^{\mathrm{T}}\mathbf{D}^{\mathrm{T}}\mathbf{S}^{\mathrm{T}} \tag{7.54}$$

To prove Eq. (7.54), we use Eq. (7.53) to obtain the relations

$$[a_p^{\dagger}, a_{\nu}]_+ = \sum_{\alpha} C_{\alpha p} S_{\nu\alpha} \tag{7.55a}$$

$$[a_{\mu}^{\dagger}, a_p]_+ = \sum_{\alpha} C_{\alpha p}^* S_{\alpha\mu} \tag{7.55b}$$

which can be used to show that

$$\langle \mathrm{vac}| a_l \ldots a_j a_i a_{\mu}^{\dagger} a_{\nu} a_i^{\dagger} a_j^{\dagger} \ldots a_l^{\dagger} |\mathrm{vac}\rangle = \langle \mathrm{vac}| a_l \ldots a_j a_{\mu}^{\dagger} a_{\nu} a_j^{\dagger} \ldots a_l^{\dagger} |\mathrm{vac}\rangle + \sum_{\alpha\beta} C_{\alpha i}^* S_{\nu\alpha} C_{\beta i} S_{\beta\mu} \tag{7.56}$$

Repeated use of Eq. (7.56) shows that Eq. (7.54) is valid. Thus, the AO density-matrix element $D_{\mu\nu}$ is only identical to the matrix element $\Delta_{\mu\nu}$ in an orthonormal basis.

Turning our attention to the two-electron case, we show in Appendix A of Paper **B** that the two-electron expectation value

$$\Gamma_{\mu\nu\gamma\delta} = \langle 0| a_{\mu}^{\dagger} a_{\gamma}^{\dagger} a_{\delta} a_{\nu} |0\rangle \tag{7.57}$$

decouples into products of expectation values of one-electron operators

$$\Gamma_{\mu\nu\gamma\delta} = \Delta_{\mu\nu}\Delta_{\gamma\delta} - \Delta_{\mu\delta}\Delta_{\gamma\nu} \tag{7.58}$$

This decoupling is similar to the decoupling of the two-electron density matrix in the molecular spin-orbital basis. It may therefore be argued that $\boldsymbol{\Delta}$ and $\boldsymbol{\Gamma}$ should be called the AO one- and two-electron density matrices, respectively. However, in order to be consistent with standard nomenclature, we shall refer to $\mathbf{D}$ as the AO density matrix, and to $\boldsymbol{\Delta}$ and $\boldsymbol{\Gamma}$ as the matrices of expectation values of the one- and two-electron operators, respectively.

From the symmetry, trace and idempotency properties of the one-electron density matrix [43, 106]

$$\boldsymbol{D}^{\dagger} = \boldsymbol{D} \tag{7.59}$$

$$\mathrm{Tr}\boldsymbol{D}\boldsymbol{S} = N_{\mathrm{el}} \tag{7.60}$$

$$\boldsymbol{D}\boldsymbol{S}\boldsymbol{D} = \boldsymbol{D} \tag{7.61}$$

we straightforwardly obtain the following relations for $\boldsymbol{\Delta}$

$$\boldsymbol{\Delta}^{\dagger} = \boldsymbol{\Delta} \tag{7.62}$$

$$\mathrm{Tr}\boldsymbol{\Delta}\boldsymbol{S}^{-1} = N_{\mathrm{el}} \tag{7.63}$$

$$\boldsymbol{\Delta}S^{-1}\boldsymbol{\Delta} = \boldsymbol{\Delta} \tag{7.64}$$

We note that Eqs. (7.59)–(7.61) are necessary and sufficient conditions for a density matrix to represent a normalized single-determinant wave function, and that Eqs. (7.62)–(7.64) are

necessary and sufficient conditions for $\mathbf{\Delta}$ to represent a normalized single-determinant wave function.

When a time-dependent external field is applied to the system, the wave function will change as a function of time. It is therefore necessary to parametrize $\mathbf{\Delta}$ to describe a change of the reference wave function $|0\rangle$ in Eq. (7.49) into another single–determinant wave function. We parametrize using an exponential operator similar to Eq. (7.2)

$$\hat{T} = \exp(i\hat{\kappa}) \tag{7.65}$$

where $\hat{\kappa}$ is a Hermitian one-electron operator

$$\hat{\kappa} = \sum_{\mu\nu} \kappa_{\mu\nu} a_\mu^\dagger a_\nu \tag{7.66}$$

and $\boldsymbol{\kappa}$ (with elements $\kappa_{\mu\nu}$) is a time–dependent Hermitian matrix. We will show that

$$|\tilde{0}\rangle = \exp(i\hat{\kappa})|0\rangle \tag{7.67}$$

is a valid normalized single-determinant wave function, and that the parametrization of Eq. (7.65) constitutes a complete parametrization.

The transformed wave function may be expressed as

$$|\tilde{0}\rangle = \exp(i\hat{\kappa})|0\rangle = \exp(i\hat{\kappa}) a_i^\dagger a_j^\dagger \ldots a_l^\dagger |\text{vac}\rangle = \tilde{a}_i^\dagger \tilde{a}_j^\dagger \ldots \tilde{a}_l^\dagger |\text{vac}\rangle \tag{7.68}$$

where we have introduced the transformed creation operators

$$\tilde{a}_\mu^\dagger = \exp(i\hat{\kappa}) a_\mu^\dagger \exp(-i\hat{\kappa}) \tag{7.69}$$

which satisfy the same anticommutation relations as the untransformed operators

$$\begin{aligned} [\tilde{a}_\mu^\dagger, \tilde{a}_\nu]_+ &= [\exp(i\hat{\kappa}) a_\mu^\dagger \exp(-i\hat{\kappa}), \exp(i\hat{\kappa}) a_\nu \exp(-i\hat{\kappa})]_+ \\ &= \exp(i\hat{\kappa})[a_\mu^\dagger, a_\nu]_+ \exp(-i\hat{\kappa}) = S_{\nu\mu} \end{aligned} \tag{7.70}$$

The exponential operators $\exp(i\hat{\kappa})$ therefore represent the manifold of operators that conserve the metric $\mathbf{S}$.

Using the Baker-Campbell-Hausdorff (BCH) expansion [43] and the anticommutation relation of Eq. (7.50), the transformed and untransformed creation operators can be related

$$\begin{aligned} \tilde{a}_\mu^\dagger &= a_\mu^\dagger + \mathrm{i}[\hat{\kappa}, a_\mu^\dagger] - \frac{1}{2}[\hat{\kappa}, [\hat{\kappa}, a_\mu^\dagger]] + \cdots \\ &= a_\mu^\dagger + \mathrm{i} \sum_\nu (\boldsymbol{\kappa}\mathbf{S})_{\mu\nu} a_\nu^\dagger - \frac{1}{2} \sum_\nu (\boldsymbol{\kappa}\mathbf{S})_{\mu\nu}^2 a_\nu^\dagger + \cdots \\ &= \sum_\nu \exp(\mathrm{i}\boldsymbol{\kappa}\mathbf{S})_{\nu\mu} a_\nu^\dagger \end{aligned} \tag{7.71}$$

In the special case where $\mathbf{S} = \mathbf{I}$, $\exp(i\boldsymbol{\kappa})$ represents a unitary transformation of the orbitals.

The expectation value of $a_\mu^\dagger a_\nu$ for the transformed state becomes

$$\tilde{\Delta}_{\mu\nu} = \langle\tilde{0}|a_\mu^\dagger a_\nu|\tilde{0}\rangle = \langle 0|\exp(-i\hat{\kappa}) a_\mu^\dagger \exp(i\hat{\kappa}) \exp(-i\hat{\kappa}) a_\nu \exp(i\hat{\kappa})|0\rangle \tag{7.72}$$

Using Eqs. (7.69) and (7.71), we straightforwardly obtain

$$\exp(-i\hat{\kappa})a_\mu^\dagger \exp(i\hat{\kappa}) \;=\; \sum_\delta \exp(-i\boldsymbol{\kappa}\mathbf{S})_{\delta\mu} a_\delta^\dagger \tag{7.73a}$$

$$\exp(-i\hat{\kappa})a_\nu \exp(i\hat{\kappa}) \;=\; \sum_\delta \exp(i\mathbf{S}\boldsymbol{\kappa})_{\nu\delta} a_\delta \tag{7.73b}$$

Inserting these expressions into Eq. (7.72) gives

$$\tilde{\boldsymbol{\Delta}} = \exp(-i\mathbf{S}^{\mathrm{T}}\boldsymbol{\kappa}^{\mathrm{T}})\boldsymbol{\Delta}\exp(i\boldsymbol{\kappa}^{\mathrm{T}}\mathbf{S}^{\mathrm{T}}) \tag{7.74}$$

which describes how $\boldsymbol{\Delta}$ transforms when the reference state $|0\rangle$ changes. If $\boldsymbol{\Delta}$ fulfills Eqs. (7.62)–(7.64), then so does $\tilde{\boldsymbol{\Delta}}$ defined in Eq. (7.72), as demonstrated in Appendix B of paper **B**.

We conclude that $\tilde{\boldsymbol{\Delta}}$ fulfills Eqs. (7.62)–(7.64) and that $\exp(i\hat{\kappa})|0\rangle$ is a normalized single-determinant wave function. It may also be shown that all matrices satisfying Eqs. (7.62)–(7.64) may be obtained by an appropriate choice of $\boldsymbol{\kappa}$, so Eq. (7.65) constitutes a complete parametrization.

### 7.4.2 Response Functions in AO-Based HF and KS Response Theory

Since the parametrization of Eq. (7.65) has the same structure as that of Eq. (7.2), the results of Section 7.2 may be straightforwardly adopted with the replacement

$$\hat{X} \to \hat{\kappa}. \tag{7.75}$$

The expansion of the expectation value in terms of the response parameters is identical to the expansion of Section 7.2.1 (using Eq. (7.75)) and the linear response function is given by

$$\langle\langle A; V(\omega)\rangle\rangle_\omega = -i\langle 0|[\hat{\kappa}^{(1)}(\omega), \hat{A}]|0\rangle \tag{7.76}$$

The quadratic response function (and higher-order response functions) may also straightforwardly be obtained from the expressions in Section 7.2.1.

The time evolution of $|\tilde{0}\rangle$ in the presence of the time-dependent perturbation may be determined using Ehrenfest's theorem[91] for the operator $a_\mu^\dagger a_\nu$

$$i\frac{\mathrm{d}}{\mathrm{d}t}\langle\tilde{0}|a_\mu^\dagger a_\nu|\tilde{0}\rangle = i\langle\tilde{0}|(\frac{\partial}{\partial t}a_\mu^\dagger a_\nu)|\tilde{0}\rangle + \langle\tilde{0}|[a_\mu^\dagger a_\nu, \hat{H}]|\tilde{0}\rangle \tag{7.77}$$

Following the derivations of section 7.2.2, the Ehrenfest theorem results in a set of nonlinear equations which define the time-dependence of $\hat{\kappa}(t)$, and these equations will be solved order by order to determine the parameters $\hat{\kappa}^{(i)}(\omega)$. The resulting equations can be directly adopted from section 7.2.2 using the replacement

$$\hat{R}_p \to a_\mu^\dagger a_\nu. \tag{7.78}$$

By introducing the generalized Hessian $\mathbf{E}^{[2]}$, metric $\mathbf{S}^{[2]}$ and property $\mathbf{g}^b$ tensors

$$E_{\mu\nu\gamma\delta}^{[2]} = \langle 0|[a_\mu^\dagger a_\nu, [\hat{H}_0, a_\gamma^\dagger a_\delta]]|0\rangle \tag{7.79}$$

$$S_{\mu\nu\gamma\delta}^{[2]} = \langle 0|[a_\mu^\dagger a_\nu, a_\gamma^\dagger a_\delta]|0\rangle \tag{7.80}$$

$$g_{\mu\nu}^b = \langle 0|[a_\mu^\dagger a_\nu, \hat{B}]|0\rangle \tag{7.81}$$

and renaming $\hat{V}^\omega$ to $\hat{B}$, the first-order response equations can be written in the form

$$\left(E^{[2]}_{\mu\nu\gamma\delta} - \omega S^{[2]}_{\mu\nu\gamma\delta}\right)\kappa^{(1)}_{\gamma\delta} = \mathrm{i}g^b_{\mu\nu} \qquad (7.82)$$

in analogue with Eq. (7.21). Introducing

$$A^{[1]}_{\gamma\delta} = -\langle 0|[a^\dagger_\gamma a_\delta, \hat{A}]|0\rangle \qquad (7.83)$$

the linear response function in Eq. (7.26) may in HF or KS theory be written in the form

$$\begin{aligned}\langle\langle A;B\rangle\rangle_\omega &=& -\mathrm{i}\langle 0|[a^\dagger_\gamma a_\delta, \hat{A}]|0\rangle\kappa^{(1)}_{\gamma\delta} \\ &=& -A^{[1]}_{\gamma\delta}\left(E^{[2]}_{\mu\nu\gamma\delta} - \omega S^{[2]}_{\mu\nu\gamma\delta}\right)^{-1}g^b_{\mu\nu}\end{aligned} \qquad (7.84)$$

We now introduce the response vector $N^B_{\gamma\delta}(\omega)$, which fulfills the real equation

$$\left(E^{[2]}_{\mu\nu\gamma\delta} - \omega S^{[2]}_{\mu\nu\gamma\delta}\right)N^b_{\gamma\delta}(\omega) = g^b_{\mu\nu}(\omega). \qquad (7.85)$$

By combining $\mu$ and $\nu$ to a single capital index $I$, and $\gamma$ and $\delta$ to a single capital index $J$, we may introduce the super-matrix/vector notation

$$\boldsymbol{E}^{[2]}\boldsymbol{N}^b = \sum_I E^{[2]}_{IJ}N^b_J = \sum_{\gamma\delta} E^{[2]}_{\mu\nu\gamma\delta}N^b_{\gamma\delta} \qquad (7.86)$$

and obtain

$$(\boldsymbol{E}^{[2]} - \omega_b\boldsymbol{S}^{[2]})\boldsymbol{N}^b = \boldsymbol{g}^b \qquad (7.87)$$

The linear response function may thus be calculated as

$$\langle\langle \hat{A};\hat{B}\rangle\rangle_\omega = -A^{[1]}_{\gamma\delta}N^B_{\gamma\delta}(\omega) \qquad (7.88)$$

The linear response function may thus be determined by solving one set of linear equations for each frequency.

Paper **B** also provides the expression for the quadratic response function and the computational expressions required for implementation.

### 7.4.3 Linear Scaling

The time-consuming step in the computation of linear and higher order response functions is the solution of the linear set of response equations (Eq. (7.85)). Coriani *et al.* [107] presented a linear-scaling implementation, where the linear equations are solved using an AO–based iterative preconditioned–conjugate–gradient method equivalent to the one that has been successfully used in the MO basis. The method uses paired trial vectors to ensure that complex eigenvalues do not arise during the iterations. The response equations are further preconditioned in an orthogonalized–atomic–orbital basis in order to reduce the condition number of $\mathbf{E}^{[2]}$ and to make $\mathbf{E}^{[2]}$ more diagonal dominant.

### 7.4.4   Kohn-Sham DFT Response Theory

In section 7.4 we have derived an atomic orbital based Hartree-Fock response theory in a manner closely related to a previously developed molecular orbital formulation [90]. This methodology cannot directly be adopted for KS-DFT, but HF response theory can also be derived in terms of an effective one electron operator which has the added advantage of facilitating the extension to Kohn-Sham DFT (KS-DFT) response theory.

We refer the reader to Section VII and VIII of paper **B**

## 7.5   Hartree–Fock and Kohn-Sham Damped Response Theory

### 7.5.1   Equivalence between Exact and Approximate HF Response Theory

In this section, we describe how the treatment of damped response theory for an exact state in Section 7.3.2 may be generalized to approximate variational methods such as HF and KS-DFT. The $\mathbf{E}^{[g]}$ and $\mathbf{S}^{[g]}$ matrices discussed in the previous sections enter in the same way as in exact theory, and therefore the procedure for obtaining damped response functions in Section 7.3.2 may also be applied in these theories. The only modification is that the excitation/deexcitation operator $R_p$ in Eq. (7.4) must be replaced by the corresponding operator in the approximate theory of interest. In single-determinant methods such as HF theory or KS-DFT, $R_p$ represents an orbital rotation generator, which mixes molecular HF or KS orbitals to generate the best possible molecular orbitals for the HF or KS determinant.

To illustrate the equivalence between exact theory and a variational approximate theory, it is convenient to express $(\mathbf{E}^{[2]} - \omega \mathbf{S}^{[2]})^{-1}$ in exact theory in the form

$$
\begin{aligned}
(\mathbf{E}^{[2]} - \omega \mathbf{S}^{[2]})^{-1} &= \begin{pmatrix} (\boldsymbol{\omega}_k - \boldsymbol{\omega})^{-1} & \mathbf{0} \\ \mathbf{0} & (\boldsymbol{\omega}_k^* + \boldsymbol{\omega})^{-1} \end{pmatrix} \\
&= \sum_{k>0} \left[ (\omega_k - \omega)^{-1} \mathbf{x}_k \mathbf{x}_k^\dagger + (\omega_k^* + \omega)^{-1} \mathbf{x}_{-k} \mathbf{x}_{-k}^\dagger \right] \\
&\rightarrow \sum_{k>0} \left[ (\omega_k - \omega - i\gamma)^{-1} \mathbf{x}_k \mathbf{x}_k^\dagger + (\omega_k + \omega + i\gamma)^{-1} \mathbf{x}_{-k} \mathbf{x}_{-k}^\dagger \right]
\end{aligned}
\tag{7.89}
$$

where we have used Eq. (7.22) and introduced complex excitation energies according to Eq. (7.37), and where the excitation vectors $\mathbf{x}_k$ are given by

$$
(x_k)_p = \delta_{pk}
\tag{7.90}
$$

and satisfy the generalized eigenvalue equation

$$
\mathbf{E}^{[2]} \mathbf{x}_k = \omega_k \mathbf{S}^{[2]} \mathbf{x}_k; \qquad \mathbf{E}^{[2]} \mathbf{x}_{-k} = -\omega_k \mathbf{S}^{[2]} \mathbf{x}_{-k}
\tag{7.91}
$$

which follows straightforwardly from Eqs. (7.22) and (7.90).

In HF and KS-DFT we may introduce also excitation vectors $\boldsymbol{X}_k$ as the eigenvectors of the generalized eigenvalue problem (in the super matrix/vector notation, see Eq. (7.86))

$$
\boldsymbol{E}^{[2]} \boldsymbol{X}_k = \omega_k \boldsymbol{S}^{[2]} \boldsymbol{X}_k; \qquad \boldsymbol{E}^{[2]} \boldsymbol{X}_{-k} = -\omega_k \boldsymbol{S}^{[2]} \boldsymbol{X}_{-k}
\tag{7.92}
$$

from which we can obtain excitation energies. For the molecular ground state, $\boldsymbol{E}^{[2]}$ can be shown to be positive definite (see paper **B**), and Eq. (7.92) may be viewed as a generalized Hermitian eigenvalue problem with $\boldsymbol{E}^{[2]}$ as the metric[1]. The excitation vectors may therefore be chosen to be orthogonal with respect to the inner product induced by $\boldsymbol{E}^{[2]}$

$$\boldsymbol{X}_g^\dagger \boldsymbol{E}^{[2]} \boldsymbol{X}_k = \omega_k \delta_{gk}; \tag{7.93}$$

and from Eq. (7.92)

$$\boldsymbol{X}_g^\dagger \boldsymbol{S}^{[2]} \boldsymbol{X}_k = \delta_{gk}; \qquad k > 0 \tag{7.94}$$

$$\boldsymbol{X}_g^\dagger \boldsymbol{S}^{[2]} \boldsymbol{X}_k = -\delta_{gk}; \qquad k < 0 \tag{7.95}$$

Using these relations, we may introduce a spectral representation of $(\boldsymbol{E}^{[2]} - \omega \boldsymbol{S}^{[2]})^{-1}$ (see paper **B**) in HF, and KS-DFT and introduce complex excitation energies in analogy with Eq. (7.89)

$$
\begin{aligned}
(\boldsymbol{E}^{[2]} - \omega \boldsymbol{S}^{[2]})^{-1} &= \sum_{k>0} \big[ (\omega_k - \omega)^{-1} \boldsymbol{X}_k \boldsymbol{X}_k^\dagger + (\omega_k^* + \omega)^{-1} \boldsymbol{X}_{-k} \boldsymbol{X}_{-k}^\dagger \big] \\
&\rightarrow \sum_{k>0} \big[ (\omega_k - \omega - i\gamma)^{-1} \boldsymbol{X}_k \boldsymbol{X}_k^\dagger + (\omega_k + \omega + i\gamma)^{-1} \boldsymbol{X}_{-k} \boldsymbol{X}_{-k}^\dagger \big]
\end{aligned}
\tag{7.96}
$$

It is clear that the equations in the approximate theories are completely equivalent to the corresponding equations in exact theory (compare Eqs. (7.96) and (7.92) to Eqs. (7.89) and (7.91)).

Therefore, all damped response equations in approximate theory have the form

$$\big[ \mathbf{E}^{[2]} - (\omega_{b...f} + i\gamma) \mathbf{S}^{[2]} \big] \bar{\mathbf{x}}^{b...f} = i\mathbf{g}^{b...f} \tag{7.97}$$

with approximate Hessian and metric matrices $\boldsymbol{E}^{[2]}$ and $\boldsymbol{S}^{[2]}$. This structure of damped response equations for a variational approximate state was also obtained by Norman *et al.* [94, 96].

In conclusion, the strategy for obtaining a formulation of damped response theory for HF and KS-DFT theory is equivalent to the one discussed in Section 7.3.2. Thus, a damped response theory formulation may be obtained by replacing all standard response parameters by their damped counterparts, and the calculation of approximate damped response functions therefore becomes a matter of solving damped response equations of the form of Eq. (7.97)

In paper **D** we presented two algorithms for solving this equation. One algorithm for the easy off-resonant region, and one algorithm for the more complex region close to an excitation energy.

### 7.5.2  Illustrative Results

In this section, we report calculations of $\langle\langle \overline{\mu_\alpha; \mu_\beta} \rangle\rangle_{\omega_b}^I$ related to the absorption spectra (see Eq. (7.48)) for single-stranded DNA strings containing one and two adenosine nucleotides referred to as $A_1$ and $A_2$ in the following. We investigate the frequency range up to 0.6 a.u. and

---

[1] $\boldsymbol{S}^{[2]}$ is not positive definite, and therefore not a valid metric

the calculations have been carried out at the HF/6-31G level of theory using the geometry of single-stranded DNA obtained from the Maestro program [108] without carrying out any additional optimizations. All calculations have been carried out using a local version of DALTON [1].

In Fig. 7.2, results for $A_1$ (first column) and $A_2$ (second column) are given. In the first row, the absorption spectra obtained from damped–response theory are shown. In the second row, absorption stick spectra containing the first 50 excitations are presented (obtained from the residues of the linear response function in standard response theory) with superimposed Lorentzian lineshape functions as in Eq. (7.46). The third row shows the density of the first 50 excited states. It is seen that the density of the excited states increases drastically at higher frequencies and for larger systems.

For $A_1$, the first 50 excitation energies yield the absorption spectrum up to a frequency of about 0.6 a.u. We again note that the absorption stick spectrum with a Lorentzian line-shape function superimposed (second row, first column) is identical to the spectrum obtained using the damped response theory (first row, first column) in accordance with the theoretical prediction.

For $A_2$, the first 50 excitation energies only include low lying states up to 0.1 a.u. (second row, second column), because the density of states increases significantly with increasing frequency. It is virtually impossible to calculate all the excited states in the frequency range between 0.1-0.6 a.u. Standard response theory therefore cannot be applied to evaluate the absorption spectrum for this frequency range. DNA strings containing more than two nucleotides will have even more low lying excited states, which furthermore increase the problems of using standard response theory to evaluate the absorption spectrum in this frequency range. However, damped response theory can be successfully used for obtaining the absorption spectra for larger systems at all frequency ranges, as can be seen in the first row, second column of Fig. 7.2, where the damped absorption spectrum for $A_2$ is given up to a frequency of 0.6 a.u.
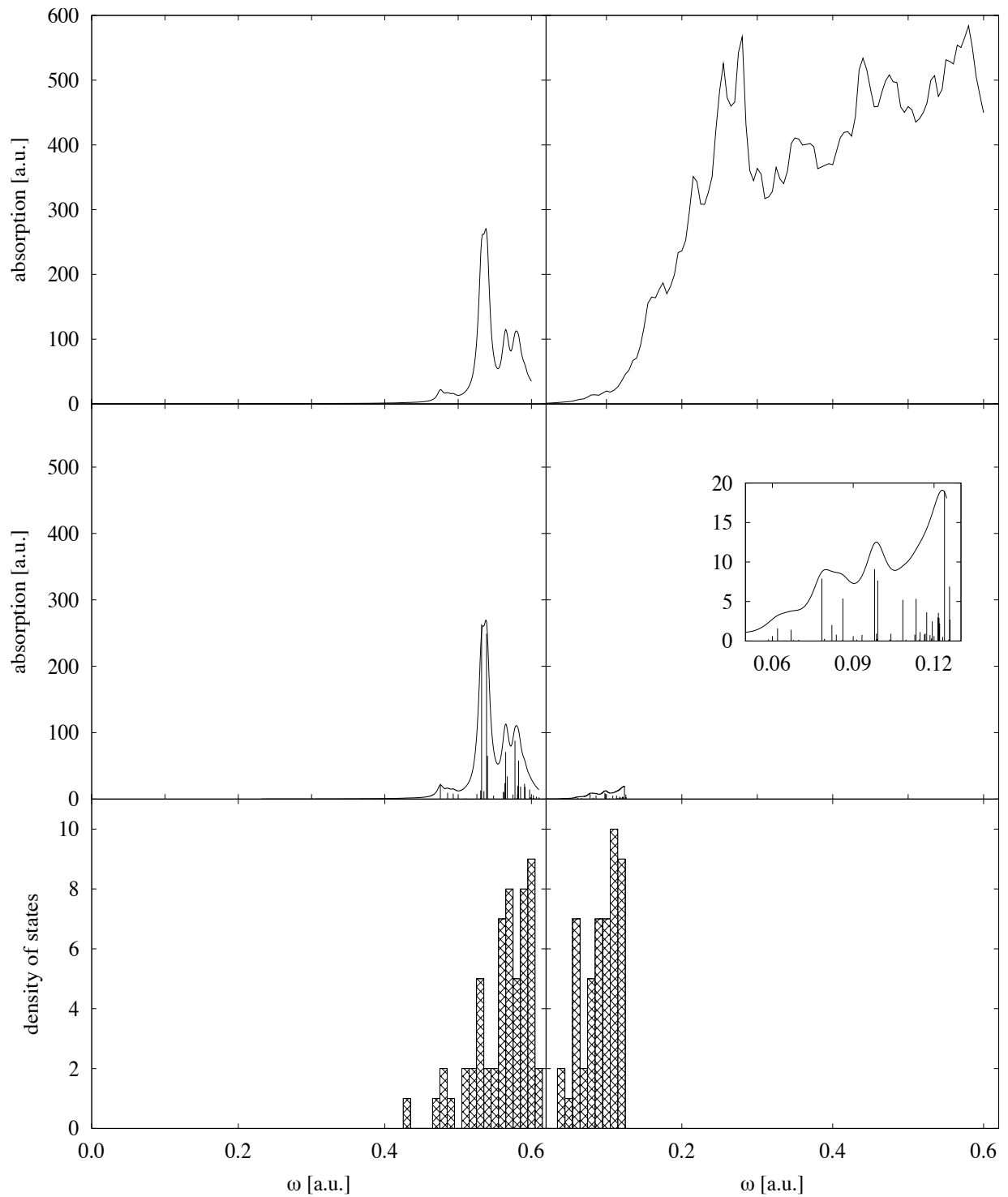
**Figure 7.2:** Absorption spectra ($xx$ component) for $A_1$ (first column) and $A_2$ (second column), $\gamma = 0.005$ a.u. Top panel: Absorption spectra obtained using the damped response theory approach described in Sec. 7.5; middle panel: First 50 excitation energies stick spectrum obtained using standard response theory with superimposed Lorentzian lineshape functions; bottom panel: Density of the first 50 excited states.

# Chapter 8

# Geometric Gradients of Linear Response Properties

In this chapter we present a Lagrangian approach for the calculation of molecular response properties which can be expressed as geometric first derivatives of generic linear response functions, their poles and residues. The approach is implemented within the linear-scaling atomic-orbital based formalism presented in section 7.4.1 at the level of HF and DFT.

Derivatives of electronic properties with respect to displacements of the nuclei, for brevity denoted as geometric derivatives herein, are one of the key ingredients in describing the effect of molecular vibrations on properties computed within the Born-Oppenheimer approximation.

As an example we consider the first geometric derivative of the transition dipole strength, which yields information on how the motion of the nuclei will affect the UV spectrum (or one-photon absorption, OPA) of a molecule through the so-called Herzberg-Teller (HT) contribution (vibronic coupling between different electronic states) [109–111]. Another example is the first geometric derivative of the excited state energy, which gives the excited-state gradient, from which the electronic excited state equilibrium geometry can be obtained.

Since the starting expressions for the transition dipole strength are in this thesis taken in accordance with the atomic-orbital formulation of response theory presented in section 7.4.1, the resulting properties are thus automatically guaranteed a linearly scaling behaviour for sufficiently sparse matrices.

Paper **F** presented the first analytic implementation of the electronic transition dipole moment derivative in a DFT framework, and this chapter deal solely with this issue.

For the geometric gradient of the linear response function or its poles, we refer the reader to paper **F**.

## 8.1 Transition Moment Lagrangian

The Lagrangian functional is build from the expression for the one-photon dipole transition moment $\mu_\alpha^{0j}$, which can be obtained from the residue of the linear response function (See Eq. (7.27)).

Introducing the spectral representation of Eq. (7.96) into the expression for the linear response function of Eq. (7.88) we obtain

$$\lim_{\omega_b \to \omega_n} (\omega_b - \omega_n)\langle\langle \hat{A}; \hat{B}\rangle\rangle_\omega = \left(A_{\gamma\delta}^{[1]} X_{\gamma\delta}^n\right)\left(X_{\mu\nu}^n g_{\mu\nu}^b\right) \tag{8.1}$$

In Eq. (8.1) we have used the Einsteins sum convention, and this will be used throughout this chapter. By comparing Eq.(8.1) and Eq. (7.27) we identify the square of the transition matrix elements as

$$A^{0n} B^{n0} = \left(A_{\gamma\delta}^{[1]} X_{\gamma\delta}^n\right)\left(X_{\mu\nu}^n g_{\mu\nu}^b\right) \tag{8.2}$$

Eq. (8.2) does not by itself allow us to identify $A^{0p}$ only $|A^{0p}|$ [90]. The sign of the transition matrix element is however not important for the description of molecular properties as transition matrix elements are always squared in molecular property expressions [90]. We may chose the identification

$$A^{0n} = \left(A_{\gamma\delta}^{[1]} X_{\gamma\delta}^n\right), \tag{8.3}$$

and choose $\hat{A} = \hat{\mu}_\alpha$. The expression of $A^{0n}$ depends on the excitation vector $X_{\gamma\delta}^n$ and orbital parameters $\kappa$. Both of these parameters have a complicated dependence on the nuclear coordinates, and we may instead of a straightforward differentiation use the Lagrange's method of undetermined multipliers to derive efficient computational expressions for the geometric derivative of the transition dipole moment.

We therefore construct the Lagrangian function for the transition moment, using the eigenvalue equation (Eq.(7.92)),the orthonormality condition (Eq. (7.94)) and the gradient condition ($E_{\mu\nu}^{[1]} = \langle \tilde{0}|[a_\mu^\dagger a_\nu, \hat{H}]|\tilde{0}\rangle = 0$) as constraints.

$$\mathcal{L} = A_{\gamma\delta}^{[1]} X_{\gamma\delta}^n - \bar{\lambda}_{\mu\nu}\left(E_{\mu\nu\gamma\delta}^{[2]} - \omega_n S_{\mu\nu\gamma\delta}^{[2]}\right) X_{\gamma\delta}^n - \bar{\omega}\left(X_{\mu\nu}^n S_{\mu\nu\gamma\delta}^{[2]} X_{\gamma\delta}^n - 1\right) - \bar{X}_{\mu\nu} E_{\mu\nu}^{[1]}. \tag{8.4}$$

The Lagrangian may be made fully variational with respect to variations in the excitation vector $\boldsymbol{X}^n$ and the orbital parameters $\kappa$ by determining the lagrangian multipliers to fulfill the equations

$$\frac{\partial \mathcal{L}}{\partial X_{\gamma\delta}^n} = 0 \Leftrightarrow A_{\gamma\delta}^{[1]} = \bar{\lambda}_{\mu\nu}(E_{\mu\nu\gamma\delta}^{[2]} - \omega_n S_{\mu\nu\gamma\delta}^{[2]}) + 2\bar{\omega} X_{\mu\nu}^n S_{\mu\nu\gamma\delta}^{[2]} \tag{8.5a}$$

$$\frac{\partial \mathcal{L}}{\partial \kappa_{\phi\chi}} = 0 \Leftrightarrow -\frac{\partial A_{\gamma\delta}^{[1]}}{\partial \kappa_{\phi\chi}} X_{\gamma\delta}^n + \bar{\lambda}_{\mu\nu}\left(\frac{\partial E_{\mu\nu\gamma\delta}^{[2]}}{\partial \kappa_{\phi\chi}} - \omega_n \frac{\partial S_{\mu\nu\gamma\delta}^{[2]}}{\partial \kappa_{\phi\chi}}\right) X_{\gamma\delta}^n = \bar{X}_{\mu\nu}\frac{\partial E_{\mu\nu}^{[1]}}{\partial \kappa_{\phi\chi}}. \tag{8.5b}$$

Eq. (8.5a) determines both $\bar{\omega}$ and $\bar{\boldsymbol{\lambda}}$. Multipling with $X_{\gamma\delta}^n$ we obtain an expression for the multiplier $\bar{\omega}$

$$\bar{\omega} = \frac{1}{2} A_{\gamma\delta}^{[1]} X_{\gamma\delta}^n. \tag{8.6}$$

Rewriting Eq. (8.5a) we obtain an equation for $\bar{\lambda}$

$$\left(E_{\mu\nu\gamma\delta}^{[2]} - \omega_n S_{\mu\nu\gamma\delta}^{[2]}\right)\bar{\lambda}_{\gamma\delta} = A_{\mu\nu}^{[1]} - 2\bar{\omega} S_{\mu\nu\gamma\delta}^{[2]} X_{\gamma\delta}^n. \tag{8.7}$$

Eq. (8.7) have the form of a standard response equation similar to Eq. (7.85) with $\omega = \omega_n$, but as the response vector have a singularity at this frequency Eq. (8.7) cannot be solved using a

standard solver. However, we may decompose $\bar{\lambda}_{\gamma\delta}$ into a component which is orthogonal to $X_{\mu\nu}^n$ and a corresponding parallel component

$$\bar{\lambda}_{\gamma\delta} = a\bar{\lambda}_{\gamma\delta}^{\perp} + bX_{\gamma\delta}^n. \tag{8.8}$$

$\lambda_{\gamma\delta}$ would satisfy Eq.(8.7) independent of the value of $b$, due to Eq. (7.92). The second term on the right hand side of Eq. (8.7) effectively project out the $X_{\mu\nu}^n$ component of $\boldsymbol{A}^{[1]}$, which means that there is no $X_{\mu\nu}^n$ component on the right hand side of Eq. (8.7) and using the spectral representaion of Eq. (7.96) we conclude that $b$ must be zero.

As Eq. (8.7) is solved by means of an iterative procedure based on trial vectors, we need to ensure that the solution vector is kept orthogonal to the excitation vector $X_{\gamma\delta}^n$ at each iteration of the procedure. See paper **E** for a more detailed discussion of the algorithm.

The parameters $\bar{X}$ may be determined from Eq. (8.5b), as differentiation with respect to the variational parameters $\kappa_{\mu\nu}$ gives a response equation from which we can determine the multipliers $\bar{X}$. using the relations

$$\frac{\mathrm{d}}{\mathrm{d}\kappa_{\phi\chi}}E_{\mu\nu\gamma\delta}^{[2]} = \frac{\mathrm{d}}{\mathrm{d}\kappa_{\phi\chi}}\langle\tilde{0}|[a_\mu^\dagger a_\nu, [\hat{H}_0, a_\rho^\dagger a_\sigma]]|\tilde{0}\rangle = E_{\phi\chi\gamma\delta\mu\nu}^{[3]} \tag{8.9}$$

$$\frac{\mathrm{d}}{\mathrm{d}\kappa_{\phi\chi}}S_{\mu\nu\gamma\delta}^{[2]} = \frac{\mathrm{d}}{\mathrm{d}\kappa_{\phi\chi}}\langle\tilde{0}|[a_\mu^\dagger a_\nu, a_\rho^\dagger a_\sigma]|\tilde{0}\rangle = S_{\phi\chi\gamma\delta\mu\nu}^{[3]} \tag{8.10}$$

$$\frac{\mathrm{d}}{\mathrm{d}\kappa_{\phi\chi}}V_{\mu\nu}^{[1]} = \frac{\mathrm{d}}{\mathrm{d}\kappa_{\phi\chi}}\langle\tilde{0}|[a_\mu^\dagger a_\nu, \hat{V}(\omega)]|\tilde{0}\rangle = V_{\mu\nu\phi\chi}^{[2]} \tag{8.11}$$

$$\frac{\mathrm{d}}{\mathrm{d}\kappa_{\phi\chi}}A_{\mu\nu}^{[1]} = -\frac{\mathrm{d}}{\mathrm{d}\kappa_{\phi\chi}}\langle\tilde{0}|[a_\mu^\dagger a_\nu, \hat{A}(\omega)]|\tilde{0}\rangle = 2A_{\phi\chi\mu\nu}^{[2]} \tag{8.12}$$

$$\frac{\mathrm{d}}{\mathrm{d}\kappa_{\phi\chi}}E_{\mu\nu}^{[1]} = \frac{\mathrm{d}}{\mathrm{d}\kappa_{\phi\chi}}\langle\tilde{0}|[a_\mu^\dagger a_\nu, \hat{H}]|\tilde{0}\rangle = E_{\mu\nu\phi\chi}^{[2]} \tag{8.13}$$

We may rewrite Eq. (8.5b) into a response equation similar to Eq. (7.85) with $\omega = 0$.

$$E_{\phi\chi\mu\nu}^{[2]}\bar{X}_{\mu\nu} = 2A_{\phi\chi\gamma\delta}^{[2]}X_{\gamma\delta}^n - E_{\phi\chi\gamma\delta\mu\nu}^{[3]}X_{\gamma\delta}^n\bar{\lambda}_{\mu\nu} \tag{8.14}$$

Note that the terms which include $S^{[3]}$ can be shown to be zero.

## 8.2 The Transition Moment Gradient

Once the Lagrange multipliers have been determined, we can obtain the geometric derivatives of the Lagrangian.

$$\frac{\mathrm{d}\mathcal{L}}{\mathrm{d}R} = \frac{\partial A_{\gamma\delta}^{[1]}}{\partial R}X_{\gamma\delta}^n - \frac{1}{2}(A_{\phi\chi}^{[1]}X_{\phi\chi}^n)\left(X_{\mu\nu}^n\frac{\partial S_{\mu\nu\gamma\delta}^{[2]}}{\partial R}X_{\gamma\delta}^n\right) \tag{8.15}$$

$$+\bar{\lambda}_{\mu\nu}\left(\frac{\partial E_{\mu\nu\gamma\delta}^{[2]}}{\partial R} - \omega_f\frac{\partial S_{\mu\nu\gamma\delta}^{[2]}}{\partial R} - \frac{\partial\omega_f}{\partial R}S_{\mu\nu\gamma\delta}^{[2]}\right)X_{\gamma\delta}^n - \bar{X}_{\mu\nu}\frac{\partial E_{\mu\nu}^{[1]}}{\partial R} \tag{8.16}$$

However the term including $\frac{\partial\omega_f}{\partial R}$ is zero since $\bar{\lambda}_{\mu\nu}S_{\mu\nu\gamma\delta}^{[2]}X_{\gamma\delta}^n = 0$.

## 8.3 Herzberg-Teller Contribution to the One-Photon Absorption Spectrum

The electric transition dipole moment $\boldsymbol{M}_{\tau\iota}$ between two rovibronic states characterized by the rovibronic wavefunctions $\Psi_\tau(\boldsymbol{r}, \boldsymbol{R})$ and $\Psi_\iota(\boldsymbol{r}, \boldsymbol{R})$, which depend on the electronic spatial coordinates $\boldsymbol{r}$ and the collective spatial coordinates $\boldsymbol{R}$ of the nuclei, is, in the adiabatic approximation, given by

$$\boldsymbol{M}_{\tau\iota} = \langle\Psi_\tau|\boldsymbol{\mu}|\Psi_\iota\rangle \approx \langle\Psi_{\tau,t}|\langle t|\boldsymbol{\mu}|i\rangle|\Psi_{\iota,i}\rangle = \langle\Psi_{\tau,t}|\boldsymbol{\mu}^{ti}|\Psi_{\iota,i}\rangle = \boldsymbol{M}_{\tau t\iota i}, \tag{8.17}$$

with the adiabatic electronic wavefunctions $|t(\boldsymbol{r}; \boldsymbol{R})\rangle$ and $|i(\boldsymbol{r}; \boldsymbol{R})\rangle$ depending explicitly on the collective spatial coordinates of the electrons and parametrically on the collective spatial coordinates of the nuclei. The wavefunctions $\Psi_{\tau,t}(\boldsymbol{R})$ and $\Psi_{\iota,i}(\boldsymbol{R})$ for the motion of the nuclei depend like the electronic transition dipole moment $\boldsymbol{\mu}^{ti}(\boldsymbol{R})$ only on the coordinates of the nuclei constituting the system of interest.

If a Taylor expansion is applied to $\boldsymbol{\mu}^{ti}(\boldsymbol{R})$, around the equilibrium molecular structure $\boldsymbol{R}_0$ of the initial electronic state, the expansion yields

$$\boldsymbol{\mu}^{ki}(\boldsymbol{R}) = \boldsymbol{\mu}^{ki}(\boldsymbol{R}_0) + \sum_\beta \frac{\partial\boldsymbol{\mu}^{ki}(\boldsymbol{R})}{\partial R_\beta}\Big|_{\boldsymbol{R}=\boldsymbol{R}_0}(R_\beta - R_{0,\beta}) + \cdots \tag{8.18}$$

Inserting this expansion to first'th order into Eq. (8.17) we obtain

$$\boldsymbol{M}_{\tau t\iota i} = \boldsymbol{\mu}^{ti}(\boldsymbol{R}_0)\langle\tau_t|\iota_i\rangle + \sum_\beta \frac{\partial\boldsymbol{\mu}^{ti}(\boldsymbol{R})}{\partial R_\beta}\Big|_{\boldsymbol{R}=\boldsymbol{R}_0}\langle\tau_t|(\hat{R}_\beta - \hat{R}_{0,\beta})|\iota_i\rangle. \tag{8.19}$$

$\boldsymbol{M}_{\tau t\iota i}$ requires the evaluation of both Franck-Condon factors $\langle\tau_t|\iota_i\rangle$ and HT integrals $\Big|_{\boldsymbol{R}=\boldsymbol{R}_0}\langle\tau_t|(\hat{R}_\beta - \hat{R}_{0,\beta})|\iota_i\rangle$, in addition to the electronic transition dipole moments and the first derivative of the electronic transition dipole moments.

The electronic transition dipole moments and first derivative of the electronic transition dipole moments can be computed analytically using the the DFT-based framework developed in this chapter, but the evaluation of Franck-Condon factors and HT integrals is beyond the scope of this thesis, and the reader is refered to paper **F**, where we present and discuss the results of a hybrid-functional DFT study of the vibronic fine structure of the $\tilde{X}(^1A_{1g})$-$\tilde{A}(^1B_{2u})$ transition in the absorption spectrum of benzene. In the electric dipole approximation, this transition is Franck-Condon forbidden ($\boldsymbol{\mu}^{kl}(\boldsymbol{R}_0) = 0$) and hence basically determined by the Herzberg-Teller integrals and electronic transition dipole-moment derivatives.

# Chapter 9

# Magnetic Circular Dichroism

## 9.1 Introduction

In an external magnetic field all matter becomes optically active, a phenomenon denoted Magneto Optical Activity (MOA), which originates from a differential interaction of the sample with the right and left circularly polarized components of the plane-polarized light. Two phenomena may occur depending on the frequency of the incident light.

- Magnetic Optical Rotation (MOR) is a rotation of the plane of polarization, which occurs when the magnetic field causes the two components of the incident light to propagate through the sample with different velocities. For a more thorough discussion of MOR, we refer the reader to paper **E**.

- Magnetic Circular Dichroism (MCD) is an induced ellipticity of the incident linearly polarized light, which occurs as the two components are absorbed to different extents [93, 112–116].

A common way to display a MCD spectrum is a plot of magnetically induced molar ellipticity $[\theta]_M$ in units of degree $dl^{-1}$ $dm^{-1}mol^{-1}G^{-1}$, normalized for unit strength of the magnetic field, against wavenumber $\tilde{\nu}$. For closed-shell molecules, MCD may be rationalized in terms of two magnetic rotatory strengths, known as the Faraday $\mathcal{A}$ and $\mathcal{B}$ terms [115–121].

The Faraday $\mathcal{A}$ term originates from the Zeeman splitting of spectral lines into left and right circularly polarized components. The $\mathcal{A}$ term only contributes in the presence of excited state degeneracy and it do not have the shape of a standard absorption peak but rather that of a derivative absorption peak, illustrated in Fig. 9.1.

Since relative intensities of the various bands in the absorption and MCD spectra can be very different, it is possible to use MCD spectroscopy in order to detect transitions that are absent or difficult to recognize in the absorption spectroscopy. The presence of nonzero $\mathcal{A}$ terms reveals the presence of degenerate states, something which is in general impossible from an ordinary absorption spectra.
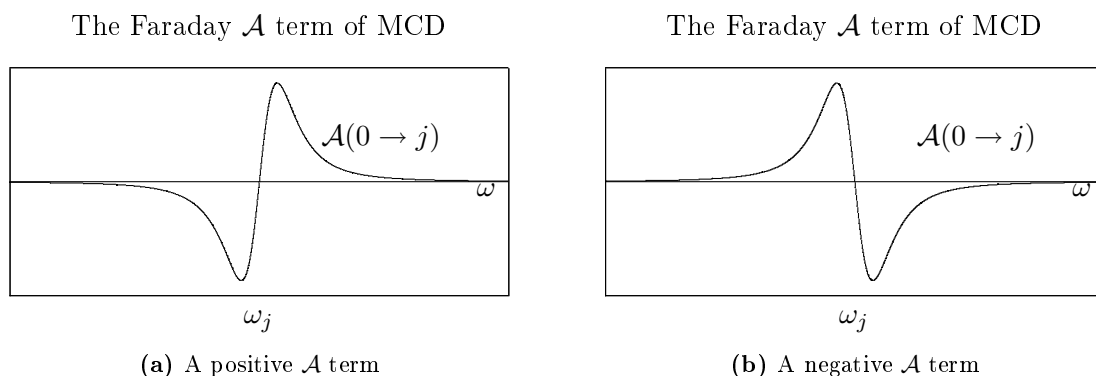
The Faraday $\mathcal{A}$ term of MCD



**(a)** A positive $\mathcal{A}$ term

The Faraday $\mathcal{A}$ term of MCD

**(b)** A negative $\mathcal{A}$ term

**Figure 9.1:** spectral profile for the Faraday $\mathcal{A}$ term for the transition to the exited state $j$

The Faraday $\mathcal{B}$ term of MCD



**(a)** A positive $\mathcal{B}$ term

The Faraday $\mathcal{B}$ term of MCD
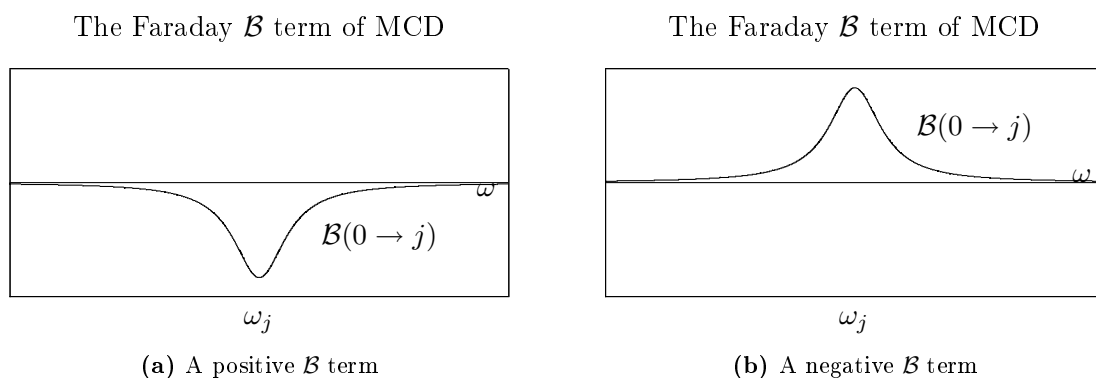
**(b)** A negative $\mathcal{B}$ term

**Figure 9.2:** spectral profile for the Faraday $\mathcal{B}$ term for the transition to the exited state $j$

The Faraday $\mathcal{B}$ term originates from a mixing of energy levels by the magnetic field and contributes regardless of the degeneracies of the involved states. The contribution from the $\mathcal{B}$ term have the shape of an absorption peak which can be either positive or negative (see Fig. 9.2) and it therefore represents a valuable supplement to UV spectra when it comes to identifying excited states, especially states hidden in UV spectra by overlapping bands.

The chapter is organized in the following way: First, we introduce the theory of MCD using damped response theory of chapter 7.3, and derive formulas for the $\mathcal{A}$ and $\mathcal{B}$ terms. Second, we show how individual $\mathcal{A}$ and $\mathcal{B}$ terms can be calculated using standard response theory, and the result obtained using CCSD and DFT. Third, we discuss a numerical instability, which can be circumvented using damped response theory.

## 9.2 Expression for the Ellipticity in terms of Response Functions

For plane-polarized light propagating in the $Z$ direction of a space-fixed frame the ellipticity $\theta$ of a sample of randomly moving molecules is, in the presence of a magnetic field directed along the $Z$ axis given by

68

$$\theta \;=\; \frac{1}{12}\omega\mu_0 clN\varepsilon_{\alpha\beta\gamma}\mathrm{Re}\left(\overline{\langle\langle\mu_\alpha;\mu_\beta,m_\gamma\rangle\rangle}_{\omega,0}\right)B_Z \tag{9.1}$$

This expression is in accordance with Ref. [93] (See Appendix 1 of paper **I** for more details). In Eq. (9.1) $\hat{m}_\alpha$ and $\hat{\mu}_\alpha$ are cartesian components of the magnetic and electric dipole operator in the molecular-fixed frame, $\omega$ is the optical (laser) frequency, $N$ is the number density, $\mu_0$ is the permeability of free space, $l$ is the length of the sample, and $c$ is the speed of light in vacuum. We have used the Einstein sum convention in connection with the Levi-Civita tensor $\varepsilon_{\alpha\beta\gamma}$, and $\overline{\langle\langle\mu_\alpha;\mu_\beta,m_\gamma\rangle\rangle}_{\omega,0}$ denotes a *damped quadratic response functions* in agreement with the notation in Section 7.3 and paper **D**.

note that the ellipticity $\theta$ is related to the molar ellipticity $[\theta]_M$ by

$$[\theta]_M \;=\; \frac{M\theta}{c\cdot l}, \tag{9.2}$$

where $\theta$ is the ellipticity in degrees, c the concentration in $g/100cm^3$, $M$ the molecular mass, and $l$ the path length in $dm$.

In order to obtain expressions which can more easily be compared to other derivations, we remind the reader that

$$\varepsilon_{\alpha\beta\gamma}\langle\langle\mu_\alpha;\mu_\beta,m_\gamma\rangle\rangle_{\omega,0}=\varepsilon_{\alpha\beta\gamma}\langle\langle\mu_\gamma;m_\beta,\mu_\alpha\rangle\rangle_{0,\omega} \tag{9.3}$$

and to ease the notation of the following sections we introduce the identifications

$$\hat{A}=\hat{\mu}_\gamma,\qquad \hat{B}=\hat{m}_\beta,\qquad \hat{C}=\hat{\mu}_\alpha \tag{9.4}$$

and change the indices of the Levi-Cevita tensor accordingly $(\varepsilon_{\alpha\beta\gamma}\to\varepsilon_{cba})$ in the expression for the ellipticity, i.e.,

$$\theta \;=\; \frac{1}{2}K\omega\mathrm{Re}\left(\varepsilon_{\alpha\beta\gamma}\overline{\langle\langle\mu_\gamma;m_\beta,\mu_\alpha\rangle\rangle}_{0,\omega}\right)=\frac{1}{2}K\omega\mathrm{Re}\left(\varepsilon_{cba}\overline{\langle\langle A;B,C\rangle\rangle}_{0,\omega}\right) \tag{9.5}$$

where $K=\frac{1}{6}\mu_0 clNB_Z$.

## 9.3 Calculating the Ellipticity using Damped Response Theory

Damped response theory can now be applied to obtain an expression for the damped quadratic response function $\overline{\langle\langle A;B,C\rangle\rangle}_{0,\omega}$

In the absorptive region where $\omega_c$ is close to an excitation energy $\omega_j$, only certain terms of the full damped quadratic response function contributes significantly, and for analysis purposes we may disregard the remaining terms. The terms that contribute in the absorptive region are the terms that would be singular in standard response theory (see Eq. (7.24) for $\omega_c=-\omega_a\approx\omega_j$).

It is therefore sufficient to consider only three terms and using the notation in paper **I**, we may write the simplified response functions as

$$\overline{\langle\langle A; B, C\rangle\rangle}_{0,\omega_c} = \sum_{p\neq 0}\sum_{q\neq 0} \frac{B^{0p}(A^{pq} - A^{00}\delta_{pq})C^{q0}}{(\omega_p + i\gamma)(\omega_q - \omega_c - i\gamma)}$$

$$+ \sum_{p\neq 0}\sum_{q\neq 0} \frac{A^{0p}B^{pq}C^{q0}}{(\omega_p + \omega_a - i\gamma)(\omega_q - \omega_c - i\gamma)} + \sum_{p\neq 0}\sum_{q\neq 0} \frac{A^{0p}(C^{pq} - C^{00}\delta_{pq})B^{q0}}{(\omega_p + \omega_a - i\gamma)(\omega_q - i\gamma)} \qquad (\omega_c \approx \omega_j).$$

$$(9.6)$$

Note that the summations run over positive indices only. Close to resonance ($\omega_c \approx \omega_j$) only $q = j_s{}^1$ will contribute significantly in the first term of Eq. (9.6), while for the second term both $q = j_s$ and $p = j_s$ will contribute. Finally in the last term only $p = j_s$ will contribute significantly. With these approximations one obtains

$$\overline{\langle\langle A; B, C\rangle\rangle}_{0,\omega_c} = \sum_{p\neq 0}\sum_{s} \frac{B^{0p}(A^{pj_s} - A^{00}\delta_{pj_s})C^{j_s0}}{(\omega_p + i\gamma)(\omega_j - \omega_c - i\gamma)}$$

$$+ \sum_{p\neq 0}\sum_{s} \frac{A^{0p}B^{pj_s}C^{j_s0}}{(\omega_p + \omega_a - i\gamma)(\omega_j - \omega_c - i\gamma)} + \sum_{q\neq 0}\sum_{s} \frac{A^{0j_s}B^{j_sq}C^{q0}}{(\omega_j + \omega_a - i\gamma)(\omega_q - \omega_c - i\gamma)}$$

$$+ \sum_{q\neq 0}\sum_{s} \frac{A^{0j_s}(C^{j_sq} - C^{00}\delta_{j_sq})B^{q0}}{(\omega_j + \omega_a - i\gamma)(\omega_q - i\gamma)} \qquad (\omega_c \approx \omega_j). \qquad (9.7)$$

Introducing the dispersion $\mathcal{D}_j(\omega)$ and absorption $\mathcal{A}_j(\omega)$ lineshape functions of Eq. (7.44), we may approximate Eq. (9.7) in the following manner

$$\overline{\langle\langle A; B, C\rangle\rangle}_{0,\omega_c} = \sum_{p\neq 0}\sum_{s} \Big( B^{0p}(A^{pj_s} - A^{00}\delta_{pj_s})C^{j_s0} \Big)\Big( \mathcal{D}_p(0) - i\mathcal{A}_p(0) \Big) i\mathcal{A}_j(\omega_c)$$

$$+ \sum_{p\neq 0}\sum_{s} \Big( B^{pj_s}C^{j_s0}A^{0p} \Big)\Big( \mathcal{D}_p(-\omega_a) + i\mathcal{A}_p(-\omega_a) \Big) i\mathcal{A}_j(\omega_c)$$

$$+ \sum_{q\neq 0}\sum_{s} \Big( B^{j_sq}C^{q0}A^{0j_s} \Big) i\mathcal{A}_j(-\omega_a)\Big( \mathcal{D}_q(\omega_c) + i\mathcal{A}_q(\omega_c) \Big)$$

$$+ \sum_{q\neq 0}\sum_{s} \Big( (C^{j_sq} - C^{00}\delta_{j_sq})B^{q0}A^{0j_s} \Big) i\mathcal{A}_j(-\omega_a)\Big( \mathcal{D}_q(0) + i\mathcal{A}_q(0) \Big) \qquad (\omega_c \approx \omega_j), \quad (9.8)$$

where we have used that $\mathcal{D}_j(\omega_c) = \mathcal{D}_j(-\omega_a) \approx 0$ (assuming $\gamma \gg |\omega_j - \omega_c|$). Taking the real part of this expression and combining terms using the Levi-Civita tensor yields

$$\text{Re}\Big( \varepsilon_{cba}\overline{\langle\langle A; B, C\rangle\rangle}_{0,\omega_c} \Big) = -2\sum_{p\neq 0}\sum_{s} \varepsilon_{cba}\text{Im}\Big( B^{0p}(A^{pj_s} - A^{00}\delta_{pj_s})C^{j_s0} \Big)\mathcal{D}_p(0)\mathcal{A}_j(\omega_c)$$

$$- 2\sum_{p\neq 0}\sum_{s} \varepsilon_{cba}\text{Im}\Big( B^{pj_s}C^{j_s0}A^{0p} \Big)\mathcal{D}_p(\omega_c)\mathcal{A}_j(\omega_c) \qquad (\omega_c \approx \omega_j), \qquad (9.9)$$

where we have also used that $\omega_a = -\omega_c$. Writing out the explicit term for $p = j_t$ in the second

---

¹$s$ denotes a component of the possibly degenerate state $j$

summation gives

$$\mathrm{Re}(\varepsilon_{cba}\overline{\langle\langle A;B,C\rangle\rangle}_{0,\omega_c}) = -2\sum_{p\neq 0}\sum_s \varepsilon_{cba}\mathrm{Im}\left(B^{0p}(A^{pj_s}-A^{00}\delta_{pj_s})C^{j_s0}\right)\mathcal{D}_p(0)\mathcal{A}_j(\omega_c)$$

$$-2\sum_{p\neq 0,p\neq\{j\}}\sum_s \varepsilon_{cba}\mathrm{Im}\left(B^{pj_s}C^{j_s0}A^{0p}\right)\mathcal{D}_p(\omega_c)\mathcal{A}_j(\omega_c)$$

$$-2\sum_{s,t}\varepsilon_{cba}\mathrm{Im}\left(B^{j_tj_s}C^{j_s0}A^{0j_t}\right)\mathcal{D}_j(\omega_c)\mathcal{A}_j(\omega_c) \qquad (\omega_c\approx\omega_j). \tag{9.10}$$

where $\{j\}$ denotes the set of (possibly degenerate) states with excitation energy $\omega_j$. The last term only contributes for a degenerate state, and according to the discussion in Section 9.1 we may define this term as the $\mathcal{A}$ term.

Assuming that the excited states are well–separated, we may use the approximation

$$\mathcal{D}_p(\omega_c) \approx \frac{1}{\omega_p-\omega_c}; \qquad \omega_c\approx\omega_j, \quad p\neq j \tag{9.11}$$

to rewrite Eq. (9.10)

$$\mathrm{Re}(\varepsilon_{cba}\overline{\langle\langle A;B,C\rangle\rangle}_{0,\omega_c}) = -2\sum_{st}\mathrm{Im}\left(B^{j_tj_s}C^{j_s0}A^{0j_t}\right)\mathcal{A}_j(\omega_c)\mathcal{D}_j(\omega_c)$$

$$-2\mathcal{A}_j(\omega_c)\sum_s\left(\sum_{p\neq 0}\frac{\mathrm{Im}(B^{0p}A^{pj_s}C^{j_s0})}{\omega_p} + 2\sum_{p\neq\{j\}}\frac{\mathrm{Im}(B^{pj_s}C^{j_s0}A^{0p})}{\omega_p-\omega_c}\right) \qquad (\omega_c\approx\omega_j), \tag{9.12}$$

We can now introduce the Faraday $\mathcal{A}$ and $\mathcal{B}$ terms in accordance with Ref. [93]

$$\mathcal{A}(0\to j) = \frac{1}{2}\sum_{st}\varepsilon_{cba}\mathrm{Im}\left(B^{j_tj_s}C^{j_s0}A^{0j_t}\right) = \frac{1}{2}\varepsilon_{cba}\sum_s B^{\tilde{j}_s\tilde{j}_s}\mathrm{Im}\left(A^{0\tilde{j}_s}C^{\tilde{j}_s0}\right) \tag{9.13a}$$

$$\mathcal{B}(0\to j) = \sum_s\varepsilon_{cba}\left(\sum_{p\neq 0}\frac{\mathrm{Im}(B^{0p}A^{pj_s}C^{j_s0})}{\omega_p} + \sum_{p\neq\{j\}}\frac{\mathrm{Im}(B^{pj_s}C^{j_s0}A^{0p})}{\omega_p-\omega}\right). \tag{9.13b}$$

For the $\mathcal{A}$ term we have expanded the real degenerate states $j_s$ in complex states $\tilde{j}_s$ which diagonalize the imaginary $\hat{B}$ operator.

Eq. (9.12) may now be expressed in terms of the Faraday $\mathcal{A}$ and $\mathcal{B}$ terms

$$\varepsilon_{cba}\mathrm{Re}(\overline{\langle\langle A;B,C\rangle\rangle}_{0,\omega_c}) = -2\mathcal{A}_j(\omega_c)\mathcal{B}(0\to j) - 4\mathcal{A}_j(\omega_c)\mathcal{D}_j(\omega_c)\mathcal{A}(0\to j) \quad (\omega_c\approx\omega_j). \tag{9.14}$$

Using that $\omega_c = \omega$ and inserting Eq. (9.14) into Eq. (9.5) we can obtain the following expression for the ellipticity

$$\theta = -\frac{1}{12}\omega\mu_0 clNB_Z\left(2\mathcal{A}_j(\omega)\mathcal{B}(0\to j) + 4\mathcal{A}_j(\omega)\mathcal{D}_j(\omega)\mathcal{A}(0\to j)\right) \qquad (\omega\approx\omega_j) \tag{9.15}$$

Noting that

$$\frac{\partial\mathcal{A}_j(\omega)}{\partial\omega} = 2\mathcal{D}_j(\omega)\mathcal{A}_j(\omega) \tag{9.16}$$

we recognize that the Faraday $\mathcal{B}$ terms are associated with an absorption lineshape function, and that the $\mathcal{A}$ terms are associated with a derivative lineshape function in agreement with previous findings

$$\theta = -\frac{1}{6}\omega\mu_0 clNB_z\left(\mathcal{A}_j(\omega)\mathcal{B}(0\to j) + \frac{\partial\mathcal{A}_j(\omega)}{\partial\omega}\mathcal{A}(0\to j)\right) \qquad (\omega\approx\omega_j). \tag{9.17}$$

Using Eq. (9.5) will therefore give a spectrum with contributions from both the Faraday $\mathcal{A}$ and $\mathcal{B}$ terms. Damped response theory may be used to determine the MCD spectra for *any* frequency range, and is therefore expected to become a very useful tool for calculating MCD spectra at arbitrary frequencies, also for large molecules.

The $\mathcal{A}$ and $\mathcal{B}$ term contributions cannot be separated using Eq. (9.5), but the spectral profile can be used to extract information about the individual $\mathcal{A}$ and $\mathcal{B}$ terms.

For clearly seperated peaks the $\mathcal{A}$ and $\mathcal{B}$ terms can be obtain according to the method-of-moments [116, 122] formula, which exploit the knowledge of the lineshape functions associated with the $\mathcal{A}$ and $\mathcal{B}$ terms [2].

$$\mathcal{B}(0 \to j) \;=\; -\frac{1}{33.53} \int_j \frac{[\theta]_M}{\tilde{\nu}} d\tilde{\nu} \tag{9.18}$$

$$\mathcal{A}(0 \to j) \;=\; \frac{1}{33.53} \int_j (\tilde{\nu} - \tilde{\nu}_0)\frac{[\theta]_M}{\tilde{\nu}} d\tilde{\nu}. \tag{9.19}$$

The units of $[\theta]_M$ is deg dl$^{-1}$ dm$^{-1}$ mol$^{-1}$ G$^{-1}$ giving the $\mathcal{A}$ term in units of D$^2\mu_B$ and the $\mathcal{B}$ term in units of D$^2\mu_B/cm^{-1}$, where D stands for Debye and $\mu_B$ is the Bohr magneton.

In the case of overlapping bands no reliable results for the individual $\mathcal{A}$ and $\mathcal{B}$ terms can be obtained. The experimentally obtained spectra face the same problem, and theoretical determined $\mathcal{A}$ and $\mathcal{B}$ terms can provide complementary insight into the origins of the MCD bands observed experimentally.

The individual $\mathcal{A}$ and $\mathcal{B}$ terms can be calculated directly using standard response function theory, and this will be the subject of the next section.

## 9.4 Faraday $\mathcal{A}$ and $\mathcal{B}$ terms using Standard Response Theory

Having defined the $\mathcal{A}$ and $\mathcal{B}$ terms of MCD in Eq. (9.13), these terms can be calculated as double and single residues of *standard* response functions, respectively. The advantage of this approach is that we directly calculate the individual $\mathcal{A}$ and $\mathcal{B}$ terms for each excited state. In contrast, a mixed spectrum containing contributions from all $\mathcal{A}$ and $\mathcal{B}$ terms is obtained using the *damped* response theory formalism in Sec. 9.3, see e.g. Eq. (9.17).

The $\mathcal{B}$ term can be identified from a single residue of the quadratic response function [123]

$$\mathcal{B}(0 \to j) = -\varepsilon_{cba}\mathrm{Im}\left\{ \lim_{\omega_b \to 0}\left( \lim_{\omega_c \to \omega_j}(\omega_c - \omega_j)\langle\langle A; B, C\rangle\rangle_{\omega_b,\omega_c} \right) \right\}. \tag{9.20}$$

In a similar manner the Faraday $\mathcal{A}$ term of Eq. (9.13a) can be obtained as a double residue of the quadratic response function

$$\mathcal{A}(0 \to j) = -\frac{1}{2}\varepsilon_{cba}\mathrm{Im}\left\{ \lim_{\omega_b \to 0}\left[ \lim_{\omega_a \to -\omega_j}(\omega_a + \omega_j)\left( \lim_{\omega_c \to \omega_j}(\omega_c - \omega_j)\langle\langle A; B, C\rangle\rangle_{\omega_b,\omega_c} \right) \right] \right\} \tag{9.21}$$

---

[2]The method-of-moments expressions rely on different lineshape functions than Eq.(7.44), but the general principle is applicable

Eq. (9.20) has already in 1999 been used to determine the $\mathcal{B}$ terms using HF and the Multi-configurational Self-Consistent-Field (MCSCF) model [123], but the result obtained in Ref. [123], have an unphysical dependence on the gauge-origin of the magnetic vector potential.

Gauge-origin independence of many magnetic properties may be obtained using the pertur-bation dependent London atomic orbitals (LAO) [124, 125], often referred to as gauge-including atomic orbitals (GIAO). In section 2.3 of paper **E**, we show that any property that can be ex-pressed as a magnetic derivative is automatically gauge-origin independent provided that LAOs are used.

The $\mathcal{A}$ and $\mathcal{B}$ terms can be expressed as a magnetic derivative of the magnetic-field perturbed excitation frequency [126] and one-photon dipole transition strength $S^{0j}_{\alpha\beta}(B)$ [127], respectively.

$$\mathcal{A}(0 \to j) = -\frac{1}{2}\varepsilon_{\alpha\beta\gamma}\sum_s \left(\frac{\partial \omega_{j_s}}{\partial B_\gamma}\bigg|_{B_\gamma=0}\right)\text{Im}(\mu^{0j_s}_\alpha \mu^{j_s 0}_\beta) \tag{9.22a}$$

$$\mathcal{B}(0 \to j) = \frac{1}{2}\varepsilon_{\alpha\beta\gamma}\text{Im}\left(\frac{dS^{0j}_{\alpha\beta}(B)}{dB_\gamma}\bigg|_{B_\gamma=0}\right), \qquad S^{0j}_{\alpha\beta}(B) = \mu^{0j}_\alpha(B)\mu^{j0}_\beta(B). \tag{9.22b}$$

Eq. (9.22b) have been the starting point for both the CCSD treatment of paper **A** and the DFT method presented in paper **E**. We note however, that Eqs. (9.21) and (9.20) can be used to determine gauge-origin independent $\mathcal{A}$ and $\mathcal{B}$ terms using the recently developed framework of Ref. [128], where perturbation dependent basis sets are an integrated part of the description. This method is superior from an implementation point of view, as almost no property specific programming is required, once the framework of Ref. [128] have been implemented.

## 9.5 Faraday $\mathcal{B}$ term within the Coupled Cluster Singles and Doubles Model

Eq. (9.22b) have been implemented at the CCSD [127] level of theory and paper **A**, applied the method to a number of selected molecules.

The complexity of most spectra, due to vibronic coupling and strongly overlapping bands, often results in a crude estimate of the magnitude of the $\mathcal{B}$ terms, and the experimentally derived values are then only expected to be slightly better than order-of-magnitude estimates[129]. Furthermore, the theoretical results do not take solvent or vibrational effects into account, thus a quantitative agreement with experiment cannot be expected. However, for non-overlapping bands the calculated $\mathcal{B}$ terms were found to be in good agreement with the experimental values.

This is illustrated in Table 9.1 where both calculated and experimental results [129, 130] are listed for Pyrimidine

We note that uncertainties of about ten percent are typical for molecular properties obtained at the CCSD level of theory. The CCSD/aug-cc-pVDZ oscillator strengths and $\mathcal{B}$ terms are therefore expected to bear such an uncertainty, although this uncertainty is still much smaller than the experimental uncertainty. The CCSD error is most obvious in the calculated excitation

| State | CCSD/aug-cc-pVDZ | | Experimental | | | |
|---|---|---|---|---|---|---|
| | $f$ | $\mathcal{B}$ term | $f$[129] | $f$[130] | $\mathcal{B}$ term[129] | $\mathcal{B}$ term$f$[130] |
| $B_1$ | 0.006 | -0.068 | 0.007 | 0.0073 | -0.06 | -0.076 |
| $B_2$ | 0.028 | 0.210 | 0.03 | 0.033 | 0.2 | 0.24 |

**Table 9.1:** The oscillator strengths $f$ and the Faraday $\mathcal{B}$ terms $(10^{-3}\mathrm{D}^2\mu_B\mathrm{cm})$ for the lowest transitions of pyrimidine.
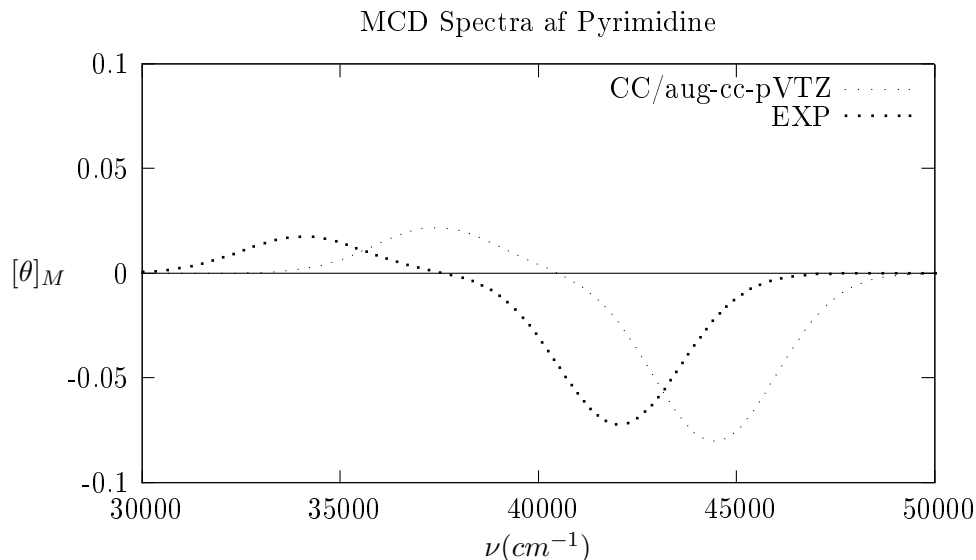


**Figure 9.3:** Pyrimidine: Comparison of experiment and simulated MCD spectra for CCSD.

energies, and the theoretical CCSD spectra must be parallel displaced in order to obtain an agreement with experiment, evident from Fig 9.3. Calculated CC3 excitation energies confirms that the major contribution for this parallel displacement is due to correlation beyond CCSD as seen when comparing vertical CCSD and CC3 equilibrium-geometry excitation energies in Table 9.2.

For overlapping bands, large deviations occurs compared to the experimental obtained $\mathcal{B}$ terms. In order to examine this deviation, lineshape functions may be superimposed onto the $\mathcal{B}$ terms in order to simulate the experimental spectrum. Using this method, the large deviation is attributed to the large cancellation of positive and negative contributions which may occur between positive and negative $\mathcal{B}$ term contributions, resulting in reduced magnitudes of experi-

| State | Vertical excitation | | Experimental | |
|---|---|---|---|---|
| | CCSD/aug-cc-pVDZ | CC3/aug-cc-pVDZ | | |
| $B_1$ | 4.64 | 4.46 | 4.22[2] | 4.29[3] |
| $B_2$ | 5.51 | 5.40 | 5.21[2] | 5.17[3] |

**Table 9.2:** Excitation energies (eV) for the lowest transitions of pyrimidine.

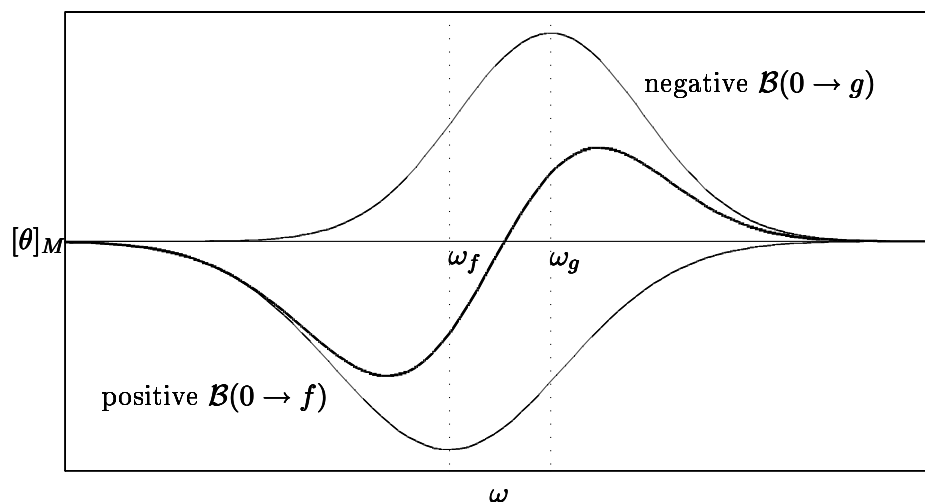The cancellation of positive and negative $\mathcal{B}$ term contributions to MCD



**Figure 9.4:** Illustation of the cancellation which occurs between a positive and a negative $\mathcal{B}$ term contribution (thin line) to the full MCD spectra (thick line). The dashed lines indicate the vertical excitation energies.

mentally measured $\mathcal{B}$ terms. This is illustrated in Fig. 9.4. In addition, the peaks of the MCD spectrum may also move, and the location of the peak maxima does not necessarly correspond to a vertical excitation energy, this is illustrated in Fig. 9.4. The calculated $\mathcal{B}$ may therefore diviate from experimental obtained $\mathcal{B}$ terms, and great caution must therefore be exercised before individual $\mathcal{B}$ terms are compared to experimentally obtained $\mathcal{B}$ terms.

For all the investigated molecules of paper **A**, the CCSD theoretically produced spectra are in good agreement with the experimental spectra, and the CCSD results of paper **A** is still the most accurate MCD results obtained to date.

## 9.6 Faraday $\mathcal{B}$ term within Kohn-Sham Density Functional Response Theory

Eq. (9.22b) have also been implemented at the DFT level of theory using the Lagrange's method of undetermined multipliers to derive efficient computational expressions for the $\mathcal{B}$ term (see paper **E**).

The method is similar to the method presented in Chapter 8 except for the last step where the lagrangian function is differentiated with respect to a magnetic field instead of the nuclear coordinates. For the full theoretical derivation, we refer the reader to paper **E**.

The $\mathcal{B}$ term of MCD represent quite a challenging task for DFT, since it requires an accurate description of both the excited states, and the magnetic perturbation. To estimate the quality of different DFT functionals, TD-DFT results have traditionally been benchmarked against results from higher level Coupled Cluster models, and for the DFT method of paper **E** we benchmark
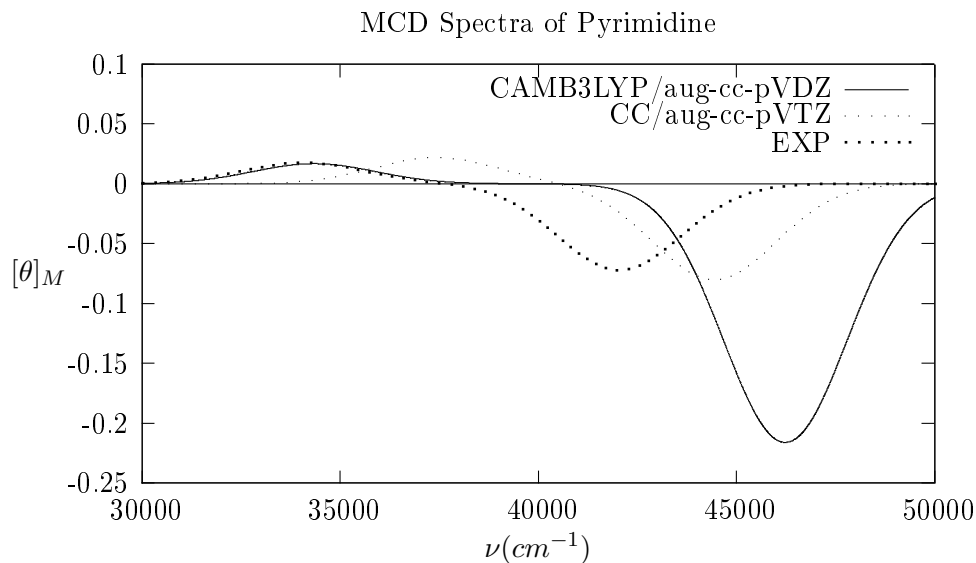
**Figure 9.5:** Pyrimidine: Comparison of simulated MCD spectra for CAMB3LYP and CCSD.

against the CCSD results of paper **A**.

The first excited state of pyrimidine was found to be quite well described, as illustrated in Table 9.3, which contains the CAMB3LYP [131] and CCSD results for the first two excited states. For the individual $\mathcal{B}$ terms, the deviation from the CCSD results seems to lack a systematic behavior and we believe that an extensive benchmark study is required before a specific DFT functional can be recommended.

| CCSD/aug-cc-pVDZ-CM [3] | | | | CAMB3LYP/aug-cc-pVDZ | | | |
|---|---|---|---|---|---|---|---|
| State | $\omega_f$ | $f$ | $\mathcal{B}$ term | State | $\omega_f$ | $f$ | $\mathcal{B}$ term |
| $1B_1$ | 4.64 | 0.006 | -0.068 | $1B_1$ | 4.548 | 0.005 | -0.065 |
| $1B_2$ | 5.51 | 0.028 | 0.210 | $1B_2$ | 5.799 | 0.046 | 0.528 |
| $2B_1$ | 6.51 | 0.006 | -0.055 | $2B_1$ | 6.301 | 0.006 | -0.069 |
| $2B_2$ | 6.68 | 0.008 | 0.017 | $1A_1$ | 6.651 | 0.042 | -0.872 |
| $1A_1$ | 6.98 | 0.027 | -0.267 | $2B_2$ | 6.836 | 0.004 | 0.0275 |

**Table 9.3:** The oscillator strengths $f$ and the Faraday $\mathcal{B}$ terms $(10^{-3}D^2\mu_B cm)$ for the lowest transitions of pyrimidine.

The TD-DFT MCD spectra was found to reproduce most of the qualitative features of the CCSD spectra, at least for the first few excited states, illustrated in figure 9.5.

Other MCD TD-DFT methods[123, 126, 127, 132–143] confirm that the TD-DFT MCD spectra reproduce most of the qualitative features of the CCSD spectra, although for this property we would discourage the use of TD-DFT results as a predictive tool, until an extensive benchmark study have been performed.

In the discussion of damped response theory, we mentioned that the density of states in-
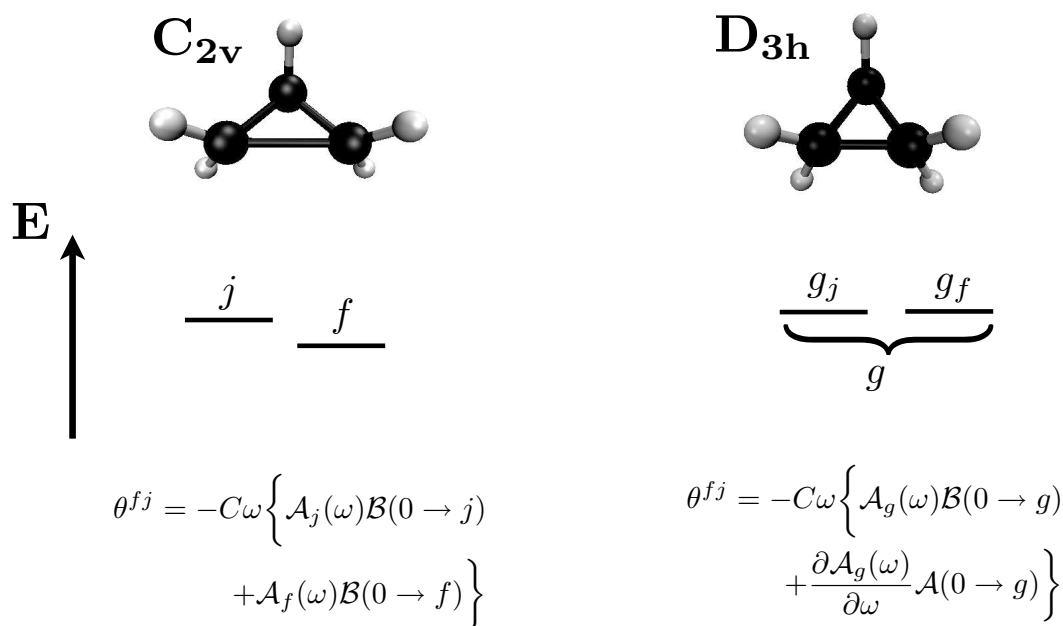
**C$_{2v}$**

**D$_{3h}$**

**E**

$$j \qquad f$$

$$g_j \qquad g_f$$

$$g$$

$$\theta^{fj} = -C\omega \left\{ \mathcal{A}_j(\omega)\mathcal{B}(0 \rightarrow j) \right.$$
$$\left. + \mathcal{A}_f(\omega)\mathcal{B}(0 \rightarrow f) \right\}$$

$$\theta^{fj} = -C\omega \left\{ \mathcal{A}_g(\omega)\mathcal{B}(0 \rightarrow g) \right.$$
$$\left. + \frac{\partial \mathcal{A}_g(\omega)}{\partial \omega} \mathcal{A}(0 \rightarrow g) \right\}$$

**Figure 9.6:** The degenerate $E'$ state ($g$) of cyclopropane in a $D_{3h}$ configuration (depicted on the right) will have both an $\mathcal{A}$ and a $\mathcal{B}$ term contribution to the ellipticity. Increasing one of the $\widehat{CCC}$ angles will break the $D_{3h}$ symmetry and give rise to the $C_{2v}$ configuration (depicted on the left), thereby breaking the degeneracy of the $E'$ state, which then evolves into two seperate states ($f$ and $j$) of $B_1$ and $B_2$ symmetry. These two states will both contribute with a $\mathcal{B}$ term.

creases significantly with increasing frequency and molecular size. Theoretical determination of individual $\mathcal{B}$ terms are therefore limited to small and medium size systems. This problem is circumvented using damped response theory, but then no reliable individual $\mathcal{B}$ terms can be obtained. In addition, the construction of theoretical MCD spectra based on individual $\mathcal{B}$ terms can be problematic for near degenerate states. For near degenerate states the construction of theoretical MCD spectra is numerically unstable. This instability is the focus of the next section and may be remedied by the use of damped response theory.

## 9.7   Numerical Instabilities

Consider the cyclopropane molecule on the right of Fig. 9.6, which has a doubly-degenerate state $g$ with two components $g_f$ and $g_j$. This degenerate state has an $\mathcal{A}$ and a $\mathcal{B}$ term contribution to the MCD spectra illustrated in Fig. 9.6.

Changing one of the $\widehat{CCC}$ angles of this molecule lowers the molecular symmetry from $D_{3h}$ to $C_{2v}$ (Fig. 9.6 left) causing the degenerate $g$ state to split into two non-degenerate states $f$ and $j$. The $f$ and $j$ states both have a $\mathcal{B}$ term contribution to the ellipticity.

Naturally, the MCD spectra should be a smooth function of the angle, and in this section we show that as the $\widehat{CCC}$ angle approaches $60°$ (i.e. going from left to right in Fig. 9.6) the two $\mathcal{B}$ terms for $f$ and $j$ turn into a $\mathcal{B}$ term and an $\mathcal{A}$ term for the degenerate $g$ state. The $\mathcal{A}$ term enters when the states $f$ and $j$ approach each other because a factor in the lineshape function

cancels a term in the original $\mathcal{B}$ terms for the states $f$ and $j$. This cancellation is the reason for the numerical instabilities observed when lineshape functions are superimposed onto the $\mathcal{B}$ terms calculated using standard response theory. In contrast, using the damped response theory formulation for MCD the lineshape functions are build into the theory and no such instability occurs.

We now prove how the two $\mathcal{B}$ terms in Fig. 9.6 (left) turn into the $\mathcal{A}$ and $\mathcal{B}$ terms in Fig. 9.6 (right) when the molecular symmetry is changed. Assuming a $\widehat{CCC}$ angle different from $60°$ the ellipticity contribution from the two states $f$ and $j$ is denoted $\theta^{fj}$ and is given as

$$\theta^{fj} = -KB_Z\omega\mathcal{A}_j(\omega)\mathcal{B}(0 \to j) - KB_Z\omega\mathcal{A}_f(\omega)\mathcal{B}(0 \to f). \tag{9.23}$$

Inserting the lineshape functions yields

$$\theta^{fj} = -\frac{KB_Z\omega\gamma}{(\omega_j - \omega)^2 + \gamma^2}\mathcal{B}(0 \to j) - \frac{KB_Z\omega\gamma}{(\omega_f - \omega)^2 + \gamma^2}\mathcal{B}(0 \to f), \tag{9.24}$$

and introducing $\mathcal{Q} = \left[(\omega_j - \omega)^2 + \gamma^2\right]\left[(\omega_f - \omega)^2 + \gamma^2\right]$ we obtain,

$$\theta^{fj} = -\frac{KB_Z\omega\gamma\left[(\omega_f - \omega)^2 + \gamma^2\right]}{\mathcal{Q}}\mathcal{B}(0 \to j) - \frac{KB_Z\omega\gamma\left[(\omega_j - \omega)^2 + \gamma^2\right]}{\mathcal{Q}}\mathcal{B}(0 \to f). \tag{9.25}$$

Since $\gamma$ is a very small number we can neglect terms containing $\gamma^3$. Inserting the $\mathcal{B}$ terms using Eq. (9.13b) then gives,

$$
\begin{aligned}
\theta^{fj} &= \frac{KB_Z\omega\gamma(\omega_f - \omega)^2}{\mathcal{Q}}\varepsilon_{cba}\left(\sum_{p\neq 0}\frac{\mathrm{Im}(B^{0p}A^{pj}C^{j0})}{\omega_p} + \sum_{p\neq\{j\}}\frac{\mathrm{Im}(B^{pj}C^{j0}A^{0p})}{\omega_p - \omega}\right) \\
&+ \frac{KB_Z\omega\gamma(\omega_j - \omega)^2}{\mathcal{Q}}\varepsilon_{cba}\left(\sum_{p\neq 0}\frac{\mathrm{Im}(B^{0p}A^{pf}C^{f0})}{\omega_p} + \sum_{p\neq\{f\}}\frac{\mathrm{Im}(B^{pf}C^{f0}A^{0p})}{\omega_p - \omega}\right). \tag{9.26}
\end{aligned}
$$

In the second term we now write out explicitly the term containing $p = f$ and in the fourth term we do the same for $p = j$,

$$
\begin{aligned}
\theta^{fj} &= \frac{KB_Z\omega\gamma(\omega_f - \omega)^2}{\mathcal{Q}}\varepsilon_{cba}\left(\sum_{p\neq 0}\frac{\mathrm{Im}(B^{0p}A^{pj}C^{j0})}{\omega_p} + \sum_{p\neq\{j,f\}}\frac{\mathrm{Im}(B^{pj}C^{j0}A^{0p})}{\omega_p - \omega}\right) \\
&+ \frac{KB_Z\omega\gamma(\omega_j - \omega)^2}{\mathcal{Q}}\varepsilon_{cba}\left(\sum_{p\neq 0}\frac{\mathrm{Im}(B^{0p}A^{pf}C^{f0})}{\omega_p} + \sum_{p\neq\{j,f\}}\frac{\mathrm{Im}(B^{pf}C^{f0}A^{0p})}{\omega_p - \omega}\right) \\
&+ \frac{KB_Z\omega\gamma(\omega_f - \omega)^2}{\mathcal{Q}}\varepsilon_{cba}\frac{\mathrm{Im}(B^{fj}C^{j0}A^{0f})}{\omega_f - \omega} + \frac{KB_Z\omega\gamma(\omega_j - \omega)^2}{\mathcal{Q}}\varepsilon_{cba}\frac{\mathrm{Im}(B^{jf}C^{f0}A^{0j})}{\omega_j - \omega}. \tag{9.27}
\end{aligned}
$$

Note that the last two terms are singular in the absence of the lineshape functions at $\omega = \omega_f$ and $\omega = \omega_j$, respectively. This does not pose a problem in damped response theory where the lineshape functions are an integrated part of the formulation, and the $(\omega_f - \omega)^{-1}$ singularity in Eq. (9.27) is removed by the $(\omega_f - \omega)^2$ factor (and similarly for the $(\omega_j - \omega)$ term). However, using the standard response theory formulation of MCD in Sec. 9.4, $\theta^{fj}$ may be numerically unstable due to the presence of the $(\omega_f - \omega)^{-1}$ and $(\omega_j - \omega)^{-1}$ factors in the individual $\mathcal{B}$ terms (see Eq. (9.13b)).

Let us now change the $\widehat{CCC}$ angle to $60°$, such that the non-degenerate states $f$ and $j$ become degenerate (i.e. $\omega_f \to \omega_g$, $\omega_j \to \omega_g$, $f \to g_f$, and $j \to g_j$ ). This changes Eq. (9.27) in the following way,

$$
\begin{aligned}
\theta^{fj} &= KB_Z\omega\mathcal{A}_g(\omega)\sum_j \varepsilon_{cba}\left(\sum_{p\neq 0}\frac{\mathrm{Im}(B^{0p}A^{pg_j}C^{g_j0})}{\omega_p} + \sum_{p\neq\{g\}}\frac{\mathrm{Im}(B^{pg_j}C^{g_j0}A^{0p})}{\omega_p - \omega_c}\right)\\
&+ \frac{KB_Z\omega\gamma(\omega_g - \omega)}{\mathcal{Q}}\sum_{jf}\varepsilon_{cba}\mathrm{Im}(B^{g_fg_j}C^{g_j0}A^{0g_f}).
\end{aligned} \tag{9.28}
$$

In this equation, we have in the first term used the approximation $\mathcal{A}_g(\omega) \approx \frac{\gamma(\omega_g-\omega)^2}{\mathcal{Q}}$ and we recognize the $\mathcal{B}(0 \to g)$ term from Eq. (9.13b). In the second term we have included terms which are zero ($B^{g_fg_f} = B^{g_jg_j} = 0$) in order to obtain the summation over degenerate components and recognize the $\mathcal{A}$ term in Eq. (9.13a),

$$
\theta^{fj} = -KB_Z\omega\mathcal{A}_g(\omega)\mathcal{B}(0 \to g) - 2\frac{KB_Z\omega\gamma(\omega_g - \omega)}{\mathcal{Q}}\mathcal{A}(0 \to g). \tag{9.29}
$$

Inserting the denominator $\mathcal{Q}$, we recognize the derivative lineshape function $\frac{\partial\mathcal{A}_g(\omega)}{\partial\omega}$,

$$
\theta^{fj} = -KB_Z\omega\left(\mathcal{A}_g(\omega)\mathcal{B}(0 \to g) + \frac{\partial\mathcal{A}_g(\omega)}{\partial\omega}\mathcal{A}(0 \to g)\right) \tag{9.30}
$$

We have thus established that $\theta^{fj}$ in Fig. 9.6 (left) turns into $\theta^{fj}$ in Fig. 9.6 (right) when the $f$ and $j$ states become degenerate. We therefore see that the $\mathcal{A}$ term is nothing more than a special occurrence of the $\mathcal{B}$ terms stemming from the excitation to a degenerate excited state. However, in order to provide a smooth description as a function of the $\widehat{CCC}$ angle, the lineshape function must be an integrated part of the description as is the case for the damped response theory formulation of MCD in Sec. 9.3. The standard response theory formulation of MCD in Sec. 9.4, where the individual $\mathcal{A}$ and $\mathcal{B}$ terms are calculated may, be subject to numerical instabilities as discussed in connection with Eq. (9.27). Care must therefore be exerted when using this approach to simulate an MCD spectrum for a molecule with near degeneracies.

In conclusion, it is therefore recommended that the individual $\mathcal{B}$ terms are calculated when possible, and that damped response theory are used in the case of near degeneracies or when the density of states becomes to large.

# Bibliography

[1] DALTON, *a molecular electronic structure program, Release 2.0*, 2005. See http://www.kjemi.uio.no/software/dalton/dalton.html.

[2] DEC, *Divide-expand-consolidate coupled-cluster (DEC-CC) program*, 2010. See http://sourceforge.net/projects/deccc/.

[3] F. Pawłowski, P. Jørgensen, J. Olsen, F. Hegelund, T. Helgaker, J. Gauss, K. L. Bak and J. F. Stanton, J. Chem. Phys. **116**(15), 6482 (2002).

[4] A. Tajti, P. G. Szalay, A. G. Császár, M. Kállay, J. Gauss, E. F. Valeev, B. A. Flowers, J. Vázquez and J. F. Stanton, J. Chem. Phys. **121**(23), 11599 (2004).

[5] E. Schrödinger, Phys. Rev. **28**(6), 1049 (1926).

[6] S. Goedecker, Rev. Mod. Phys. **71**(4), 1085 (1999).

[7] S. Goedecker and G. E. Scuseria, Comp. Sci. Eng. **5**(4), 14 (2003).

[8] J. Almlöf, K. Faegri Jr. and K. Korsell, J. Comp. Chem. **3**(3), 385 (1982).

[9] R. Ahlrichs, Theor. Chim. Acta. **33**(2), 157 (1974).

[10] V. Dyczmons, Theor. Chim. Acta. **28**(3), 307 (1973).

[11] M. Häser and R. Ahlrichs, J. Comp. Chem. **10**(1), 104 (1988).

[12] D. S. Lambrecht and C. Ochsenfeld, J. Chem. Phys. **123**(18), 184101 (2005).

[13] L. Greengard and V. Rokhlin, J. Comp. Phys. **73**(2), 325 (1987).

[14] C. A. White, B. G. Johnson, P. M. W. Gill and M. Head-Gordon, Chem. Phys. Lett. **230**(1-2), 8 (1994).

[15] M. C. Strain, G. E. Scuseria and M. J. Frisch, Science. **271**, 51 (1996).

[16] M. Challacombe and E. Schwegler, J. Chem. Phys. **106**(13), 5526 (1997).

[17] Y. Shao and M. Head-Gordon, Chem. Phys. Lett. **323**(5-6), 425 (2000).

[18] E. Schwegler and M. Challacombe, J. Chem. Phys. **105**(7), 2726 (1996).

[19] E. Schwegler, M. Challacombe and M. Head-Gordon, J. Chem. Phys. **106**(23), 9708 (1997).

[20] C. Ochsenfeld, C. A. White and M. Head-Gordon, J. Chem. Phys. **109**(5), 1663 (1998).

[21] P. Hohenberg and W. Kohn, Phys. Rev. **136**(3B), B864 (1964).

[22] W. Kohn and L. J. Sham, Phys. Rev. **140**(4A), A1133 (1965).

[23] J. Pérez-Jordá and W. Yang, Chem. Phys. Lett. **241**(4), 469 (1995).

[24] R. E. Stratmann, G. E. Scuseria and M. J. Frisch, Chem. Phys. Lett. **257**(3-4), 213 (1996).

[25] M. Challacombe, J. Chem. Phys. **113**(22), 10037 (2000).

[26] J. Kong, S. T. Brown and L. Fusti-Molnar, J. Chem. Phys. **124**(9), 094109 (2006).

[27] J. L. Whitten, J. Chem. Phys. **58**(10), 4496 (1973).

[28] E. J. Baerends, D. E. Ellis and P. Ros, Chem. Phys. **2**(1), 41 (1973).

[29] B. I. Dunlap, J. W. D. Connolly and J. R. Sabin, J. Chem. Phys. **71**(8), 3396 (1979).

[30] B. I. Dunlap, J. W. D. Connolly and J. R. Sabin, J. Chem. Phys. **71**(12), 4993 (1979).

[31] S. Boys and I. shavitt, University of Wisconsin Rept. WIS-AF-13. (1959).

[32] M. D. Newton, N. S. Ostlund and J. A. Pople, J. Chem. Phys. **49**(11), 5192 (1968).

[33] M. D. Newton, J. Chem. Phys. **51**(9), 3917 (1969).

[34] F. P. Billingsley and J. E. Bloor, Chem. Phys. Lett. **4**(1), 48 (1969).

[35] F. P. Billingsley and J. E. Bloor, J. Chem. Phys. **55**(11), 5178 (1971).

[36] F. Weigend, Physical Chemistry Chemical Physics. **4**, 4285 (2002).

[37] A. Sodt, J. E. Subotnik and M. Head-Gordon, J. Chem. Phys. **125**(19), 194109 (2006).

[38] B. Dunlap, J Mol Struc.(Theochem). **501**, 221 (2000).

[39] Y. Jung, A. Sodt, P. Gill and M. Head-Gordon, P Natl Acad Sci Usa. **102**, 6692 (2005).

[40] O. Vahtras, J. Almlöf and M. Feyereisen, Chem. Phys. Lett. **213**(5-6), 514 (1993).

[41] R. T. Gallant and A. St-Amant, Chem. Phys. Lett. **256**(6), 569 (1996).

[42] M. J. G. Peach, P. Benfield, T. Helgaker and D. J. Tozer, J. Chem. Phys. **128**(4), 044118 (2008).

[43] T. Helgaker, P. Jørgensen and J. Olsen. *Molecular Electronic-Structure Theory*. John Willey & Sons, Chichester, 2002.

[44] G. D. Purvis and R. J. Bartlett, J. Chem. Phys. **76**(4), 1910 (1982).

[45] J. Noga and R. J. Bartlett, J. Chem. Phys. **86**(12), 7041 (1987).

[46] C. Møller and M. S. Plesset, Phys. Rev. **46**(7), 618 (1934).

[47] K. Raghavachari, G. W. Trucks, J. A. Pople and M. Head-Gordon, Chem. Phys. Lett. **157**(6), 479 (1989).

[48] J. E. Subotnik and M. Head-Gordon, J. Chem. Phys. **122**(3), 034109 (2005).

[49] J. Almlöf, Chem. Phys. Lett. **181**(4), 319 (1991).

[50] M. Haser and J. Almlof, J. Chem. Phys. **96**(1), 489 (1992).

[51] D. S. Lambrecht, B. Doser and C. Ochsenfeld, J. Chem. Phys. **123**(18), 184102 (2005).

[52] B. Doser, D. S. Lambrecht and C. Ochsenfeld, Phys. Chem. Chem. Phys. **10**, 3335 (2008).

[53] B. Doser, D. S. Lambrecht, J. Kussmann and C. Ochsenfeld, J. Chem. Phys. **130**(6), 064107 (2009).

[54] C. Ochsenfeld, J. Kussmann and D. S. Lambrecht, Linear-scaling methods in quantum chemistry, in *Reviews in computational chemistry, Volume 23*, edited by K. B. Lipkowitz and T. R. Cundari. VCH Publishers, Inc., New York, 2007.

[55] O. Christiansen, H. Koch and P. Jørgensen, Chem. Phys. Lett. **243**(5-6), 409 (1995).

[56] M. Ziółkowski, B. Jansík, P. Jørgensen and J. Olsen, J. Chem. Phys. **131**(12), 124112 (2009).

[57] S. F. Boys, Rev. Mod. Phys. **32**(2), 296 (1960).

[58] C. Edmiston and K. Ruedenberg, Rev. Mod. Phys. **35**(3), 457 (1963).

[59] C. Edmiston and K. Ruedenberg, J. Chem. Phys. **43**(10), S97 (1965).

[60] W. von Niessen, J. Chem. Phys. **56**(9), 4290 (1972).

[61] J. Pipek and P. G. Mezey, J. Chem. Phys. **90**(9), 4916 (1989).

[62] J. Pipek, Int. J. Quantum Chem. **36**, 487 (1989).

[63] D. A. Kleier, T. A. Halgren, John H. Hall and W. N. Lipscomb, J. Chem. Phys. **61**(10), 3905 (1974).

[64] V. Magnasco and A. Perico, J. Chem. Phys. **47**(3), 971 (1967).

[65] F. Aquilante, T. B. Pedersen, A. S. de Meras and H. Koch, J. Chem. Phys. **125**(17), 174101 (2006).

[66] J. E. Subotnik, A. D. Dutoi and M. Head-Gordon, J. Chem. Phys. **123**, 114108 (2005).

[67] P. Pulay, Chem. Phys. Lett. **100**(2), 151 (1983).

[68] S. Saebø and P. Pulay, Ann. Rev. Phys. Chem. **44**(1), 213 (1993).

[69] R. B. Murphy, M. D. Beachy, R. A. Friesner and M. N. Ringnalda, J. Chem. Phys. **103**(4), 1481 (1995).

[70] G. Reynolds, T. J. Martinez and E. A. Carter, J. Chem. Phys. **105**(15), 6455 (1996).

[71] M. Schütz, G. Hetzer and H.-J. Werner, J. Chem. Phys. **111**(13), 5691 (1999).

[72] C. Hampel and H.-J. Werner, J. Chem. Phys. **104**(16), 6286 (1996).

[73] J. E. Subotnik, A. Sodt and M. Head-Gordon, J. Chem. Phys. **125**(7), 074116 (2006).

[74] J. E. Subotnik, A. Sodt and M. Head-Gordon, J. Chem. Phys. **128**(3), 034103 (2008).

[75] G. Hetzer, M. Schutz, H. Stoll and H.-J. Werner, J. Chem. Phys. **113**(21), 9443 (2000).

[76] M. Schütz and H.-J. Werner, J. Chem. Phys. **114**(2), 661 (2001).

[77] M. Schütz, J. Chem. Phys. **113**, 9986 (2000).

[78] G. E. Scuseria and P. Y. Ayala, J. Chem. Phys. **111**(18), 8330 (1999).

[79] J. E. Subotnik, A. Sodt and M. Head-Gordon, J. Chem. Phys. **125**(7), 074116 (2006).

[80] N. Flocke and R. J. Bartlett, J. Chem. Phys. **121**(22), 10935 (2004).

[81] S. Li, J. Ma and Y. Jiang, J. Comp. Chem. **23**, 237 (2001).

[82] M. Kobayashi and H. Nakai, J. Chem. Phys. **129**(4), 044103 (2008).

[83] D. G. Fedorov and K. Kitaura, J. Chem. Phys. **123**(13), 134103 (2005).

[84] J. Friedrich, M. Hanrath and M. Dolg, J. Chem. Phys. **126**(15), 154110 (2007).

[85] J. W. Boughton and P. Pulay, J. Comp. Chem. **14**, 736 (1993).

[86] R. K. Nesbet, Phys. Rev. **155**(1), 51 (1967).

[87] R. K. Nesbet, Phys. Rev. **175**(1), 2 (1968).

[88] P. Sałek, S. Høst, L. Thøgersen, P. Jørgensen, P. Manninen, J. Olsen, B. Jansík, S. Reine, F. Pawłowski, E. Tellgren, T. Helgaker, and S. Coriani, J. Chem. Phys. **126**(11), 114110 (2007).

[89] M. Ziółkowski, V. Weijo, P. Jørgensen and J. Olsen, J. Chem. Phys. **128**(20), 204105 (2008).

[90] J. Olsen and P. Jørgensen, J. Chem. Phys. **82**, 3235 (1985).

[91] P. Ehrenfest, Z. Phys. **45**, 455 (1927).

[92] A. S. Davydov. *Quantum Mechanics*. Pergamon Press Ltd, 1965.

[93] L. D. Barron. *Molecular Light Scattering and Optical Activity. Second Edition revised and enlarged.* Cambridge University Press, Cambridge, 2004.

[94] P. Norman, D. M. Bishop, H. J. A. Jensen and J. Oddershede, J. Chem. Phys. **123**(19), 194103 (2005).

[95] R. W. Boyd. *Nonlinear Optics*. Academic, San Diego, 1992.

[96] P. Norman, D. M. Bishop, H. J. A. Jensen and J. Oddershede, J. Chem. Phys. **115**(22), 10323 (2001).

[97] P. W. Milonni and J. H. Eberly. *Lasers*. Wiley, 1988.

[98] E. Wigner, *Math. Naturw. Anz. Ung. Akad. Wiss.* **53**, 477 (1935).

[99] K. Kristensen, P. Jørgensen, A. J. Thorvaldsen and T. Helgaker, J. Chem. Phys. **129**(21), 214103 (2008).

[100] K. Sasagane, F. Aiga and R. Itoh, J. Chem. Phys. **99**, 3738 (1993).

[101] O. Christiansen, C. Hättig and P. Jørgensen, Int. J. Quantum Chem. **68**, 1 (1998).

[102] M. A. Ball and A. D. McLachlan, Mol. Phys. **7**, 501 (1964).

[103] A. D. McLachlan and M. A. Ball, Rev. Mod. Phys. **36**, 844 (1964).

[104] F. Smet, J. Tillieu and A. V. Groenendael, Int. J. Quantum Chem. **17**(3), 531 (1980).

[105] M. A. Spackman, J. Chem. Phys. **94**(2), 1288 (1991).

[106] T. Helgaker, H. Larsen, J. Olsen and P. Jørgensen, Chem. Phys. Lett. **327**, 397 (2000).

[107] S. Coriani, S. Høst, B. Jansík, L. Thøgersen, J. Olsen, P. Jørgensen, S. Reine, F. Pawłowski, T. Helgaker, and P. Sałek, J. Chem. Phys. **126**, 154108 (2007).

[108] MAESTRO *v. 8.5*, 2005. See http://www.schrodinger.com.

[109] R. Berger, C. Fischer and M. Klessinger, J. Phys. Chem. A. **102**(36), 7157 (1998).

[110] N. Lin, X. Zhao, A. Rizzo and Y. Luo, J. Chem. Phys. **126**(24), 244509 (2007).

[111] F. Santoro, A. Lami, R. Improta, J. Bloino and V. Barone, J. Chem. Phys. **128**(22), 224311 (2008).

[112] M. Faraday, Philos. Mag. **28**, 294 (1846).

[113] M. Faraday, Philos. Trans. R. Soc. London. **136**, 1 (1846).

[114] D. J. Caldwell and H. Eyring. *The Theory of Optical Activity*. Wiley-Interscience, New York, 1971.

[115] A. D. Buckingham and P. J. Stephens, Adv. Res. Chem. Phys. **17**, 399 (1966).

[116] P. N. Schatz and A. McCaffery, Q. Rev. Chem. Soc. **23**, 552 (1969).

[117] R. Serber, Phys. Rev. **41**, 489 (1932).

[118] P. J. Stephens, Chem. Phys. Lett. **2**, 241 (1968).

[119] P. J. Stephens, J. Chem. Phys. **52**, 3489 (1970).

[120] P. J. Stephens, Ann. Rev. Phys. Chem. **25**, 201 (1974).

[121] P. J. Stephens, Adv. Chem. Phys. **35**, 197 (1976).

[122] C. H. Henry, S. E. Schnatterly and C. P. Slichter, Phys. Rev. **137**(2A), A583 (1965).

[123] S. Coriani, P. Jørgensen, A. Rizzo, K. Ruud and J. Olsen, Chem. Phys. Lett. **300**, 61 (1999).

[124] London, F., J. Phys. Radium. **8**(10), 397 (1937).

[125] T. Helgaker and P. Jørgensen, J. Chem. Phys. **95**(4), 2595 (1991).

[126] M. Seth, M. Krykunov, T. Ziegler and J. Autschbach, J. Chem. Phys. **128**(23), 234102 (2008).

[127] S. Coriani, C. Hattig, P. Jørgensen and T. Helgaker, J. Chem. Phys. **113**(9), 3561 (2000).

[128] A. J. Thorvaldsen, K. Ruud, K. Kristensen, P. Jørgensen and S. Coriani, J. Chem. Phys. **129**(21), 214108 (2008).

[129] A. Castellan and J. Michl, J. Am. Chem. Soc. **100**, 6824 (1978).

[130] A. Kaito, M. Hatano and A. Tajiri, J. Am. Chem. Soc. **99**, 5241 (1977).

[131] T. Yanai, D. P. Tew and N. C. Handy, Chem. Phys. Lett. **393**(1-3), 51 (2004).

[132] G. A. Peralta, M. Seth and T. Ziegler, J. Chem. Theory Comput. **3**, 434 (2007).

[133] D. Ganyushin and F. Neese, J. Chem. Phys. **128**(11), 114117 (2008).

[134] H. Solheim, K. Ruud, S. Coriani and P. Norman, J. Phys. Chem. A. **112**, 9615 (2008).

[135] M. Krykunov, M. Seth, T. Ziegler and J. Autschbach, J. Chem. Phys. **127**(24), 244102 (2007).

[136] Y. Honda, M. Hada, M. Ehara, H. Nakatsuji and J. Michl, J. Chem. Phys. **123**(16), 164113 (2005).

[137] M. Seth, T. Ziegler and J. Autschbach, J. Chem. Phys. **129**(10), 104105 (2008).

[138] M. Seth, M. Krykunov, T. Ziegler, J. Autschbach and A. Banerjee, J. Chem. Phys. **128**(14), 144105 (2008).

[139] M. Seth and T. Ziegler, J. Chem. Phys. **124**(14), 144105 (2006).

[140] M. Seth, T. Ziegler and J. Autschbach, J. Chem. Phys. **122**(9), 094112 (2005).

[141] M. Seth, T. Ziegler, A. Banerjee, J. Autschbach, S. J. A. van Gisbergen and E. J. Baerends, J. Chem. Phys. **120**(23), 10942 (2004).

[142] H. Solheim, K. Ruud, S. Coriani and P. Norman, J. Chem. Phys. **128**(9), 094103 (2008).

[143] H. Solheim, L. Frediani, K. Ruud and S. Coriani, Theor. Chem. Accounts. **119**, 231 (2008).